ANAS Transactions **Earth Sciences** **1 / 2019**

Geology and geophysics

http://www.journalesgia.com

ISOTOPE-GEOCHEMICAL CHARACTERISTICS OF HYDROCARBONS ON THE NORTH-WESTERN FLANK OF SOUTH CASPIAN BASIN

Feyzullayev A.A.

İnstitute of Geology and Geophysics of Azerbaijan National Academy of Sciences
119, H. Javid Ave., Baku, Azerbaijan, AZ1143: fakper@gmail.com

Keywords: *oil, gas, source rocks, organic matter, geochemistry, correlation, South Caspian basin*

Summary. This paper details aspects of isotope-geochemical features for oil and gas on the N-W flank of South Caspian basin (Gobustan, western Absheron regions and adjacent offshore area), where natural oil and gas seepages are associated with tectonic faults and mud volcanoes (MVs). Oils concerned with MVs are biodegraded, having predominantly naphthenic-paraffinic base and less than 0.5% sulfur content. Oil samples and hydrocarbon extracts of source rock were analyzed using gas chromatography, mass spectrometry and their combination (biomarker analysis). Oil–oil and oil–source rock correlations are used. The values of the complex biomarker parameters of selected oil samples correspond to Tertiary source rocks with the similar organic facies accumulated in deep-water conditions with some terrestrial contribution. Oils have low to moderate organic maturities (Ro = 0.75-0.85). Relationship between the isotope composition of carbon (ICC) for aliphatic and aromatic fractions of oils and rock extracts (oil-rock correlation) shows that the source of commercial oil reserves in the Productive series (lower Pliocene) is mainly Miocene deposits (Diatom, Chokrak and Upper Maykop strata). The source of gases is from the sedimentary cover as is evidenced by the 3He/4He ratio values. They also have been derived from mixed marine organic-rich source facies. Such gas is not from the thermal destruction of oils. Calculated depth of oil source corresponds to 6.1-8.6 km (gas source – from 8.1 to 15.8 km). The isotopically heavy ICC of CO_2 in gases is most probably the microbial destruction of hydrocarbons at shallow depths (no deeper than 2 km).

© 2019 Earth Science Division, Azerbaijan National Academy of Sciences. All rights reserved.

1. Introduction

The north-western flank of the South Caspian basin (SCB) includes Gobustan, western Absheron regions and adjacent offshore area (Fig. 1). This area is a strongly folded region with high density of development of structures and outcrops with a wide stratigraphic range (from Pliocene to Paleogene). Natural oil and gas surface seepages associated with tectonic faults and mud volcanoes are widely developed.

The purpose of this paper is to detail different aspects of isotope-geochemical features of oil and gas in this region.

2. Results of studies and discussion

2.1. Oil and gas seepages

2.1.1. Oil seeps

Oil seeps concerned with mud volcanoes (MV) are biodegraded except for the oil at the northwesternmost volcano, Demirchi, at the offset of the Greater Caucasus (Fig. 2). All oils have predominantly naphthenic-paraffinic base and less than 0.5% sulfur content.

The isotopic composition of carbon (ICC) of crude oil ranges from -28.2 to -25.0‰ and the pristine/phytane (Pr/Ph) ratio ranges from 0.9 to 2.0. The studied oil seeps from MVs are classified into two types: isotopically heavy and isotopically light. The gas chromatography – mass spectrometry (GC-MS) traces show low diasteranes and an almost equal distribution of C_{27-29} sterane compounds, though C_{28} sterane is often slightly dominant.

2.1.2. Gas seepages

Gases play an important role in mud volcanoes process. The source of these significant gas volumes is from the sedimentary cover as is evidenced by the $^3He/^4He$ ratio values, which vary within $(0.28\text{-}9.0)*10^{-7}$ (average $1.2*10^{-7}$).

Methane dominates in all the samples of the MV gases (89.1-99.5 %). There are small amounts of $CH_{2\text{-}6}$, CO_2, N_2, He and Ar (Valayev and Grinchenko, 1984).

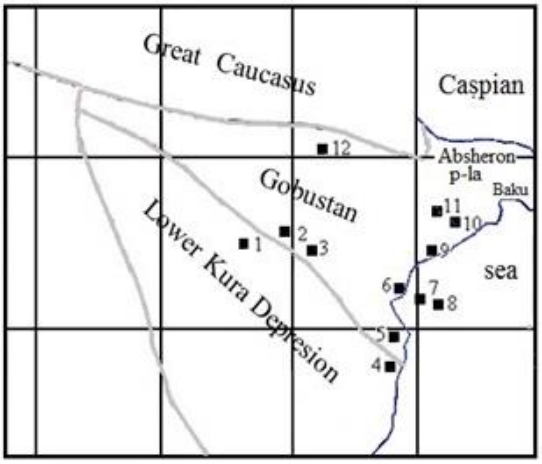


Figure 1. Scheme of location the studied region, petroleum fields and mud volcanos:1 – Kalamaddyn; 2 – Hajiveli; 3 – Umbaki; 4 – Pirsaat; 5 – Dashgil; 6 – Kyanizadag; 7 – Sangachaldeniz; 8 – Duvanny-deniz; 9 – Garadag; 10 – Guzdek; 11 – Kergez; 12 – Jangi (mud volcano)

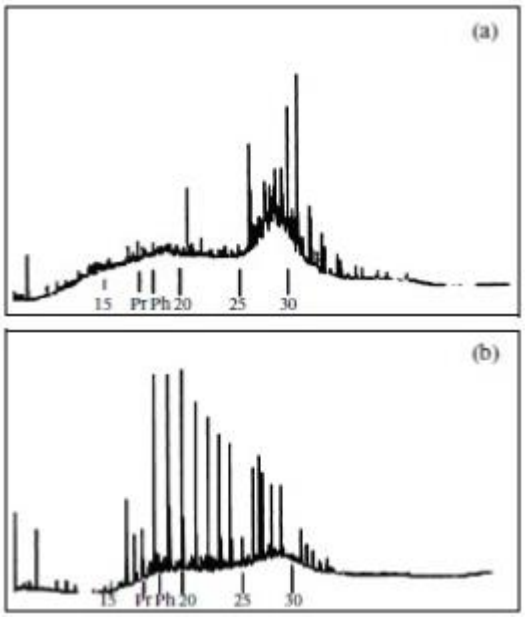


Figure 2. Examples of gas–liquid chromatograms of the saturated fraction of oils from mud volcanoes in Azerbaijan: (a) biodegraded oil (Kyrlykh MV) and (b) non-biodegraded oil (Demirchi MV)

The isotope compositions of carbon of methane and ethane display significant variability: respectively, -58.4 to -39.4‰ and -23.3 to -29.6‰. The isotopically lightest samples are interpreted as a mixed biogenic and thermogenic gases. The isotopically heaviest samples are indicative of a thermogenic origin (Fig. 3).

The CO_2 concentration in gases of MVs ranges from 0.05 to 18.2%. Values of $\delta^{13}C$ (CO_2) from more than 80 examined MVs vary widely: from -49.6 to +25.6‰ and indicate the presence of multiple sources of CO_2. The rarely encountered isotopically super-heavy CO_2 (> +5‰) has special interest.

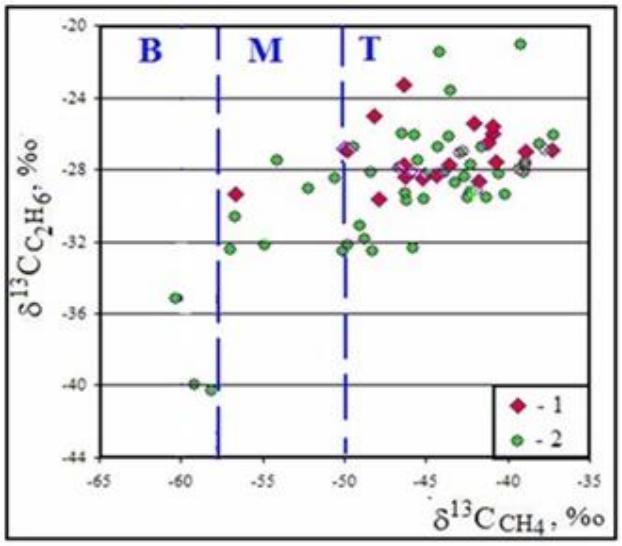


Figure 3. ICC of CH_4 vs. ICC of C_2H_6 in gases of mud volcanoes (1) and petroleum

2.2. Reservoir oils and gases

2.2.1. Reservoir oils

Examination of oils was carried out using gas chromatography and mass-spectrometry techniques and their combination (biomarker analysis). Some oils are mixtures of biodegraded and non-biodegraded oils. Unaltered oils have similar n-alkane distributions, indicating an algae contribution typical for lacustrine, lagoonal or pelagic sedimentation environments.

The pristane / phytane (Pr/Ph) ratio is between 1.3 and 1.5 for the majority of oils. Such values are typical for oils generated by source facies of marine origin when the oxygen-enriched photic zone is located above anoxic water mass and sediments. For some samples values of Pr/Ph ratio were found to be below 1.3, apparently suggesting more reducing conditions in the water layer, less thermal maturity or, more likely, biodegradation impact.

Pristane/n-C_{17} and Phytane/n-C_{18} ratios (Fig. 4) suggest that the source rocks were in transition between oxidizing and reducing conditions with similar molecular characteristics. Variation in isoprenoid/n-alkane ratio values is controlled exclusively by the extent of biodegradation. These parameters suggest that oils were generated by several source rocks with similar facies.

The carbon preference index (CPI) values, derived from gas chromatographic analyses (Marzi et al., 1993), change in the narrow range (1.02±0.02), indicating moderate input of terrestrial organic material.

Gross composition of oils (Fig.5) indicates that they are sourced from similar organic facies.

Sterane distributions (C_{27}, C_{28} and C_{29}) show close similarity between studied oils (dispersion is

around 3%), thus also indicating, that the oils have been generated by similar source facies (Fig. 6-8).

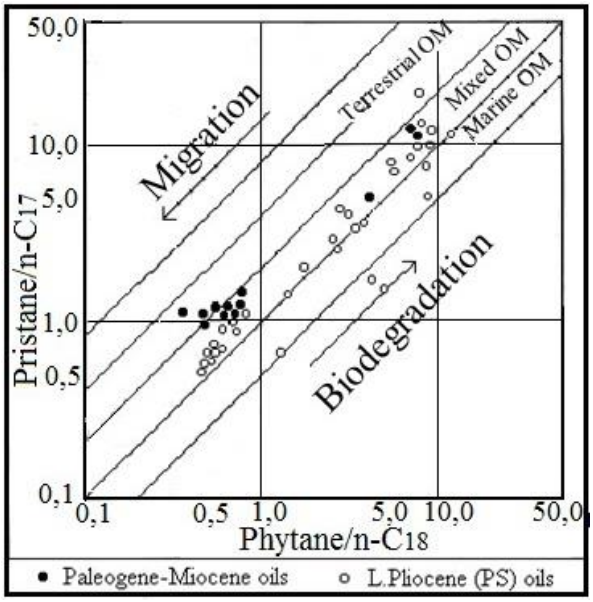


Figure 4. Crossplot of Pristane/n-C_{17}vs. Phytane/n-C_{18} in oils

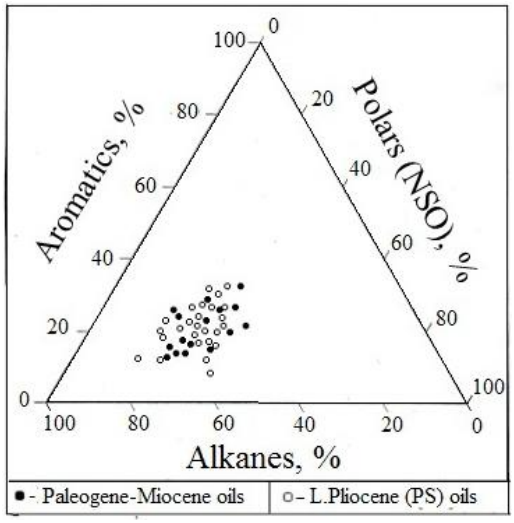


Figure 5. Triangle diagram of the oil group composition from Paleogene-Miocene and Low Pliocene reservoirs

The values of other complex biomarker parameters, such as C_{28}/C_{29} sterane ratio, hopane/(hopane +moretane) ratio, content of oleanane and gammacerane, tricyclic and pentacyclic-terpanoids, testify to Tertiary source rocks with similar organic facies accumulated in deep-water conditions with some terrestrial contribution. Moderate input of terrestrial organic material is confirmed by the carbon preference index (CPI) values, derived from gas chromatographic analyses (Marzi et al., 1993), which change in the narrow range (1.02±0.02). Norhopanes to hopanes ratio is low, typical for clastic source rocks.

Although all of the above biomarker indexes indicate the formation of oils from similar organic facies, the $\delta^{13}C$ ratio of whole oils, varying between -27.52 and -23.83 ‰ suggests their formation in different source rocks.

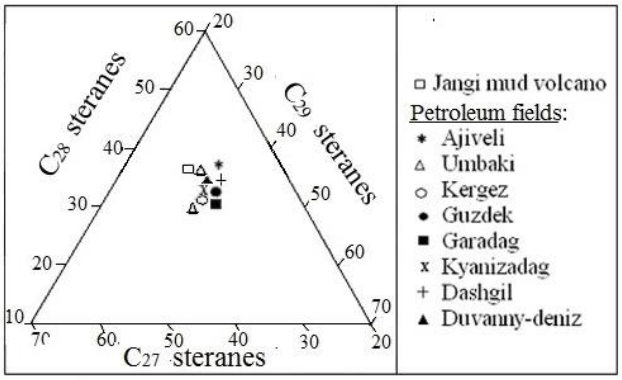


Figure 6. Relative percentage of C_{27}:C_{28}:C_{29} regular steranes in oils

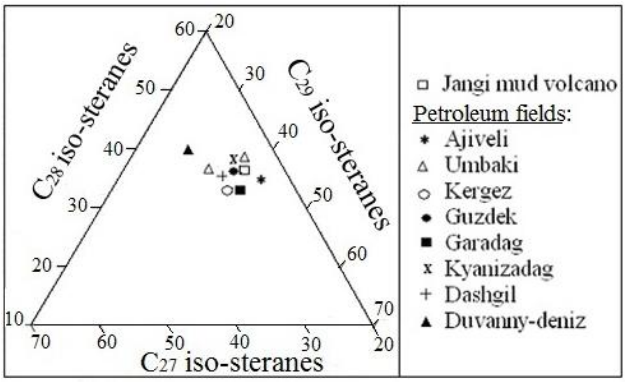


Figure 7. Relative percentage of C_{27}:C_{28}:C_{29} isosteranes in oils

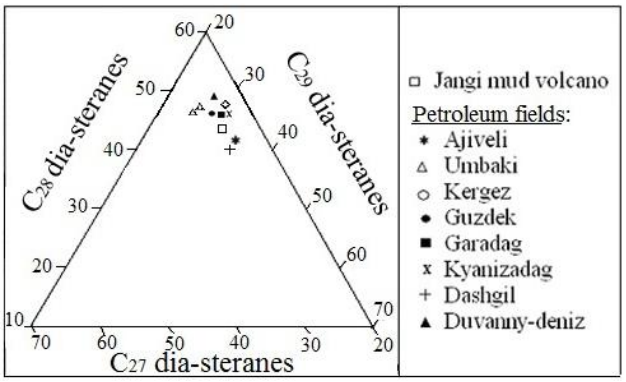


Figure 8. Relative percentages of C_{27}:C_{28}:C_{29} diasteranes in oils

The relationship between the ICC of aliphatic and aromatic fractions of oils and rock extracts (oil-rock correlation) indicates that the source of commercial oil reserves in the Productive series is mainly Miocene deposits (Diatom, Chokrak and Upper Maykop strata) (Fig. 9).

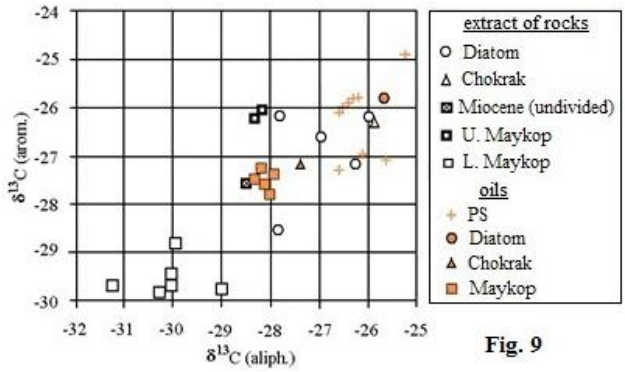


Figure 9. The relationship between the ICC of aliphatic and aromatic fractions of oils and rock extracts

2.2.2. Reservoir gases

17 gas samples were examined from 13 fields of the Gobustan and adjacent Absheron and offshore areas. All gases are associated with oil accumulations. The samples are taken from reservoirs occurring in the depth interval from 520 to 4268 m and cover wide geographic and stratigraphic ranges.

The natural gases display significant differences in both molecular and isotopic composition. Methane dominates in all samples (89-99.8%). Gas wetness ranges from less than 1% (Sangachal-deniz field) to greater than 12% (Pirsaat field). The character of the gas wetness variability with depth most probably reflects the location in the section of peak oil generation and the zone of biogenic gases.

Values of the iC_4/nC_4 ratios vary in the range 0.36-4.4 and decrease with depth due to either thermal maturity as a result of the generation of nC_4 or alteration through microbial processes, which preferentially remove nC_4 and therefore cause an increase in the ratio.

Methane carbon isotopic composition ranges from 58 to 37‰ relative to the PDB standard. The stable carbon isotopic composition of ethane also displays a wide range. Unlike mud volcanoes, which are represented predominantly by thermogenic hydrocarbon gases, the gases of the petroleum fields have both thermogenic and biochemical origins, as well as being mixed (see Fig.3).

Examination of the dataset reveals an increasing tendency in the methane and ethane $\delta^{13}C$ values with depth. Such a trend is consistent with increasing thermal maturity of gases. Due to vertical migration the introduction of isotopically heavier gas in the shallow section is observed.

As well as in mud volcanoes the presence of isotopically super-heavy CO_2 was detected also in gases of petroleum fields. In gases of the petroleum fields this type of CO_2 is found only to a depth of about 2 km, regardless of the stratigraphic affiliation of the reservoir (Fig. 10).

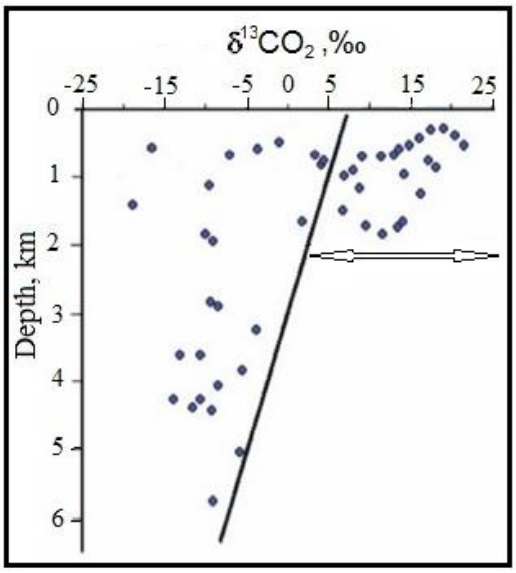


Figure 10. The carbon isotopic composition of carbon dioxide in gases of petroleum fields vs. depth

The mechanism of oil biodegradation is able to explain the nature of isotopically heavy CO_2 in gases of petroleum fields and mud volcanoes. The presence of isotopically super-heavy CO_2 and the possibility of its generation by the oxidation of hydrocarbons were mentioned by Zarttman et al. (1961), Kissin and Pakhomov (1967), Galimov (1973), Irwin et al. (1977), Pallasser R.J. (2000) and Wilhelms et al. (2001).

This result is confirmed by the comparative analysis of distribution of $\delta^{13}C$ CO_2 and CH_4 for mud volcanoes separately with and without oil seeps (Fig. 11). The heaviest $\delta^{13}C$ values of CO_2 and the lowest $\delta^{13}C$ values of CH_4 are typical for mud volcanoes with oil seeps (Feyzullayev and Movsumova, 2010).

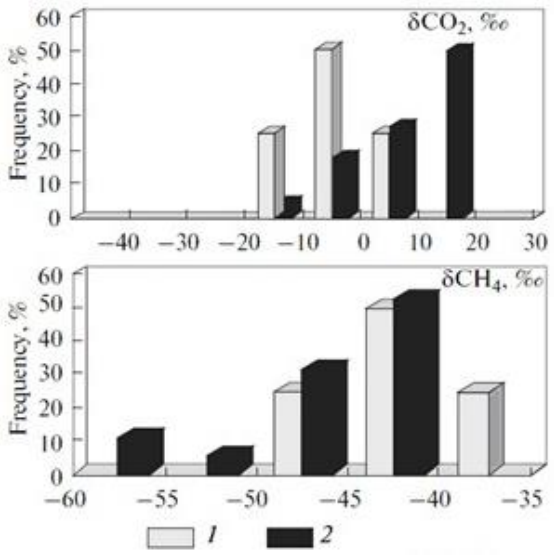


Figure 11. Histograms of the distribution of $\delta^{13}C$ CO_2 values (in‰) of CO_2 and CH_4: (1) mud volcanoes without oil seeps and (2) mud volcanoes with oil seeps

2.3. Maturity of oils and gases

A number of isotopic geochemical parameters are used for assessments of oil and gas maturity (Peters and Moldovan, 1993).

Isomerization of C_{29}-ethylcholestanes and methyl-phenantrane index (MPI) are the most often used biomarker ratios for oil maturity assessments. Based on empirically derived relationships between values of these parameters and the thermal history of sedimentary basins their values are converted to equivalent vitrinite reflectance (Ro) values.

Gas maturity estimates are based on an empirically derived relation between carbon isotopic composition of HC gases and vitrinite reflectance (Ro) (Faber, 1987).

Values of isomerization of C_{29}-ethylcholestanes ratio for studied oils vary between 0.3-0.5 with an average value of 0.39 and a tendency for an increase in the direction of the regional subsidence of the strata. Such values indicate a low degree of maturity.

The majority of methyl-phenathrene index (MPI-1) values reported as vitrinite reflectance equivalence (Req.) are within 0.6-0.9 in agreement with the estimates of thermal maturity of oils corresponding to the upper part of oil window.

Values of trisnorhopane ratio Ts/(Ts+Tm) vary within 0.21-0.30 (0.26 average) and indicate that the oils were generated at different hydrocarbon-generating stages and/or from diverse source rocks.

There are no maturity differences between non-degraded oils and condensates.

Based on the estimates of the maturity of the gases from mud volcanoes (Feyzullayev et al., 2015), their gases migrate to the surface from considerable depths (7 to 15 km), corresponding to the zone of generation of gas-condensate (vitrinite reflectance R_0 = 1.3-1.8%). In this connection the primary gas must be fatty. Gas sampled in the quiet period of MV activity is predominantly methane and the gas is classified as dry. Gas wetness {100 x (C_2+/C_1+)} values range from 0.01 to 0.62%. The explanation is that during quite periods the gas migrates through the thick clay mass filling the channel of the volcano, accompanied by a contrasting gas chromatographic effect. However, during the eruption of mud volcanoes HC gases reach the surface through an open channel without a gas chromatographic effect. In this case the initial fatty composition of gases is reflected by the black color of the products of their combustion (Feyzullayev, 2010) (Fig. 12) and the detection of "frozen" drops of liquid HCs from the burning gas on the surface of the volcano.

As a whole the maturity estimates for mud volcano HC gases are in agreement with those for HC fields, varying within 1.30-2.10% R_{eq}. At the same time, slightly higher maturity of mud volcano gases is noted (R_{eq}=1.55% on average vs. 1.42% for reservoir gases).



Figure 12. Eruptions of Lokbatan MV in 1997 (on the top) and 2001 years

The maturity of oils is lower in comparison with gas. The present-day maturity of the MV oils is 0.65% - 0.80% R_{eq}. and agrees well with maturity of the reservoir oils, allowing one conclude that the MV oils are a product of the destruction of oil accumulation in structures, pierced by MV. Therefore the maximal depth of the MV oils does not exceed the depth of corresponding reservoir oils, about 4.9 km offshore (8 March field, well 580) and 5.3 km onshore (Kalamaddyn field, well 3) (Feyzullayev, 2012).

The stratigraphic locations of the HC sources change towards regional subsidence of strata (from southern slope of the Great Caucasus to the central deep buried part of SCB) from Mesozoic to Paleogene-Miocene (gas) and from Oligocene to Miocene (oil) (Feyzullayev and Aliyeva, 2003; Guliyev et al., 2004).

Using the relationship between R_o and depth for the SCB a generalized model was created for vertical zonality of oil and gas generation in the SCB. The interval of oil and gas formation occupies a depth range of 5-15 km, with a hypsometric shift between the zones of liquid and gas generation. The oil generation interval is confined to 5-9 km (peak generation at 7-8 km) and the gas source is located between 8 and 15 km (peak generation at 11-12 km) (Fig. 13).

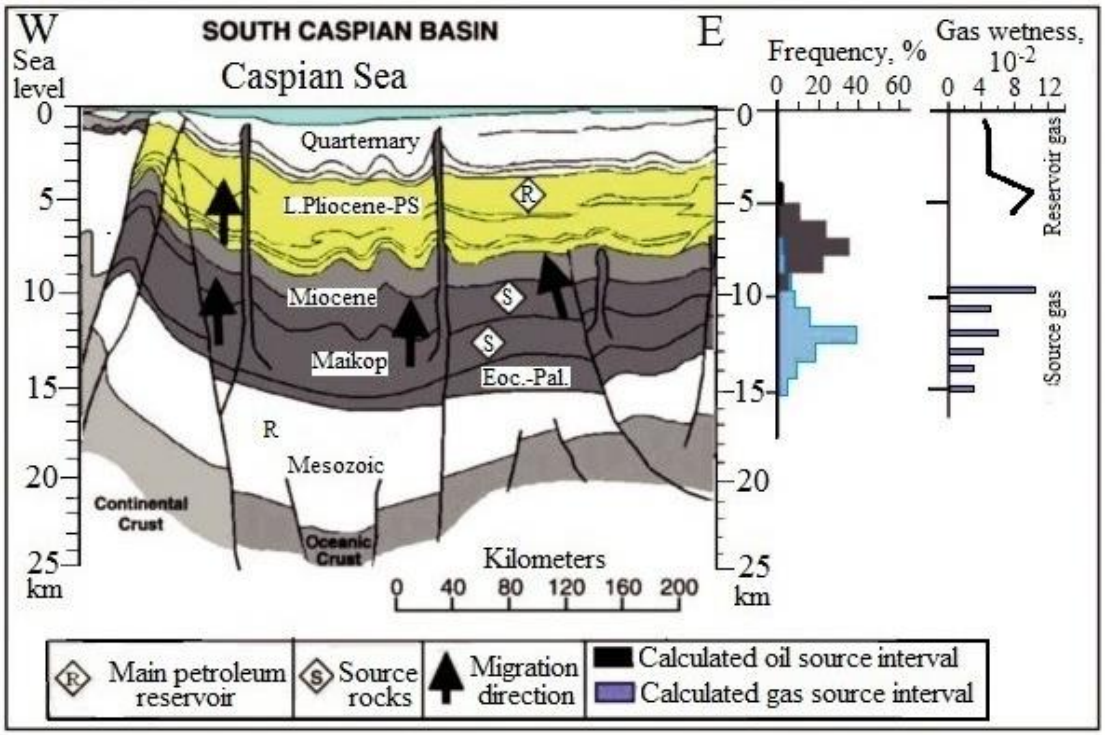


Figure 13. WE directed geological profile across the SCB with chart of calculated depths of oil and gas generation

3. Conclusion

Examination of hydrocarbons using gas chromatography and mass-spectrometry techniques showed that some oils are mixtures of biodegraded and non-biodegraded oils. Unaltered oils have similar n-alkane distributions indicating algae contribution typical for lacustrine, lagoonal or pelagic sedimentation environments.

Molecular characterization of selected oil samples indicates that most of the oils are sourced from similar Tertiary, slightly calcareous, mixed terrestrial-marine kerogen and have low to moderate organic maturities (R_o = 0.75-0.85).

Gas also has been derived from mixed marine organic-rich source facies (more humic and less anoxic). Such gas is not from the thermal destruction of oils.

Thermal disequilibrium from the rapid subsidence delayed hydrocarbon generation and increased the minimum depth required for the onset of liquid hydrocarbon generation. Several oils display characteristics consistent with multiple phases of trap charging.

Oil-to-oil and source rock-to-oil correlations based on carbon isotopic ratios suggest that the Miocene interval (Diatom, Chokrak and Upper Maykop strata) has played the principal role in formation of commercial oil accumulations in Lower Pliocene reservoirs.

Liquid HCs and gas are generated by different stratigraphic intervals located at different depths. HC gases are sourced from the strata ranging in depth interval from 8 to 15 km, with the tendency for increase in depth towards regional subsidence. Calculated depth of oil source corresponds to 5-9 km.

The isotopically heavy carbon of the CO_2 in gases of MVs and fields is most probably synthesized by the microbial destruction of hydrocarbons in an open system. This process takes place at shallow depths (no deeper than 2 km) and, correspondingly, at low temperatures (no higher than 40°C for SCB).

4. Acknowledgment

The author is deeply grateful to all colleagues who participated in the field and analytical studies.

REFERENCES

Faber E. About isotopic geochemistry of gaseous hydrocarbons. Erdol, Erdgas, Kohle, V. 103, Iss. 5, 1987, pp. 210-218 (in German).

Feyzullayev A.A. Mud volcanoes in the South Caspian basin: nature and estimated depth of its products. Natural Science, V. 4, № 7, 2012, pp. 445-453.

ЛИТЕРАТУРА

Faber E. Zur isotopengeochemie gasformiger Kohlenwasserstoffe. Erdol, Erdgas, Kohle, V. 103, Iss. 5, 1987, pp. 210-218.

Feyzullayev A.A. Mud volcanoes in the South Caspian basin: nature and estimated depth of its products. Natural Science, V. 4, № 7, 2012, pp. 445-453.

Feyzullayev A.A. Physicochemical interactions in the sedimentary rock – fluid system in the South Caspian basin in connection with oil-gas ontogenesis. Proceedings of ANAS, The Sciences of Earth, № 4, 2010, pp. 28-45 (in Russian).

Feyzullayev A.A., Aliyeva Es.A. Estimation of the various source rocks contribution in oil pools formation. Proceedings of EAGE 65 Conference and Exhibition. Stavanger. Norway, 2-5 June, 2003.

Feyzullayev A.A., Movsumova U.A. The nature of the isotopically heavy carbon composition of carbon dioxide and bicarbonates in the waters of mud volcanoes in Azerbaijan. Geochemistry International, V. 48, № 5, 2010, pp. 517-522.

Feyzullayev A.A., Tagiyev M.F., Lerche I. On the origin of hydrocarbons in the main Lower Pliocene reservoirs of the South Caspian Basin, Azerbaijan. Energy, Exploration & Exploitation, V. 33, № 1, 2015, pp. 1-14.

Galimov E.M. Carbon isotopes in oil and gas geology. Nedra. Moscow, 1973, 384 p. (in Russian).

Guliyev I.S., Feyzullayev A.A., Huseynov D.A. Geochemical features and source of fluids of mud volcanoes in South Caspian basin in lights of new data at isotopes C, H, and O. Geochimiya, № 7, 2004, 792-800 (in Russian).

Irwin H., Curtis C., Coleman M. Isotopic evidence for source of diagenetic carbonates formed during burial of organic rich sediments. Nature, V. 269, Iss. 5625, 1977, pp. 209-213.

Kissin I.G., Pakhomov S.N. On the possibility of generation of hydrocarbonic acid in the interiors under moderately high temperatures. Doklady AS of the USSR, V. 174, № 2, 1967, pp. 451-454 (in Russian).

Marzi R., Torkelson, B.E., Olson R.K. A revised carbon preference index. Organic Geochemistry, V. 20, № 8, 1993, pp. 1303-1306.

Pallasser R.J. Recognising biodegradation in gas/oil accumulations through the ^{13}C compositions of gas components. Org. Geochem., V. 31, № 12, 2000, pp. 1363-1373.

Peters K.E., Moldowan J.M. The biomarker guide: interpreting molecular fossils in petroleum and ancient sediments. Prentice Hall. Englewood Cliffs, New Jersey, 1993, 363 p.

Valyaev B.M., Grinchenko Yu.I. Source of isotopically "ultraheavy" carbon dioxide in natural gases. In: Proceedings of 10th AllUnion symposium on Stable Isotopes in Geochemistry, Moscow, Russia, 1984, p. 170 (in Russian).

Wilhelms A., Larter S.R., Head I. et al. Biodegradation of oil in uplifted basins prevented by deep burial sterilization. Nature, V. 411, 2001, pp. 1034-1037.

Zartman R.E., Wasserburg G.J., Reynolds J.H. Helium, argon and carbon in some natural gases. J. Geophys. Res., V. 66, 1961, pp. 277-286.

Feyzullayev A.A., Aliyeva Es.A. Estimation of the various source rocks contribution in oil pools formation. Proceedings of EAGE 65 Conference and Exhibition. Stavanger. Norway, 2-5 June, 2003.

Feyizullayev A.A., Movsumova U.A. The nature of the isotopically heavy carbon composition of carbon dioxide and bicarbonates in the waters of mud volcanoes in Azerbaijan. Geochemistry International, V. 48, № 5, 2010, pp. 517-522.

Feyzullayev A.A., Tagiyev M.F., Lerche I. On the origin of hydrocarbons in the main Lower Pliocene reservoirs of the South Caspian Basin, Azerbaijan. Energy, Exploration & Exploitation, V. 33, № 1, 2015, pp. 1-14.

Irwin H., Curtis C., Coleman M. Isotopic evidence for source of diagenetic carbonates formed during burial of organic rich sediments. Nature, V. 269, Iss. 5625, 1977, pp. 209-213.

Marzi R., Torkelson, B.E., Olson R.K. A revised carbon preference index. Organic Geochemistry, V. 20, № 8, 1993, pp. 1303-1306.

Pallasser R.J. Recognising biodegradation in gas/oil accumulations through the ^{13}C compositions of gas components. Org. Geochem., V. 31, № 12, 2000, pp. 1363-1373.

Peters K.E., Moldowan J.M. The biomarker guide: interpreting molecular fossils in petroleum and ancient sediments. Prentice Hall. Englewood Cliffs, New Jersey, 1993, 363 p.

Wilhelms A., Larter S.R., Head I. et al. Biodegradation of oil in uplifted basins prevented by deep burial sterilization. Nature, V. 411, 2001, pp. 1034-1037.

Zartman R.E., Wasserburg G.J., Reynolds J.H. Helium, argon and carbon in some natural gases. J. Geophys. Res., V. 66, 1961, pp. 277-286.

Валяев Б.М., Гринченко Ю.И. Источник изотопно-тяжелой углекислоты в природных газах. В материалах 10 Всесоюзного симпозиума по стабильным изотопам в геохимии. Москва, Россия, 1984, с.170.

Галимов. Э.М. Изотопы углерода в нефтегазовой геологии. Недра. Москва, 1973, 383 с.

Гулиев И.С., Фейзуллаев А.А., Гусейнов Д.А. Геохимические особенности и источники флюидов грязевых вулканов Южно-Каспийского осадочного бассейна в свете новых данных по изотопии С, Н, и О. Геохимия, № 7, 2004, с. 792-800.

Киссин И.Г., Пахомов С.Н. О возможности генерации углекислоты в недрах при умеренно высоких температурах. Докл. АН СССР, Т. 174, № 2, 1967, с. 451-454.

Фейзуллаев А.А. Физико-химические взаимодействия в системе осадочная порода-флюид в Южно-Каспийском бассейне в связи с онтогенезом нефти и газа. Известия НАН Азербайджана. Науки о Земле, № 4, 2010, с. 28-45.

ИЗОТОПНО-ГЕОХИМИЧЕСКАЯ ХАРАКТЕРИСТИКА УГЛЕВОДОРОДОВ СЕВЕРО-ЗАПАДНОГО ФЛАНГА ЮЖНО-КАСПИЙСКОГО БАССЕЙНА

Фейзуллаев А.А.
Институт геологии и геофизики НАНА
AZ1148, г.Баку, просп. Г.Джавида, 119: fakper@gmail.com

Резюме. В данной статье подробно рассматриваются различные аспекты изотопно-геохимических особенностей нефтей и газов СЗ борта Южно-Каспийского бассейна (Гобустан, западный Абшерон и прилегающая прибрежная зона), где естественные проявления нефти и газа связаны с тектоническими нарушениями и грязевыми вулканами (ГВ). Нефти ГВ биодеградированы, имеют преимущественно нафтен-парафиновую основу с содержанием серы менее 0,5%. Образцы нефти и углеводородного экстракта материнских пород анализировались с помощью газовой хроматографии, масс-спектрометрии и их комбинации (биомаркерный анализ). Проведена корреляция нефть – нефть и нефть – материнская порода, и установлено, что нефти соответствуют породам третичного возраста с органическими фациями, накопленными в глубоководных условиях с некоторым вкладом наземного органического материала. Нефти характеризуются низкой или умеренной зрелостью (Ro = 0,75-0,85). Зависимость между изотопным составом углерода (ИСУ) алифатической и ароматической фракций нефтей и экстрактов пород показывает, что источником промышленных запасов нефти в продуктивной толще (нижний плиоцен)

являются в основном миоценовые отложения (диатом, чокрак и верхний майкоп). Источником газов является осадочный чехол, о чем свидетельствуют значения отношения $^3He/^4He$. Газы также были образованы из смешанной морской (преобладает) и наземной органической фаций. Газы не являются продуктом термического крекинга нефтей. Расчетная глубина источника нефти соответствует 6,1-8,6 км (источника газа – от 8,1 до 15,8 км). Изотопно-тяжелый ИСУ CO_2 в газах, скорее всего, связан с микробным разрушением углеводородов на небольших глубинах (не глубже 2 км).

Ключевые слова: *нефть, газ, материнские породы, органическое вещество, геохимия, корреляция. Южно-Каспийский бассейн*

CƏNUBİ XƏZƏR HÖVZƏSİNİN ŞİMAL-QƏRB CİNAHINDA KARBOHİDROGENLƏRİN İZOTOP-GEOKİMYƏVİ SƏCİYYƏSİ

Feyzullayev Ə.Ə.
AMEA Geologiya və Geofizika İnstitutu
AZ1143, Bakı şəh., H.Cavid prosp.,119: fakper@gmail.com

Xülasə. Bu məqalədə Cənubi Xəzər hövzəsində (Qobustan, Qərbi Abşeron rayonları və bitişik sahil zonası) neft və qazın izotop-geokimyəvi xüsusiyyətlərinin müxtəlif aspektləri təhlil edilir. Burada geniş yayılmış neft və qazın təbii təzahürləri tektonik qırılmalar və palçıq vulkanları (PV) ilə əlaqədardır. Bioloji aşınmaya məruz qalmış və kükürdün miqdarı 0,5%-dən az olan PV neftləriı, əsasən, naften-parafin tərkiblidir. Neftin və ana süxurların karbohidrogen ekstraktının nümunələri qaz- xromatoqrafiya, mass-spektrometriya və onların kombinasiyası (biomarker analizi) üsullarının köməyi ilə öyrənilmişdir. Neft-neft və neft-ana süxur korrelyasiyası aparılmış və müəyyən edilmişdir ki, neftlər, əsasən, dərinsu şəraitində yığılmış Miosen yaşlı üzvi materialdan əmələ gəlmişdir. Neftlərin yetkinliyi aşağı və ya orta dərəcəyə (Ro = 0,75-0,85) uyğundur. Neftlərin və süxur ekstraktlarının alifatik və aromatik fraksiyaların karbonunun izotop tərkibləri (KİT) arasındakı asılılıq Məhsuldar qatda (alt Pliosen) olan sənae neft ehtiyatlarının mənbəyinin əsasən Miosen çöküntüləri (Diatom, Çokrak və üst Maykop) olduğunu göstərir. Qazların mənbəyi $^3He/^4He$ nisbətinin qiymətlərinə görə çöküntü örtüyüdür. Qazlar da qarışıq dəniz (dominant) və yerüstü üzvi fasiyalardan əmələ gəlmişdir və onlar neftlərin termal krekinqinin məhsulu deyil. Hesablanmış neft mənbəyin dərinliyi 6,1-8,6 km-ə bərabərdir (qaz mənbəyi 8,1-dən 15,8 km-ə qədərdir). Qazlarda CO_2 ağır KİT-nin dayaz dərinliklərdə (2 km-dən dərin olmayan) karbohidrogenlərin mikrobial dağılması ilə əlaqədardır.

Açar sözlər*: neft, qaz, ana süxurlar, üzvi maddə, geokimya, korrelyasiya, Cənubi Xəzər hövzəsi*

ANAS Transactions **Earth Sciences** **1 / 2019**

Geology and geophysics

http://www.journalesgia.com

DANGEROUS ATMOSPHERIC EVENTS: A NEW PHYSICAL-MATHEMATICAL APPROACH

Arsen'yev S.A.[1], Eppelbaum L.V.[2], Ermakov N.N.[3]

[1]Dept. of Earth and Planetary Physics of Schmidt's Institute of the Earth's Physics, Russian Academy of Sciences

10 Bolshaya Gruzinskaya str., Moscow, Russia, 123995: Arsy7@mail.ru

[2]School of Geosciences, Raymond and Beverly Sackler Faculty of Exact Sciences. Tel Aviv University Ramat Aviv, 6997801, Tel Aviv, Israel: levap@post.tau.ac.il

[3]School of Chemistry, Raymond and Beverly Sackler Faculty of Exact Sciences. Tel Aviv University Ramat Aviv, 6997801, Tel Aviv, Israel: ermakov@post.tau.ac.il

***Keywords**: tornado, long tide gravity waves, Earth-Moon-Sun gravity system, soliton, dangerous environmental phenomena*

Summary. A significant progress has been recently reached in a long-range forecast of such dangerous atmospheric events as catastrophic and violent tornadoes (EF3-EF5 level). Eppelbaum (2013) elaborated non-stochastic long-term prediction method using pattern recognition theory and Fourier analysis. He detected a close correlation tie of the total tornado numbers per annum with the gravity system of the Earth – Moon – Sun producing the tide forces. However, physical meaning of this effect leaves undisclosed. In present work, we propose a physical-mathematical model which elucidates the process of violent tornado initiation. It occurs in two main stages. At first, the gravitational forces and the hurricane winds in the upper troposphere form the long tide non-linear waves in the lower troposphere. The gale-force winds in the top troposphere arise at intrusion of air cold masses into the warm areas and are usually connected to the fast synoptic cyclones bearing thundery cloudiness and rains. The arisen gravitational non-linear waves rush at the speed of tide waves $V = (gH)^{1/2}$ along the subcloud inversion. After this, gravitational waves fall on (and it is absorbed into) thunderstorm supercells which are already formed inside the cold atmospheric front. In the result of the meteorological field adaption, a pressure inside the thunderstorm supercells decreases, wind rotation becomes stronger and generates a violent tornado. Various environmental examples illustrate an applicability of the developed approach. The theoretical results show a good agreement with the field observations. The proposed new physical-mathematical methodology can be conceptually applied to analysis of other environmental phenomena.

© 2019 Earth Science Division, Azerbaijan National Academy of Sciences. All rights reserved.

1. Introduction

Dangerous atmospheric events produce annual damage of many dozens billion US $ only in the USA (Smith and Katz, 2013; Eppelbaum and Isakov, 2015). Tornadoes are the natural processes of the highest possible intensity in the atmosphere. Velocity of wind in the violent tornadoes exceeds 516 km/hour; therefore they generate great destructive forces. In scientific literature (e.g., Nalivkin, 1969) are given many examples of the total destruction of small towns by tornado. Therefore, the problem of their analysis is high actual (e.g., Doswell and Burgess, 1993; Arsen'yev et al., 2000, 2001, 2004; 2010; Marshall, 2002; Drton et al., 2003; Hirth et al., 2008; Garner, 2012; Naylor and Gilmore, 2012; Wurman et al., 2012; Eppelbaum, 2013; Eppelbaum and Isakov, 2015; Markowski and Richardson, 2014; Laing, 2015; Huang et al., 2016; Paulikas and Schmidlin, 2017).

An influence of solar activity and Moon and Sun gravity fields on many Earth's processes is well-known (e.g., Chizevsky, 1976; Arsen'yev, 1995, 1998; Gadirov, 2001; Sidorenkov, 2002; Belyakov et al., 2008; Scafetta and West, 2008; Gray et al., 2012; Alizadeh et al., 2017) and is studied by physical, statistical, probabilistic and analytical approaches. The Moon-Sun gravity fields, besides atmospheric phenomena, influence to the spread of epidemics and the productivity of many crops (e.g., Chizevsky, 1976), mud volcanism (e.g., Alizadeh et al., 2017),

earthquake triggering (e.g., Tanaka et al., 2004), driving plate tectonics (e.g., Riguzzi et al., 2010) and to many other analyzed and do not investigated yet effects.

The most popular methodology for modelling the catastrophic weather phenomena (tornado, hurricanes, strong wind) are: (a) the statistical approach based on the probability density function, and (b) the deterministic approach, basing on the numerical solution the differential equations of the atmospheres-ocean dynamics. Representation about modern statistical methods of the tornado forecast can be obtained from articles: Eppelbaum (2013), Eppelbaum and Isakov (2015) where reviews of the basic works development in the given direction were presented. In particular, Eppelbaum (2013) has developed a method for the forecast of number of tornado per year, using the historical data of tornado observation in the USA during 63 years, from 1950 to 2012. In the analysis of these data he revealed the maxima (initial harmonics) in spectra of tornado which coincide with the factors describing the tidal gravity forces of the Moon and Sun (a simplified scheme of the Earth-Moon-Sun interaction is presented in Figure 1). The maximum of 2.9 years coincides with the Moon's resonance period. It is the minimal period which can be caught in a spectrum because Nyquist-Kotelnikov's period (Nyquist, 1928; Kotelnikov, 1933) in our case is equal to two years, and the period of digitization is equal to one year. The maximum of 18.6 years corresponds to the Moon's nodal period. A spectrum of number of tornado per year has also a second harmonic of the Moon's nodal period of 9.3 years. The maximum of 63 years is near to the maximum of 64 years which corresponds to the long-period part of the Moon's gravity field variations. In the tornado spectra there is also a peak 4.2 years which corresponds to the Sun activity. It determines the duration of the rise from the minimum to maximum number of sunspots during of Sun activity (e.g., de Jager, 1959; Landscheidt, 1995, 2013). Thus, time changes in gravity fields of the Sun – Moon – Earth system is connected with the interannual variability of tornado series. Statistical methods though allow predicting number of tornado per year; however do not describe the physical mechanism of the tornado activity relative to the gravity fields of the celestial bodies. To clarify "how it works", we should attract the models of tornado based on solutions of the equations of geophysical hydrodynamics.

Arsen'yev et al. (2010) were done a review of the modern numerical models allowing to calculating the structure of tornado. A lot of models reproducing existential evolution and internal structure of the weak (EF0-EF1) and strong (EF2-EF3) tornadoes was developed. Their common shortcoming is the simplified description of the turbulence effect with two scales utilization. The basic scale corresponds to an average wind velocity in tornado. Other stochastic, minor scale describes the small-scale turbulence. It provides the energy dissipation and reduces average velocity of a wind in tornado.

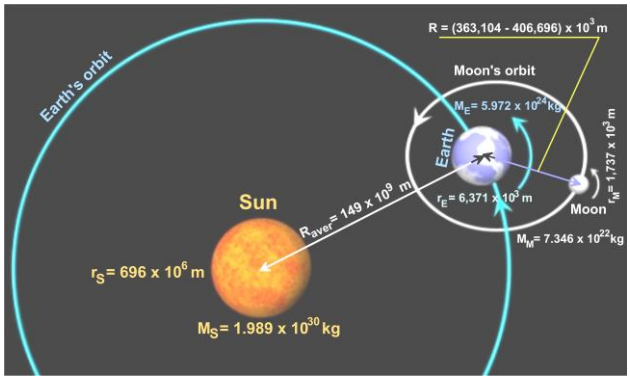


Figure 1. A simplified scheme (not to scale) of the Sun-Moon-Earth interaction with their masses (M) and distances (R) between the Sun and Earth and Moon and Earth and radiuses (r). Subscripts S, E and M denote Sun, Earth and Moon, respectively (after Eppelbaum, 2019)

However, Lorenz (1953) has shown on an example of two-dimensional model that the basic average current is stable, if all lengths of waves of the turbulent disturbances in a flow are less than the length of a wave of the basic current (i.e., a spectrum of the basic current and small-scale turbulence are not overlap). Nevertheless, if in turbulent current there are longer components, for example, convective jets and cells, thermic bubbles, vortical rollers, internal waves, coherent and other eddies, then spectrum of the basic and turbulent current have the common zone, which is filled by mesoscale eddies. In this case the basic current may be unstable and it can increase in time, due to the nonlinear interaction with the mesoscale eddies (Kardashov and Eppelbaum, 2008). The theory of the mesoscale turbulence stated in Arsen'yev et al. (2010) and Nikolaevskiy (2003) allows taking into account in an explicit form the presence of the third intermediate mesoscale in a spectrum of atmospheric currents. Application of this theory to problems of calculation of tornado and tropical hurricanes has allowed to obtain the violent tornadoes (EF4-EF5) and super typhoons due to amplification of the average wind getting energy from the mesoscale eddies (Arsen'yev et al., 2004, 2010). Classification of the mesoscale eddies is presented in Arsen'yev et al. (2010). These eddies fill thunderstorm supercell generating tornado, or arise from the superheated ocean surface producing tropical hurricanes. Instability and growth of the average current arise from

performance of the special conditions which are established by the theory of the mesoscale turbulence. The energy and angular velocity of the mesoscale eddies should be sufficiently large.

Different mechanism for amplification of the weak rotatory tornadogenesis thunderstorm supercell is the superposition of an average wind inside this supercell and the long tidal gravitational wave in the troposphere attacking the supercell.

This investigation is an evaluation of some basis ideas on the tornado mathematical modeling presented earlier in Arsen'yev (2011).

2. Long non-linear tide waves in troposphere

Kardashov et al. (2000) and Eppelbaum and Kardashov (2001) have shown that the majority of geological, geophysical and environmental processes in the Earth are characterized by nonlinear behavior. Let us consider the typical distribution of the temperature T in the Earth's troposphere (Figure 2).

A characteristic feature of the squall storms is the presence of clouds which have a thin inversion layer at the bottom boundary. Within this inversion, the temperature increases with altitude, but above and below this phenomenon the temperature decreases (Figure 2). An inversion arises at a condensation level, slightly above the bottom boundary of the clouds, because inside the cloud the temperature increases due to emission of the latent heat of vaporization (obviously, this process has a nonlinear character). It is essential that the inversion has disabling features which make it stable. The volume of air ascending from below the inversion is colder than the surrounding air and is pushed downward by the Archimedes forces. Similarly, warmer air, which enters the inversion from the top, is pushed upward. This allows us to simulate the inversion by a streamline $\zeta(x, y)$ surface. Here, horizontal wind velocities u and v may exist, and the vertical velocity w satisfies to the impermeability condition:

$$\text{when } z=\varsigma,\ w=\frac{\partial \varsigma}{\partial t}+u\frac{\partial \varsigma}{\partial x}+v\frac{\partial \varsigma}{\partial y}. \qquad (1)$$

In addition, the vertical turbulent stresses in the inversion must be continuous

$$\text{when } z=\varsigma,\ \Re_x^z=\Re_x^0, \Re_y^z=\Re_y^0. \qquad (2)$$

Here $\Re_x^z$ and $\Re_y^z$ are the turbulent tensions at the lower boundary layer of atmosphere (LBLA), $\Re_x^0$ and $\Re_y^0$ are the turbulent tensions at the lower boundary of the middle troposphere (MT), ζ is the disturbance level of the inversion surface, z-axis is directed downward from the unperturbed level of $z = 0$, Earth's surface (ES) is at the level of $z = H$ (Figure 2).

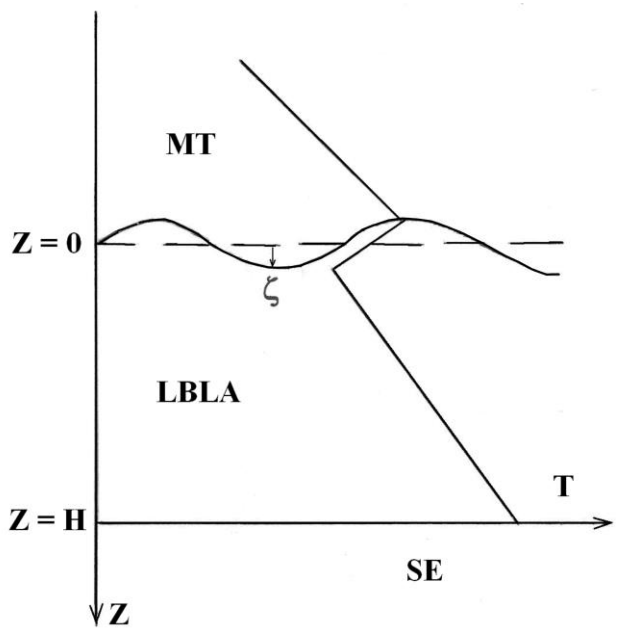


Figure 2. System of coordinates and temperature of air in the lower boundary layer of atmosphere (LBLA) and in the middle troposphere (MT). Position of the inversion layer is denoted by line ζ, letters SE designate the surface of the Earth (SE)

If the inversion in any area is destroyed by powerful movement upward, then condition (1) does not hold and the air gathers to the spots forming powerful thunderstorm *Cb* clouds (Snow, 1984). However, if the vertical motions are insufficient to break the inversion and condition (1) takes place, then and gravity waves arise on the inversion surface. The problem of studying these waves on the surface with different temperatures and velocities for the first time was set in the 19th century by Kelvin and Helmholtz (Lamb, 1945). The complete solution of this problem, which takes into account the compressibility of air and temperature variability, was obtained by D.L.Laikhman in 1947 (Khrgian, 1978). This solution describes internal waves in the troposphere. However, the fundamental mode, corresponding to gravity waves in the atmosphere with a uniform density, is omitted in this solution. This mode appears in the analysis of the Laplace tidal equations in atmosphere (Dikiy, 1969). It should be noted that a consideration of the movements in the lower atmospheric boundary layer associated with this mode is practically important. In present paper, this problem is solved for the long gravity waves, for which takes place the static condition

$$gp=\frac{\partial p}{\partial z}. \qquad (3)$$

For these waves the wavelength λ much greater than the thickness $H(\lambda \gg H)$. Thus, we use the theory of shallow water, which is created in geophysical hydrodynamics for analysis of long waves in particular tides (Gill, 1982; Pedlosky, 1992).

The density ρ and pressure of air p which are included in Eq. (3) change with the altitude. To determine these changes, we use the following equation

$$p = R_c \rho T, \tag{4}$$

where R_c = 287 м^2/с^2 and ^{0}K is the specific gas constant of the dry air.

The effects of humidity are not important in the LBLA at altitudes below the level of condensation, which practically coincides with the level of z = 0 (Figure 2). Since we are interested in the movement within the LBLA at $z \geq \zeta$, an influence of humidity can be neglected. Let us take the logarithm of Eq. (4) and take the derivative of the result with respect to z. We obtain

$$\frac{1}{p}\frac{dp}{dz} = \frac{1}{\rho}\frac{d\rho}{dz} + \frac{1}{T}\frac{dT}{dz}. \tag{5}$$

Substituting pressure p in Eq. (5) from Eq. (4) and the gradient dp/dz from Eq. (3), we find

$$\frac{g}{TR_C} = \frac{1}{\rho}\frac{d\rho}{dz} + \frac{1}{T}\frac{dT}{dz}.$$

Thus, we find the law defining the change of density with altitude

$$\frac{1}{\rho}\frac{d\rho}{dz} = \frac{1}{T}(\gamma_0 - \gamma), \tag{6}$$

where $\gamma = \frac{dT}{dz}$ and $\gamma_0 = \frac{g}{R_c} = 3.42 \cdot 10^{-2}$ °C/m is a constant. It is temperature gradient in a uniform density atmosphere, because on assumption $\gamma_0 = \gamma$, $\frac{\partial \rho}{\partial z} = 0$.

If $\gamma > \gamma_0$, then the air density increases with altitude since $d\rho/dz < 0$. This situation is practically rare. It may occur during intense heating of the LBLA in the day time in the summer and corresponds to an unstable state of atmosphere, because the heavy air is at the top, the light air is at the bottom, and $\gamma > \gamma_0 > \gamma_a$, where γ_a = 10^{-2} ^{0}C/m is the dry-adiabatic temperature gradient. Upon cooling of the lower atmospheric boundary layer in the stormy weather, we have the condition $\gamma \cong \gamma_0$, which corresponds to a uniform density atmosphere. The case $\gamma > \gamma_0$, where the air density decreases with altitude is the most frequent one (conventional) and is observed above the LBLA in the middle troposphere (*MT*). This corresponds to the stable stratification where heavy air is on the bottom (Arsen'yev, 2011). Thus, we will consider the case $\gamma \cong \gamma_0$, in which the stratification inside the LBLA is unstable ($\gamma_0 > \gamma_a$). This means that the air inside the LBLA is mixed by turbulent convection and turbulence generated by the vertical shear of the mean wind velocity.

The condition ρ = *const* allows us to vertically integrate Eq. (3) from $z = \zeta$ до z and to obtain the law of the air pressure changing *versus* height inside the LBLA

$$p = p_0 + g\rho(z - \zeta), \tag{7}$$

where p_0 is the pressure at the level of $z = \zeta$.

Let us direct the x-axis along the wind current at the lower boundary of the middle troposphere *MT* and denote the wind velocity at this boundary by the letter *W*. Strong winds within the middle troposphere *MT* tend to quadratic law of resistance in the inversion. That is, if $z = \zeta$

$$\Re_0^x = C_g W^2, \tag{8}$$

where C_g is the coefficient of a resistance.

In Eqs. (2) and (8) the tangential wind stress is divided by the air density (ρ = 1.3 kg/m^3). This means that we consider the kinematic (referred to the average density of air) tangential wind stress. Flows within the LBLA that emerge under the influence of the wind *W* are also directed along the x-axis, since we neglect the Coriolis force due to not large thickness of the LBLA. Therefore, cross currents along the y-axis are irrelevant, and we may write the equations of motion and continuity in the form of

$$\frac{\partial u}{\partial t} = -\frac{1}{\rho}\frac{\partial p}{\partial x} - \frac{\partial \Re_x^z}{\partial z} + A_L \frac{\partial^2 u}{\partial x^2}, \tag{9}$$

$$\frac{\partial u}{\partial z} + \frac{\partial w}{\partial z} = 0\ , \tag{10}$$

where A_L is the coefficient of the horizontal shear turbulent viscosity.

Eqs. (9) and (10) contain the turbulent tensions and vertical velocities w inside the LBLA. We can eliminate these factors by the vertical integration from $z = \zeta$ to $z = H$. As a result, Eq. (10) will have the following form:

$$\frac{\partial \zeta}{\partial t} = \frac{\partial S}{\partial x}, \tag{11}$$

where $S = \int_\zeta^H u dz$ is the total vertical flow.

In deriving Eq. (11) we take into account the boundary conditions (1), (2) and condition at the Earth's surface *ES*

$$\text{when } z = H, \qquad u = w = 0. \tag{12}$$

It is easy to exclude the pressure p from Eq. (9) using the law (7)

$$\frac{1}{\rho}\frac{\partial p}{\partial x} = \frac{1}{\rho}\frac{\partial p^0}{\partial x} - g\frac{\partial \varsigma}{\partial x}. \tag{13}$$

It is convenient to present the level of inversion ζ as the sum of the statical ζ_s and the dynamical ζ_d components: $\zeta = \zeta_s + \zeta_d$. Then, if the statical tilts of the inversion level are balanced by pressure gradients on the inversion

$$\frac{1}{\rho}\frac{\partial p_0}{\partial x} = g\frac{\partial \varsigma_S}{\partial x},$$

then Eq. (13) may be written as

$$\frac{1}{\rho}\frac{\partial p}{\partial x} = -g\frac{\partial \varsigma_d}{\partial x}. \tag{14}$$

Substituting Eq. (14) into Eq. (9) and omitting the index d (hereinafter we consider only the dynamics tilts of the level ζ_d) we find

$$\frac{\partial u}{\partial t} = g\frac{\partial \varsigma}{\partial x} - \frac{\partial \Re_x^z}{\partial z} + A_L\frac{\partial^2 u}{\partial x^2}. \tag{15}$$

Let us integrate Eq. (15) by z in the *LBLA*. We obtain

$$\frac{\partial S}{\partial t} = gH\frac{\partial \varsigma}{\partial x} - \Re_x^H + \Re_x^0 + A_L\frac{\partial^2 S}{\partial x^2}. \tag{16}$$

A system of Eqs. (16) and (11) is closed one with regard to the unknown parameters S and ζ, if the turbulent stresses are known on the upper and lower boundaries of the LBLA or their relationship with S or ζ.

3. Problem solution

Let us find the solution of Eqs. (11) and (16) in the form of a progressive wave traveling with velocity V: $S = F(x - Vt)$. Then Eq. (11) gives the algebraic relationship between S and ζ. Denoting $\chi = x - Vt$, we get (index χ with F denotes derivative by χ)

$$\frac{\partial S}{\partial x} = F_\chi;\ \frac{\partial S}{\partial t} = -V F_\chi;\ \frac{\partial \varsigma}{\partial t} = \frac{\partial S}{\partial x} = F_\chi = -\frac{1}{V}\frac{\partial S}{\partial t} = -\frac{\partial}{\partial t}\left(\frac{S}{V}\right).$$

Integrating over time t, we obtain

$$S = -\zeta V, \tag{17}$$

because the integration constant is equal to zero (when $S = 0$ and $\zeta = 0$). Eq. (17) allows us to eliminate the level ζ from Eq. (16):

$$\frac{\partial S}{\partial t} = -\left(\frac{gH}{V}\right)\frac{\partial S}{\partial x} - \Re_x^H + \Re_x^0 + A_L\frac{\partial^2 S}{\partial x^2}. \tag{18}$$

For the friction stress at the lower boundary of the LBLA, we may use the law that is well known in the theory of long waves (Gill, 1988; Arsen'yev, 1989)

$$\Re_x^H = \omega_f S. \tag{19}$$

Here ω_f is the frequency of friction which may be estimated with the help of following formula (Arsen'yev, 1989)

$$\omega_f = \frac{3A}{H^2(1-n)^2}, \tag{20}$$

where $n = z_0/H$, z_0 is the height of the roughness on the Earth's surface and A is the coefficient of the vertical shear turbulent viscosity. On the other hand, the frictional stress at the upper boundary of LBLA is determined by Eq. (8). In this formula, the following relation may connect the wind velocity W at the lower boundary MT with the wind velocity at the upper boundary u^0 of the LBLA

$$u^0 = kW, \tag{21}$$

where k is the wind coefficient. If the jump on a passage of the wind velocity through the inversion is absent, then $k = 1$. Otherwise, $0 < k < 1$, because the wind velocity decreases with the altitude decreasing.

The total flow S may be expresses through the wind velocity u^0, if we use the shallow water theory, which well describes long waves (Gill, 1982; Pedlosky, 1992). In this theory all parts of long wave are moving with the same velocity $u^0 = u$, except for a thin near-ground atmospheric boundary layer with a thickness approximately 10 m, where the wind velocity decreases rapidly to zero. In this case the friction is concentrated near the level $z = H$ and the relation (19) has a place. For the model of long wave $S = uH$, and Eq. (8) may be written in the following form

$$\Re_x^0 = \left(\frac{C_g}{k^2H^2}\right)S^2. \tag{22}$$

Substituting Eqs. (22) and (19) to Eq. (18) we obtain an equation for the parameter S

$$\frac{\partial S}{\partial t} = -\left(\frac{g H}{V}\right)\frac{\partial S}{\partial x} - \omega_f S + \alpha S^2 + A_L \frac{\partial^2 S}{\partial x^2}, \quad (23)$$

where $\alpha = \frac{C_g}{k^2 H^2}$.

At the same time, we should underline that we find a solution in the form of progressing wave $S = F(\chi)$.

Then $\frac{\partial S}{\partial t} = VF_\chi$, $\frac{\partial S}{\partial x} = F_\chi$, $\frac{\partial^2 S}{\partial x^2} = F_{\chi\chi}$, and Eq. (23) takes the form

$$A_L F_{\chi\chi} + \alpha F^2 - \omega_f F + V\left(1 - \frac{gH}{V^2}\right)F_\chi = 0. \quad (24)$$

The studied tidal gravitational waves propagate with the Lagrange velocity $V = (gH)^{1/2}$. Hence Eq. (24) may be transformed as

$$A_L F_{\chi\chi} + \alpha F^2 - \omega_f F = 0. \quad (25)$$

Eq. (25) is easy to solve by F_χ multiplication. In this case

$$\frac{A_L}{2}\frac{d}{d\chi}\left[\left(\frac{dF}{d\chi}\right)^2\right] + \frac{\alpha}{3}\frac{dF^3}{d\chi} - \frac{\omega_f}{2}\frac{dF^2}{d\chi} = 0. \quad (26)$$

From here, by integrating, we find

$$\left(\sqrt{\frac{3A_L}{2\alpha}}\right)F_\chi = F\sqrt{\beta - F}, \quad (27)$$

where $\beta = \frac{3}{2}\frac{w_f}{\alpha}$. The constant of integration is equal to zero, because $F \to 0$, $F_\chi \to 0$ if $\chi \to \infty$.

In Eq. (27) variables are separated

$$\frac{dF}{F\sqrt{\beta - F}} = d\chi\sqrt{\frac{2\alpha}{3A_L}}.$$

Hence, again integrating, we obtain

$$-\frac{2}{\sqrt{\beta}}arcth\left(\sqrt{\frac{\beta - F}{\beta}}\right) = \chi\sqrt{\frac{2\alpha}{3A_L}}$$

or

$$\sqrt{\frac{\beta - F}{\beta}} = -th\left(\chi\sqrt{\frac{\alpha\beta}{6A_L}}\right). \quad (28)$$

The identity $\tanh^2 x \equiv 1 - \operatorname{sech}^2 x$ is true. Consequently,

$$\frac{\beta - F}{\beta} = 1 - \operatorname{sech}^2\chi\sqrt{\frac{\beta\alpha}{6A_L}}.$$

Thus,

$$S = F = \beta\operatorname{sech}^2\left(\frac{\chi}{\Delta}\right), \quad (29)$$

$$u = \left(\frac{\beta}{H}\right)\operatorname{sech}^2\left(\frac{\chi}{\Delta}\right), \quad (30)$$

$$\zeta = \left[\frac{\beta}{(gH)^{1/2}}\right] = \beta\operatorname{sech}^2\left(\frac{\chi}{\Delta}\right). \quad (31)$$

Here

$$\Delta = \sqrt{\frac{4A_L}{\omega_f}} = H(1-n)\sqrt{\frac{4A_L}{3A}}. \quad (32)$$

is the wide of solitons (29) – (32).

It should be noted that importance of applications of such mathematical models as solitons in the applied and environmental geophysics was underlined in Kardashov et al. (2000).

Using solutions (7) and (31), we find changes in pressure in the LBLA

$$p = p^0 + g\rho z - g\rho\frac{\beta}{\sqrt{gH}}\operatorname{sech}^2\left(\frac{\chi}{\Delta}\right). \quad (33)$$

In particular, at the Earth's surface, when $z = H$

$$p = p^0 + g\rho H - g\rho\frac{\beta}{\sqrt{gH}}\operatorname{sech}^2\left(\frac{\chi}{\Delta}\right). \quad (34)$$

From Eqs. (30) and (34) is evident that during pass of the solitary tide wave, the pressure decreases but the wind velocity increases. Duration of the solitary tide wave may be estimated by the following formula

$$t_* = \frac{\Delta}{V} = \sqrt{\frac{4A_L}{g\omega_f H}}. \quad (35)$$

As example, Figures 3 and 4 show calculation of oscillations of the surface pressure and the wind velocity with utilization of the following parameters: $C_g = 10^{-2}$, $k = 0.7$, $H = 980$ m, $p_0 = 888.4$ GPa, $g = 9.8$ m/s^2, $\rho = 1.3$ kg / m^3, $z_0 = 0.05$ m (grass, rye), $A = 129.7$ m^2 / s, $A_L = 2.16\cdot10^6$ m^2/s. In this case $\Delta = 147\cdot10^3$ m, $\beta = 30380$ m^2/s, $\alpha = 2.08\cdot10^{-8}$. From Figures 4 and 5 we see that the maximal wind velocity reaches 31 m/s, and time of its passage (see Eq. (35)) is 25 minutes. The minimal pressure is equal to 973.76 GPa, and the width of the soliton is 147 km, i.e. the solitary tide wave is the mesoscale atmospheric phenomenon that occurs during hurricane winds in the middle troposphere. In this case the maximum value of W is 44.3 m/s.

The obtained solution describes a squall storms which are observed in the natural conditions. According to (Nalivkin, 1969; Khromov and Mamon-

tova, 1974), a squall storm is short-term and strong increase in the average wind velocity without rotation in the areas of heavy storms or fast cyclones, with cloud and rain. Squall storms lead to sea disasters. For example, in March 1878, the British frigate "*Eurydice*" was overturned by a squall storm and almost immediately went down along with its crew. The same accident has occurred with the Russian linear ship *"Mermaid"* on September 19, 1893, in the Baltic Sea, 178 seamen were lost. On the land, the squall storms may destroy lightweight buildings and cause a windfall in the woods. For example, at region of Upper Volga River (nearby of the Lake *Seliger*, Russia) on July 29, 2017, a squall storm with the wind velocity up to 35 m/s and duration of 20 minutes has caused the significant damage to farms. Trees were uprooted and roofs were blown away, fences were torn down, and panes of windows were broken. In San Francisco on November 21, 1910, a squall storm has attacked the fortified town houses. They remained standing but experienced a strong tremor. The duration of the storm was only 2 min, but the wind velocity reached 100 km/h. Nalivkin (1969, p.148) notes that it was: «As if a huge, long, and narrow air wave flew over the city».

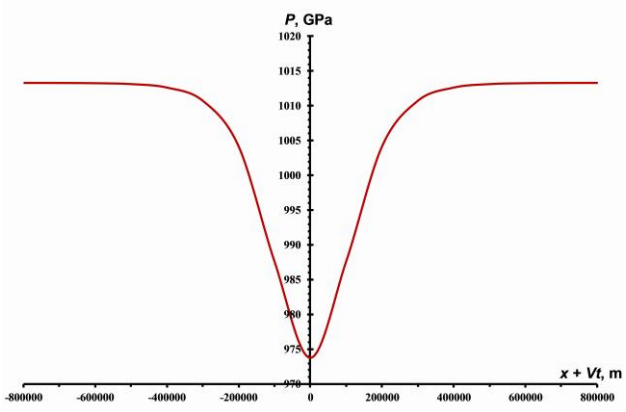


Figure 3. Calculation of the pressure at the ground *P* during the time of the squall storm. Minimal and maximal registered pressures were 973.756, and 1013.25 GPa, respectively. Anomalous pressure difference was 34.49 GPa

Figure 5 shows an example of a real squall storm. We see as on the background of weak southwest wind a strong solitary perturbation appears in the form of the north-west wind with a maximum wind velocity of 31 m/s. The wind soliton is very narrow, but during 10 min the wind velocity increases from 3 to 31 m/s, and then during 15 min decreases to 2 m/s. The total lifetime of this storm was t = 25 min. There was no air rotation that is typical for the whirlwinds and tornadoes. The calculated theoretical values of the maximal wind velocity and time of existence of the solitary tidal wave, excited by a gale-force wind in the middle and top troposphere, coincide with supervision. Thus, the theory explains process of the squall storms formation and gives us the method for calculation of this phenomenon.

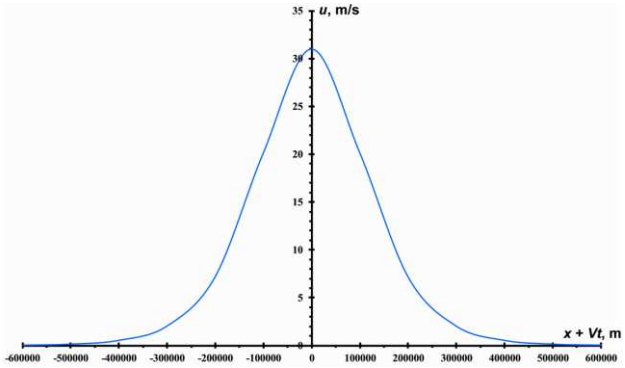


Figure 4. Calculation of the wind velocity at the ground on passage of the squall storm. The maximal wind velocity was 31 m/s

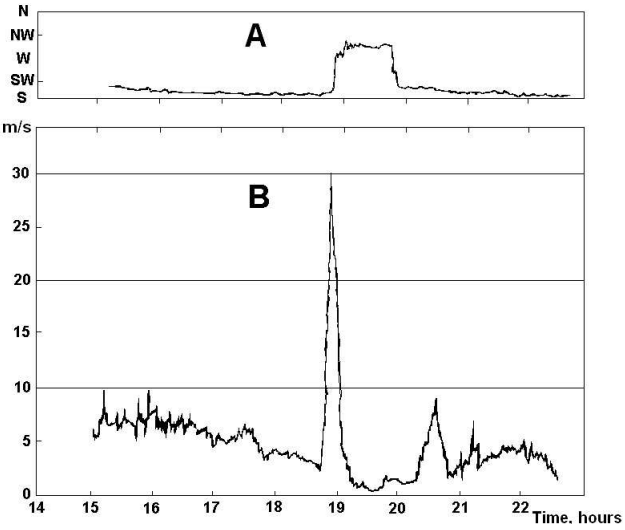


Figure 5. Observations of the wind direction (A) and wind velocity (B) during the time of the squall storm (Nalivkin, 1969, Fig. 80). The maximal wind velocity was 31 m/s

4. Tornado appearing

Squall storms propagate on the subcloud inversion layer. However, such inversions do not exist always. For instance, large vertical velocity caused by intensive updrafts on a cold atmospheric front, destroy theirs. But the vertical airflows generate the thunderclouds *Cb* (Snow, 1984; Arsen'yev et al., 2010; Laing, 2015). If the several slight thunderstorms are amalgamating, then one large supercell arises which may generate a tornado. Snow (1984) mentioned that this effect does not happen in 40% of all cases. However, in other cases, tornado arises inside a supercell and rapidly propagates down to the Earth's surface (e.g., Wurman et al., 2012).

Process of tornado appearance can be presented as capture of a squall storm by the thundery supercell. Running on a surface of inversion, the squall storm falls into supercell where this inversion is destroyed. And the long wave of a squall storm remains inside a supercell because inversion here is absent. Thus, a squall storm soliton should be captured by the supercell with further adaptation of air pressure and wind velocity to each other. This mutual adaptation of the meteorological fields also results in appearance of tornado in which the wind velocity and the gradient of air pressure can reach greatest values.

Usually, the thundery supercell is weakly-rotating due to, e.g., the shear eddy instability (Arsen'yev et al., 2000, 2010). Air rotation inside a supercell is described by the cyclostrophic balance

$$\frac{\partial p}{\partial x}=\rho\frac{v^2}{r}, \qquad (36)$$

where r is the radial coordinate oriented outside from the rotation center.

Capture of a storm by the thundery supercell results in pressure drop within a supercell that causes amplification of the wind rotation and produces of tornado. To find the wind velocity in tornado development, it is necessary to change χ in Eq. (34) to r, then to differentiate Eq. (34) with respect to r, and substitute the result into Eq. (36). Resolving the resulting equation with respect to the azimuthal velocity v, we derive the formula for the wind velocity in a developing tornado

$$v=\mathrm{sec}h\left(\frac{r}{\Delta}\right)\sqrt{\frac{2g\beta r}{V\Delta}th\left(\frac{r}{\Delta}\right)}. \qquad (37)$$

The surface air pressure inside the tornado is defined by the functional relation in Eq. (34).

5. The proposed theory verification

Physical-environmental model of tornado may be presented as a strongly rotating air column that originated in a cumulo-nimbus thundercloud and reaches the Earth's surface (Doswell and Burgess, 1993; Arsen'yev et al., 2010; Markowski and Richardson, 2014). Hurricane winds, which are typical for tornado cause serious damages. Therefore, moving tornado usually contains many different fragments of buildings, cars, trees, clods of spoil, water, and dust. This creates essential difficulties with the measurements of the physical quantities. Bluestein (1999) described the basic methods for the field study of tornadoes in the United States. He suggested that the remote metrology of wind velocity and direction with the Doppler radars (including those mounted on cars) is the most effective methodology. Another method is measurements of the wind velocity and wind direction, air temperature and pressure, humidity and electromagnetic fields with the help of self-contained portable equipment complexes mounted in the expected trajectories of the tornadoes. Figure 6 shows the air pressure measured inside a tornado on July 8, 1995 near Allison town (Texas) by scientists from the Langmuir's Laboratory at New Mexico, USA (Winn et al., 1999). The measurements were carried out with the use of a small device called a "tortoise" which was buried on the way of the tornado. It can be seen from Figure 2 that the air pressure is strongly fluctuated near the earth's surface inside a tornado, especially near the center. It can relate to many meso-eddies inside tornado (Arsen'yev et al., 2010). Nevertheless, the pressure monotonously decreases to the tornado's center after averaging these fluctuations (see squares in Figure 7). The maximal drop of the air pressure in the tornado is not large, about 50 hectoPascal. However, in according to Eq. (36), the wind velocity inside tornado is determined by the radial gradients of the pressure (but not by the pressure itself). Thus, sharp spatial variations of the air pressure inside tornado can induce a strong wind.

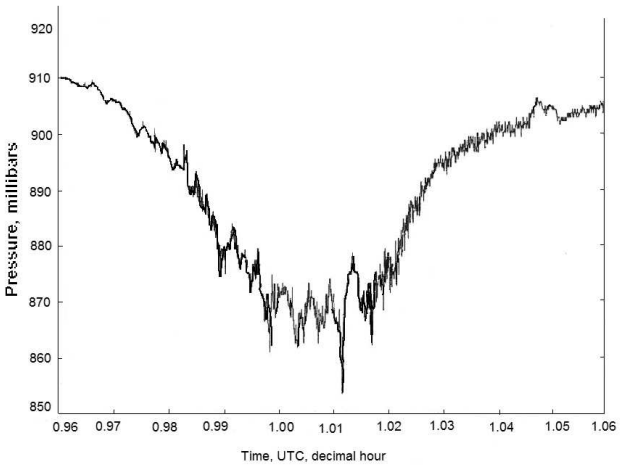


Figure 6. Metering data of the air pressure in a large tornado (after Winn et al., 1999)

The solid curve in Figure 7 shows the air pressure calculated by Eq. (34) with following parameters: H = 980 m, g = 9.8 m/s^2, V = 98 m/s, p_0 = 785.15 hectoPascal; ρ = 1.3 kg/m^3, A = 1.7 m/s^2, A_L = 67.3 m/s^2, C_g = 0.02, k =1, z_0 = 0.05 m (grass, rye). The values of β and Δ are equal to 384.6 m^2/s and 7101.8 m, respectively. For convenience, we introduce the evaluation time $t = T_* - 3636$ seconds, where T_* is the current measured time in sec shown in Figure 6. Thus, the origin of the coordinates is shifted to the point T_* = 3636 seconds = 1.01 hour along the time axis, and the image shown in

Figure 7 is symmetrical relative to this origin. The coincidence of the theoretical curve with the measurements results (Figure 7) confirms our theory.

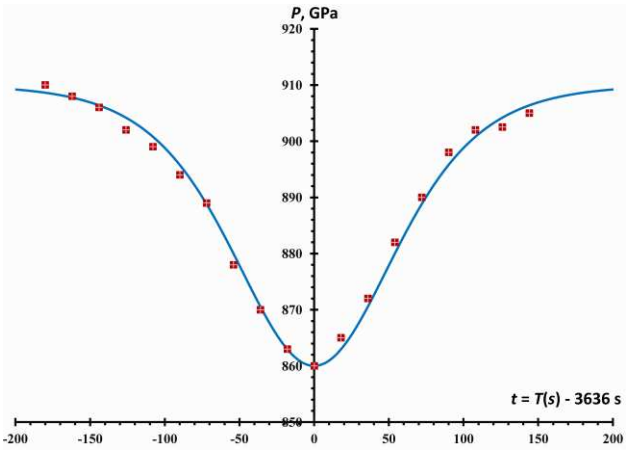


Figure 7. Theoretical computation of the air pressure in a large tornado are presented by blue solid curve. Small red squares show the averaged pressure corresponding to the observations drawn in Figure 5

To verify Eq. (37) we use the data of the Doppler radar measurements of wind velocity inside a tornado (Wurman and Gill, 2000). These data are shown in Figure 8 by squares. The solid curve in Figure 8 shows the theoretical calculations using Eq. (37) with the following parameters: H = 980 m, g = 9.8 m/s^2, A = 300 m/s^2, A_L = 3.96 m/s^2, C_g = 0.02, k = 1, z_0 = 0.05 m; hence β = 67,500 m^2/s and Δ = 130 m. An agreement of the theoretical calculations with measurements turned out to be worse in this case than for the air pressure calculation. Additional secondary maxima on the curve of measured wind velocity are seen in Figure 4 (at $r \approx$ 300m, $r \approx$ 650 m, $r \approx$ 780 m, $r \approx$ -500 m, and $r \approx$ -780 m). They are evidently connected with the large mesoscale turbulent eddies that fill the tornado. Thus, the tornado was measured at a time close to the moment of its origin, and therefore turned out to be multi-eddy. Due to this fact, the wind velocity abates much more slowly when moving away from the tornado center than it is predicted from the theory.

As is shown in (Arsen'yev et al., 2010), the mesoscale eddies inside tornado can transfer the energy to the average flow and, consequently, they decrease in size, kinetic energy, and angular momentum with a time. Therefore, we calculated the wind velocity for one more, a large powerful tornado that is close to the mature stage. The circles in Figure 9 show wind velocity measured with a Doppler radar at the height of 100 m in the F5-class tornado (Monastersky, 1999; Burgess et al., 2002). This violent tornado attacked Oklahoma City (USA) on May 3, 1999, damaged more than 4000 houses and 47 business buildings, 48 people died, many people received wounds of varying severities. According to Monastersky (1999), the maximum wind velocity was 144 m/s (512 km/h or 318 ml/h). Figure 9 also shows the 10% relative error. This is unavoidable, because the measurements were carried out in uncontrollable field conditions. Figure 9 shows also the theoretical curve calculated with application of Eq. (37) under following values of parameters: t = 0, $\chi = r$, H = 980 m, g = 9.8 m/s^2, A = 355, 55 m/s^2, A_L = 19,591.84 m/s^2, C_g = 0.02, k =1, z_0 = 0.05 m, so that β = 80,000 m^2/s and Δ = 8,400 m. Figure 9 indicates that the theoretical calculations and field measurements coincide within 10% accuracy.

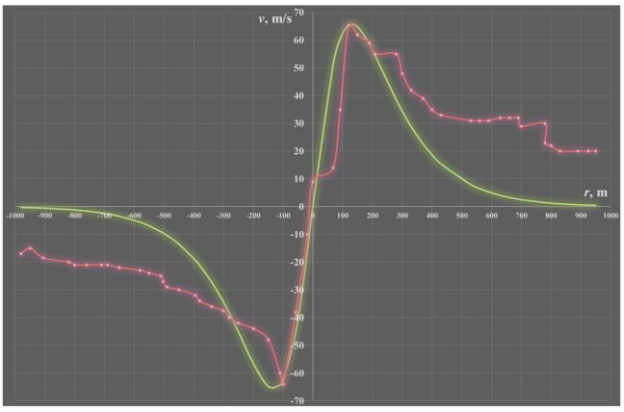


Figure 8. Comparison of the theoretical computation of the angular wind velocity v in tornado (green solid curve) and physical observations of the wind velocity in tornado (red curve with white points) (last curve after Wurman and Gill, 2000)

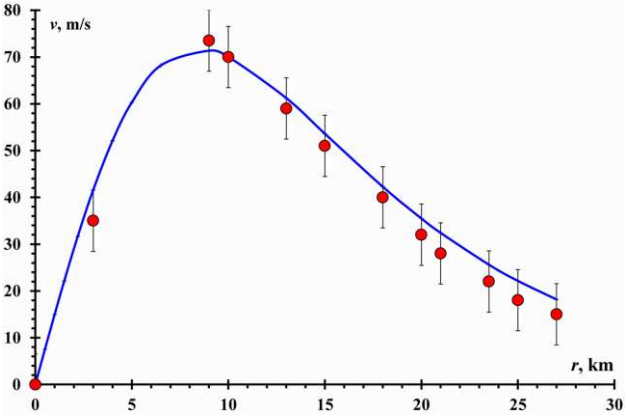


Figure 9. Comparison of theoretical computation of the angular wind velocity v in tornado (blue solid line) with observations in EF5 tornado on 03 May 1999 (red circles)

6. Analysis of obtained results and brief discussion

A good compliance between the theoretical and measurement data indicates the applicability of Eqs. (34)-(37) for calculation of the real tornadoes. Besides the surface air pressure and wind velocity, there are other important parameters. Figure 10 demonstrates the radial distribution of vorticity in

the F5 tornado, which corresponds to Figure 9. The calculations were done using the following expression

$$\Omega = \mathrm{rot}_z\, v = \frac{\partial v}{\partial r} + \frac{v}{r}\ , \qquad (38)$$

Here v is determined by Eq. (37).

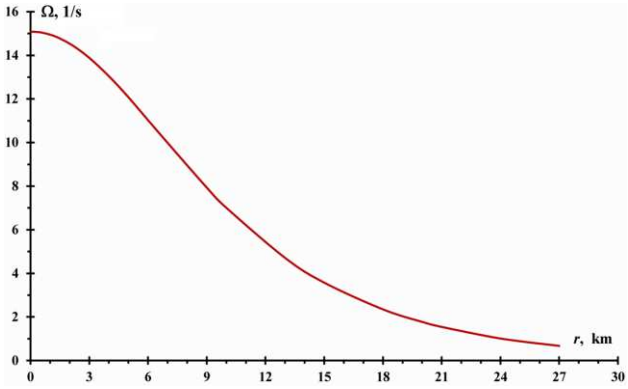


Figure 10. The radial distribution of a vorticity for the violent tornado EF5 (see Figure 8)

As it is clearly seen from Figure 10, the vorticity is maximal in the tornado center; for an EF5 tornado, it attains to a very high value of 15 Hz. For comparison, we must note that in tropical hurricanes and typhoons $\Omega \approx 10^{-3}$ Hz (Arsen'yev et al., 2010).

Figure 11 shows the eddy force calculated for the EF5 tornado

$$F_E = [v \times \mathrm{rot}\, v] = v\Omega = \frac{\partial}{\partial r}\left(\frac{v^2}{2}\right) + \frac{v^2}{r}. \qquad (39)$$

This is a sum of the dynamical thrust and the centrifugal force, which is associated with a pressure by Eq. (36)

$$F_E = \frac{\partial}{\partial r}\left(\frac{v^2}{2} + \frac{p}{\rho}\right). \qquad (40)$$

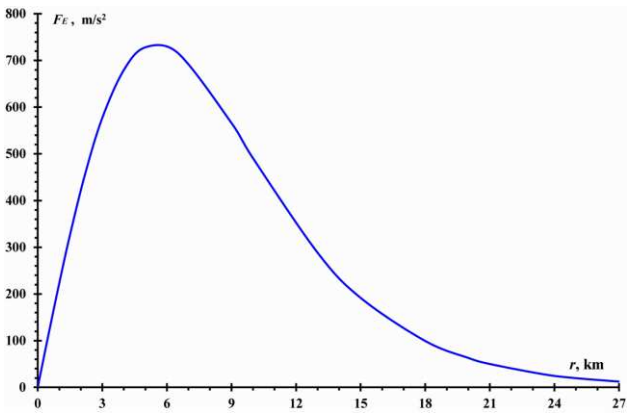


Figure 11. Computation of the vortex force for the violent tornado (Figure 8) realized by Eq. (40)

The eddy force enters into the Gromeka-Lamb vectorial equation

$$\frac{\partial v}{\partial t} + grad\left(\frac{v^2}{2}\right) - [v \times rot\, v] = -\frac{1}{\rho} grad\ p + \eta \Delta v, \qquad (41)$$

which follow from the Naiver-Stokes equation (Lamb, 1945; Vasil'yev, 1958).

If the eddy force is absent (F_E = 0), then Eq. (39) implies the equation

$$\frac{dv}{v} = -\frac{dr}{r}. \qquad (42)$$

This solution is the law of hyperbolic wind-velocity abatement $v = v_0 \frac{r_0}{r}$, which corresponds to the Ranque eddy in an ideal fluid without friction (Vasil'yev, 1958; Saffman, 2000). We can see from Figure 11 that $F_E \neq 0$, i.e., the Ranque eddy does not occur in our case, because the air motion in tornado passes under the presence of turbulent friction. The maximum value of $F_{E\text{-}max}$ = 740 m/s^2 is attainable at the inner boundary of the "wall of the hurricane". Multiplying $F_{E\text{-}max}$ by ρ = 1.3 kg/m^3 we find $\Phi \approx 962$ n/m^3. On the house with a volume 10^3 m^3 tornado acts with a force $962 \cdot 10^3$ n. This force is equal to weight of a mass 98 metric tons. To reduce this wind force building(s) should have the streamline aerodynamic form. Damage to buildings could be totally avoided if the buildings were located underground.

It is necessary to underline that the presented methodology may be flexibly modified for investigation of other atmospheric and solid Earth phenomena.

Conclusions

In this work, a novel physical-mathematical model of creating the violent tornadoes in troposphere (as result of the tidal gravity wave influence), has been developed. In the years of increasing gravity activity within the Earth-Moon-Sun system, is necessary to expect an increment of number and intensity of the squall storms which represent strong tidal nonlinear waves in troposphere. Therefore, at that time an increased number of the violent tornadoes should be observed. The present investigation enabled to establish an analytical connection between the numbers of tornadoes per year with the tidal forces, which was found earlier as result of statistical analysis of the observed data. It should be noted that this approach may be effectively applied to studying other environmental effects associated with the Moon-Sun activity.

REFERENCES

Alizadeh A.A., Guliyev I.S., Kadirov F.A., Eppelbaum L.V. Geosciences in Azerbaijan. V. II – Economic minerals and applied geophysics. Springer. Heidelberg – N.Y., 2017, 340 p.

Arsen'yev S.A. Dynamics of shelf water. Moscow State University. Moscow, 1989, 96 p. (in Russian).

Arsen'yev S.A. Irregular Earth's rotation and dynamics of the gas-liquid geospheres. Doklady of the Russian Academy of Sciences, V. 343, № 2, 1995, pp. 251-254.

Arsen'yev S.A. About origin of the synoptic variability in ocean. Moscow University Physics Bulletin, V. 39, № 6 (Alerton Press, Inc., USA), 1998, pp. 40-44.

Arsen'yev S.A. Mathematical modeling of tornadoes and squall storms. Geosciences Frontiers, V. 2, № 2, 2011, pp. 215-221.

Arsen'yev S.A., Nikolaevskiy V.N., Shelkovnikov N.K. Eddy instability and initiation of tornado. Moscow University Physics Bulletin, V. 41, № 1 (Alerton Press, Inc., USA), 2000, p. 50-54.

Arsen'yev S.A., Nikolaevskiy V.N. Modelling of tornadoes by turbulence theory with Eddy Angular Momentum. Trans. of the SIAM Conference on Mathematical and Computational Sciences. Issue in the Geosci. Boulder, CO USA, 2001, p. 13.

Arsen'yev S.A., Gubar A.Yu., Nikolaevskiy V.N. Self-organization of tornado and hurricanes in atmospheric currents with mesoscale eddies. Doklady of the Russian Academy of Sciences, V. 396, № 4, 2004, pp. 588-593.

Arsen'yev S.A., Babkin V.A., Gubar A.Yu., Nikolaevskiy V.N. Theory of mesoscale turbulence. Eddies of atmosphere and ocean. Inst. of Computer Sciences, Regular and Chaotic Dynamics. Moscow-Izhevsk, 2010, pp. 365-371 (in Russian).

Bluestein H.B. A history of severe-storm-intercept field programs. Weather and Forecasting, V. 14, 1999, pp. 558-577.

Belyakov A.S., Lavrov A.S., Nikolaev A.V. Seismoacoustic emission, earthquakes, and Lunar-Solar tides. Doklady Earth Sciences (Springer), V. 420, № 4, 2008, pp. 670-671.

Burgess D.W., Magsig M.A., Wurman J., Dowell D.C., Richardson Y. Radar observations of the 3 May 1999 Oklahoma City Tornado. Weather and Forecasting, V. 17, 2002, pp. 456-471.

Chizevsky A.L. The Earth echo of the Sun's storms. Mysl' Publ. Moscow, 1976, 367 p. (in Russian).

De Jager C. Structure and dynamics of the solar atmosphere. Springer-Verlag. Berlin- Gottingen-Heidelberg, 1959, 362 p.

Doswell C.A., Burgess D.W. Tornadoes and tornadic storms: A review of conceptual models. In: The Tornado: Its Structure, Dynamics, Prediction, and Hazards. Geophys. Monogr. V. 79, Amer. Geophys. Union, 1993, pp. 161-172.

Dikiy L.A. The theory of oscillations of the Earth's atmosphere. Gidrometeoizdat. Leningrad, 1969, 196 p. (in Russian).

Drton M., Marzban C., Guttorp P., Schaefer J.T. A Markov chain model of tornadic activity. American Meteorological Society, V. 131, № 12, 2003, pp. 2941-2953.

Eppelbaum L.V. Non-stochastic long-term prediction model for US tornado level. Natural Hazards, V. 69, 2013, pp. 2269-2278.

Eppelbaum L.V. Potential geophysical fields: geological and environmental applications. Elsevier. Amsterdam, 2019, 551 p.

Eppelbaum L., Isakov A. Implementation of the geo-correlation methodology for predictability of catastrophic weather events: long-term US tornado season and short-term hurricanes. Environmental Earth Sciences, V. 74, 2015, pp. 3371-3383.

Eppelbaum L.V., Kardashov V.R. Analysis of strongly nonlinear processes in geophysics. In: Proceed. of the Chapman Conference on Exploration Geodynamics. Moresi, L. and Müller, D. (eds.). Dunsborough, Western Australia, 2001, pp. 43-44.

Garner J.M. Environments of significant tornadoes occurring within the warm sector versus those occurring along surface baroclinic boundaries. Electronic Jour. of Severe Storms Meteor., V. 7, № 5, 2012, pp. 1-28.

Gill A.E. Atmosphere-ocean dynamics. Academic Press. N.Y. – London, 1982, 644 p.

Gray L.J., Beer J., Geller M., Haigh J.D., Lockwood M., Matthes K., Cubasch U., Fleitmann D., Harrison G., Hood L., Luterbacher J., Meehl G.A., Shindell D., van Geel B., White W. Solar influences on climate. Review of Geophys-

ЛИТЕРАТУРА

Alizadeh A.M., Guliyev I.S., Kadirov F.A., Eppelbaum L.V. Geosciences in Azerbaijan. V. II – Economic minerals and applied geophysics. Springer. Heidelberg – N.Y., 2017, 340 p.

Arsen'yev S.A. Irregular Earth's rotation and dynamics of the gas-liquid geospheres. Doklady of the Russian Academy of Sciences, V. 343, № 2, 1995, pp. 251-254.

Arsen'yev S.A. About origin of the synoptic variability in ocean. Moscow University Physics Bulletin, V. 39, № 6 (Alerton Press, Inc., USA), 1998, pp. 40-44.

Arsen'yev S.A. Mathematical modeling of tornadoes and squall storms. Geosciences Frontiers, V. 2, № 2, 2011, pp. 215-221.

Arsen'yev S.A., Nikolaevskiy V.N., Shelkovnikov N.K. Eddy instability and initiation of tornado. Moscow University Physics Bulletin, V. 41, № 1 (Alerton Press, Inc., USA), 2000, p. 50-54.

Arsen'yev S.A., Nikolaevskiy V.N. Modelling of tornadoes by turbulence theory with Eddy Angular Momentum. Trans. of the SIAM Conference on Mathematical and Computational Sciences. Issue in the Geosci. Boulder, CO USA, 2001, p. 13.

Arsen'yev S.A., Gubar A.Yu., Nikolaevskiy V.N. Self-organization of tornado and hurricanes in atmospheric currents with mesoscale eddies. Doklady of the Russian Academy of Sciences, V. 396, № 4, 2004, pp. 588-593.

Bluestein H.B. A history of severe-storm-intercept field programs. Weather and Forecasting, V. 14, 1999, pp. 558-577.

Belyakov A.S., Lavrov A.S., Nikolaev A.V. Seismoacoustic emission, earthquakes, and Lunar-Solar tides. Doklady Earth Sciences (Springer), V. 420, № 4, 2008, pp. 670-671.

Burgess D.W., Magsig M.A., Wurman J., Dowell D.C., Richardson Y. Radar observations of the 3 May 1999 Oklahoma City Tornado. Weather and Forecasting, V. 17, 2002, pp. 456-471.

De Jager C. Structure and dynamics of the solar atmosphere. Springer-Verlag. Berlin- Gottingen-Heidelberg, 1959, 362 p.

Doswell C.A., Burgess D.W. Tornadoes and tornadic storms: A review of conceptual models. In: The Tornado: Its Structure, Dynamics, Prediction, and Hazards. Geophys. Monogr. V. 79, Amer. Geophys. Union, 1993, pp. 161-172.

Drton M., Marzban C., Guttorp P., Schaefer J.T. A Markov chain model of tornadic activity. American Meteorological Society, V. 131, № 12, 2003, pp. 2941-2953.

Eppelbaum L.V. Non-stochastic long-term prediction model for US tornado level. Natural Hazards, V. 69, 2013, pp. 2269-2278.

Eppelbaum L.V. Potential geophysical fields: geological and environmental applications. Elsevier. Amsterdam, 2019, 551 p.

Eppelbaum L., Isakov A. Implementation of the geo-correlation methodology for predictability of catastrophic weather events: long-term US tornado season and short-term hurricanes. Environmental Earth Sciences, V. 74, 2015, pp. 3371-3383.

Eppelbaum L.V., Kardashov V.R. Analysis of strongly nonlinear processes in geophysics. In: Proceed. of the Chapman Conference on Exploration Geodynamics. Moresi, L. and Müller, D. (eds.). Dunsborough, Western Australia, 2001, pp. 43-44.

Garner J.M. Environments of significant tornadoes occurring within the warm sector versus those occurring along surface baroclinic boundaries. Electronic Jour. of Severe Storms Meteor., V. 7, № 5, 2012, pp. 1-28.

Gill A.E. Atmosphere-ocean dynamics. Academic Press. N.Y. – London, 1982, 644 p.

Gray L.J., Beer J., Geller M., Haigh J.D., Lockwood M., Matthes K., Cubasch U., Fleitmann D., Harrison G., Hood L., Luterbacher J., Meehl G.A., Shindell D., van Geel B., White W. Solar influences on climate. Review of Geophys-

ler, D. (eds.). Dunsborough, Western Australia, 2001, pp. 43-44.
Gadirov V.G. Natural alterations in oil output. Facts and hypotheses. Geophysics: News in Azerbaijan, № 3, 2001, pp. 21-24 (in Azerbaijani).
Garner J.M. Environments of significant tornadoes occurring within the warm sector versus those occurring along surface baroclinic boundaries. Electronic Jour. of Severe Storms Meteor., V. 7, № 5, 2012, pp. 1-28.
Gill A.E. Atmosphere-ocean dynamics. Academic Press. N.Y. – London, 1982, 644 p.
Gray L.J., Beer J., Geller M., Haigh J.D., Lockwood M., Matthes K., Cubasch U., Fleitmann D., Harrison G., Hood L., Luterbacher J., Meehl G.A., Shindell D., van Geel B., White W. Solar influences on climate. Review of Geophysics, V. 50, 2012, pp. 1-53. RG1006, DOI: 10.1029/2011RG000387.
Hirth B.D., Schroeder J.L., Weiss C.C. Surface analysis of the rear-flank downdraft outflow in two tornadic supercells. Monthly Weather Review, V. 136, 2008, pp. 2344-2363.
Huang Z., Fan X., Cai L., Shi S.Q. Tornado hazard for structural engineering. Natural Hazards, V. 83, 2016, pp. 1821-1842.
Kardashov V.R., Eppelbaum L.V. Mathematical models of strongly nonlinear geophysical phenomena. Trans. of the 5th Europ. Conf. of Mathematicians. Amsterdam, The Netherlands, 2008, 2 p.
Kardashov V.R., Eppelbaum L.V., Vasilyev O.V. The role of nonlinear source terms in geophysics. Geophysical Research Letters, V. 27, № 14, 2000, pp. 2069-2073.
Khrgian A.H. Physics of atmosphere. Gidrometeoizdat. Leningrad, 1978, 532 p. (in Russian).
Khromov S.P., Mamontova L.N. Meteorological dictionary. Gidrometeoizdat. Leningrad, 1974, 567 p. (in Russian).
Kotelnikov V.A. On the carrying capacity of the ether and wire in telecommunications. Trans. of the First All-Union Conf. on Problems of Communic. Izd. Upr. Svyazi RKKA. Moscow, 1933 (in Russian).
Laing A. Mesoscale convective systems. In: Encyclopedia of Atmospheric Sciences. North G.R., Pyle J.A., Zhang F., (eds.). Elsevier. The Netherlands, 2nd Edition, 2015, pp. 339-354.
Lamb H. Hydrodynamics. Dover. USA, 1945, 760 p.
Landscheidt T. The cosmic function of the golden section. In: HSG: Sterne, Mond und Kometen. Bremen und die Astronomie. Richter, P.H., (ed.) Verlag H.M. Hauschild, Bremen, 1995, pp. 240-276 (in German).
Landscheidt T. Solar activity of EL Nino and LA Nina. 2013. http://www.john-daly.com/sun-enso/sun-enso.htm.
Lorenz E.N. The interaction between a mean flow and random disturbances. Tellus, V. 21, № 3, 1953, pp. 289-307.
Markowski P., Richardson Y. What we know and don't know about tornado formation. Physics Today, V. 67, № 9, 2014, pp. 25-31.
Marshall T.P. Tornado damage survey at Moore, Oklahoma. Weather Forecasting, V. 17, 2002, pp. 582-598.
Monastersky R. Oklahoma tornado sets wind records. Science News, V. 155, № 2, 1999, pp. 308-309.
Nalivkin D.V. Hurricanes, storms and tornadoes. Nauka. Leningrad, 1969, 487 p. (in Russian).
Naylor J., Gilmore M.S. Environmental factors influential to the duration and intensity of tornadoes in simulated supercells. Geophysical Research Letters, V. 39, 2012, pp. 1-5. L17802. DOI: 10.1029/2012GL053041.
Nikolaevskiy V.N. Angular momentum in geophysical turbulence: continuum. Spatial averaging method. Kluwer (Springer). Dordrecht, 2003, 244 p.
Nyquist H. Certain topics in telegraph transmission theory. Trans. AIEE, V. 47, 1928, pp. 617-644.
ics, V. 50, 2012, pp. 1-53. RG1006, DOI: 10.1029/2011RG000387.
Hirth B.D., Schroeder J.L., Weiss C.C. Surface analysis of the rear-flank downdraft outflow in two tornadic supercells. Monthly Weather Review, V. 136, 2008, pp. 2344-2363.
Huang Z., Fan X., Cai L., Shi S.Q. Tornado hazard for structural engineering. Natural Hazards, V. 83, 2016, pp. 1821-1842.
Kardashov V.R., Eppelbaum L.V. Mathematical models of strongly nonlinear geophysical phenomena. Trans. of the 5th Europ. Conf. of Mathematicians. Amsterdam, The Netherlands, 2008, 2 p.
Kardashov V.R., Eppelbaum L.V., Vasilyev O.V. The role of nonlinear source terms in geophysics. Geophysical Research Letters, V. 27, № 14, 2000, pp. 2069-2073.
Laing A. Mesoscale convective systems. In: Encyclopedia of Atmospheric Sciences. North G.R., Pyle J.A., Zhang F., (eds.). Elsevier. The Netherlands, 2nd Edition, 2015, pp. 339-354.
Lamb H. Hydrodynamics. Dover. USA, 1945, 760 p.
Landscheidt T. Solar activity of EL Nino and LA Nina. 2013. http://www.john-daly.com/sun-enso/sun-enso.htm.
Lorenz E.N. The interaction between a mean flow and random disturbances. Tellus, V. 21, № 3, 1953, pp. 289-307.
Markowski P., Richardson Y. What we know and don't know about tornado formation. Physics Today, V. 67, № 9, 2014, pp. 25-31.
Marshall T.P. Tornado damage survey at Moore, Oklahoma. Weather Forecasting, V. 17, 2002, pp. 582-598.
Monastersky R. Oklahoma tornado sets wind records. Science News, V. 155, № 2, 1999, pp. 308-309.
Naylor J., Gilmore M.S. Environmental factors influential to the duration and intensity of tornadoes in simulated supercells. Geophysical Research Letters, V. 39, 2012, pp. 1-5. L17802. DOI: 10.1029/2012GL053041.
Nikolaevskiy V.N. Angular momentum in geophysical turbulence: continuum. Spatial averaging method. Kluwer (Springer). Dordrecht, 2003, 244 p.
Nyquist H. Certain topics in telegraph transmission theory. Trans. AIEE, V. 47, 1928, pp. 617-644.
Paulikas M.J., Schmidlin T.W. US tornado fatalities in motor vehicles (1991-2015). Natural Hazards, V. 87, 2017, pp. 121-143.
Pedlosky J. Geophysical fluid dynamics. Springer-Verlag. N.Y. Heidelberg – Berlin, 1992, 710 p.
Riguzzi F., Panza G., Varga P., Doglioni K. Can Earth's rotation and tidal despinning drive plate tectonics? Tectonophysics, V. 484, 2010, pp. 60-73.
Scafetta N., West B.J. Is climate sensitive to solar variability? Physics Today, March 2008, pp. 50-51.
Snow J.T. The tornado. Scientific American, V. 250, 1984, pp. 86-97.
Smith B., Katz R.W. US billion-dollar weather and climate disasters: data sources, trends, accuracy and biases. Natural Hazards, V. 67, 2013, pp. 387-410.
Tanaka, S., Ontake, M. and Sato, H. Tidal triggering of earthquakes in Japan related to the regional tectonic stress. Earth, Planet, Space, V. 56, 2004, pp. 511-515.
Vasil'yev O.F. Mechanics of the spiral and circulatory flows. A foundation. Gostechizdat. Moscow – Leningrad, 1958, 145 p. (in Russian).
Winn W.P., Hunyady S.J., Aulich G.D. Pressure at the ground in a large tornado. Jour. of Geophysical Research, V. 104 (D18), 1999, pp. 22067-22082.
Wurman J., Dowell D., Richardson Y., Markowski P., Ramussen E., Burgess D., Wicker L., Bluestein H.B. The second verification of the origins of rotation in tornadoes experiment Vortex2. Bull. of the American Meteorological Society, V. 8, 2012, pp. 1147-1170.

Paulikas M.J., Schmidlin T.W. US tornado fatalities in motor vehicles (1991-2015). Natural Hazards, V. 87, 2017, pp. 121-143.
Pedlosky J. Geophysical fluid dynamics. Springer-Verlag. N.Y. Heidelberg – Berlin, 1992, 710 p.
Riguzzi F., Panza G., Varga P., Doglioni K. Can Earth's rotation and tidal despinning drive plate tectonics? Tectonophysics, V. 484, 2010, pp. 60-73.
Saffmen P.G. Dynamics of eddies. Nauchny mir. Moscow, 2000, 376 p. (in Russian).
Scafetta N., West B.J. Is climate sensitive to solar variability? Physics Today, March 2008, pp. 50-51.
Sidorenkov N.S. Atmospheric processes and the Earth's evolution. Gidrometeoizdat. St. Petersburg, 2002, 365 p. (in Russian).
Snow J.T. The tornado. Scientific American, V. 250, 1984, pp. 86-97.
Smith B., Katz R.W. US billion-dollar weather and climate disasters: data sources, trends, accuracy and biases. Natural Hazards, V. 67, 2013, pp. 387-410.
Tanaka S., Ontake M. and Sato H. Tidal triggering of earthquakes in Japan related to the regional tectonic stress. Earth, Planet, Space, V. 56, 2004, pp. 511-515.
Vasil'yev O.F. Mechanics of the spiral and circulatory flows. A foundation. Gostechizdat. Moscow- Leningrad, 1958, 145 p. (in Russian).
Winn W.P., Hunyady S.J., Aulich G.D. Pressure at the ground in a large tornado. Jour. of Geophysical Research, V. 104 (D18), 1999, pp. 22067-22082.
Wurman J., Dowell D., Richardson Y., Markowski P., Rasmussen E., Burgess D., Wicker L., Bluestein H.B. The second verification of the origins of rotation in tornadoes experiment Vortex2. Bull. of the American Meteorological Society, V. 8, 2012, pp. 1147-1170.
Wurman J., Gill S. Fine scale radar observation of the Dimmit, Texas (2 June 1995) Tornado. Monthly Weather Review, V. 128, № 7, 2000, pp. 2135-2164.
Wurman J., Gill S. Fine scale radar observation of the Dimmit, Texas (2 June 1995) Tornado. Monthly Weather Review, V. 128, № 7, 2000, pp. 2135-2164.
Landscheidt T. Die kosmische Function des Goldenen Schnitts. In: HSG: Sterne, Mond und Kometen. Bremen und die Astronomie. Richter, P.H., (ed.) Verlag H.M. Hauschild, Bremen, 1995, pp. 240-276.
Арсеньев С.А. Динамика вод шельфов. Московский Государственный Университет. Москва, 1989, 96 с.
Арсеньев С.А., Бабкин В.А., Губарь А.Ю., Николаевский В.Н. Теория мезомасштабной турбулентности. Вихри атмосферы и океана. Ин-т компьютерных наук, регулярной и хаотической динамики. Москва-Ижевск, 2010, с. 365-371.
Васильев О.Ф. Основы механики винтовых и циркуляционных потоков. Гостехиздат. Москва-Ленинград, 1958, 145 с.
Дикий Л.А. Теория колебаний земной атмосферы. Гидрометеоиздат. Ленинград, 1969, 196 с.
Котельников В.А. О пропускной способности эфира и проволоки в электросвязи. Материалы к I Всесоюзному съезду по вопросам технической реконструкции дела связи и развития слаботочной промышленности. Издательство Управления Связи РККА. Москва, 1933.
Наливкин Д.В. Ураганы, бури и смерчи. Наука. Ленинград, 1969, 487 с.
Сидоренков Н.С. Атмосферные процессы и вращение Земли. Гидрометеоиздат. Санкт-Петербург, 2002, 365 с.
Сэффмэн Ф.Дж. Динамика вихрей. Научный мир. Москва, 2000, 376 с.
Хиргиан А.Н. Физика атмосферы. Гидрометеоиздат. Ленинград, 1978, 532 с.
Хромов С.П., Мамонтова Л.Н. Метеорологический словарь. Гидрометеоиздат. Ленинград, 1974, 567 с.
Чижевский А.Л. Земное эхо солнечных бурь. Мысль. Москва, 1976, 376 с.
Qədirov V.G. Neft hasilatında təbii dəyişikliklər. Faktlar və fərziyyələr. Geofizika: Azerbaycanda xəbərlər, № 3, 2001, pp. 21-24.

ОПАСНЫЕ АТМОСФЕРНЫЕ ЯВЛЕНИЯ: НОВЫЙ ФИЗИКО-МАТЕМАТИЧЕСКИЙ ПОДХОД

Арсеньев С.А.[1], Эппельбаум Л.В.[2], Ермакова Н.Н.[3]
[1]Отделение планетарной геофизики и геодинамики Института Физики Земли им. О.Ю. Шмидта, Российская Академия Наук
123995, Россия, Москва, Большая Грузинская ул., 10: Arsy7@mail.ru
[2]Отделение Наук о Земле, Факультет точных наук им. Раймонда и Беверли Саклер, Тель-Авивский Университет
6997801, Израиль, Тель-Авив, Рамат Авив: levap@post.tau.ac.il
[3]Отделение химии, Факультет точных наук им. Раймонда и Беверли Саклер, Тель-Авивский Университет
6997801, Израиль, Тель-Авив, Рамат Авив: ermakov@post.tau.ac.il

Резюме. В последнее время достигнут значительный прогресс в долгосрочном прогнозе таких опасных атмосферных явлений, как катастрофические и сильные торнадо (уровень EF3-EF5). Л. Эппельбаумом в 2013 году разработан нестохастический долговременный метод предсказания на основе использования метода долгосрочного прогнозирования с использованием теории распознавания образов и Фурье-анализа. Им выявлена тесная корреляция между общим количеством торнадо в год и параметрами гравитационной системы, продуцирующей приливные эффекты. Однако физический смысл этой связи оставался нераскрытым. В представленной работе предлагается новая физико-математическая модель, объясняющая процесс возникновения мощных торнадо. Модель включает два главных этапа. Вначале гравитационные силы и ураганные ветры в верхней тропосфере образуют нелинейные длинные волны в нижней тропосфере. Затем возникают штормовые ветры в верхней тропосфере (при проникновении холодных масс воздуха в теплых районах), связанные обычно с быстрыми синоптическими циклонами, несущими грозовую облачность и дожди. Возникающие гравитационные нелинейные волны устремляются со скоростью приливных волн $V = (gH)^{1/2}$ вдоль инверсии субоблака. После этого гравитационные волны падают (и поглощаются) суперячейкой грозы, которая уже сформировалась внутри холодного атмосферного фронта. В результате адаптации метеорологического поля давление внутри грозовой суперячейки уменьшается, вращение ветра усиливается, что порождает сильный торнадо. Различные примеры иллюстрируют применимость разработанного подхода, причем теоретические результаты хорошо согласуются с практическими наблюдениями. Предложенная новая физико-математическая методология может быть концептуально применена для анализа других явлений, происходящих в атмосфере Земли.

Ключевые слова*: торнадо, длинные приливные гравитационные волны, гравитационная система Земля-Луна-Солнце, солитон, опасные атмосферные феномены*

TƏHLÜKƏLİ ATMOSFER HADİSƏLƏRİ: YENİ FİZİKİ-RİYAZİ YANAŞMA

Arsenyev S.A.[1], Eppelbaum L.V.[2], Yermakova N.N.[3]
[1]Rusiya Elmlər Akademiyası O.Y.Şmidt adına Yer Fizikası İnstitutunun Planetar geofizika və geodinamika bölməsi,
123995, Rusiya, Moskva şəh., Bolşaya Qruzinskaya küç., 10: Arsy7@mail.ru
[2]Geoelmlər məktəbi, Reymond və Beverli Sakler adına Dəqiq Elmlər fakültəsi, Təl-Əviv Universiteti
6997801, Israil, Təl-Aviv, Ramat Aviv: levap@post.tau.ac.il
[3]Kimya məktəbi, Reymond və Beverli Sakler adına Dəqiq Elmlər fakültəsi, Təl-Əviv Universiteti
6997801, Israil, Təl-Aviv, Ramat Aviv: ermakov@post.tau.ac.il

Xülasə. Son vaxtlar fəlakətli və güclü tornadolar (səviyyə EF3-EF5) kimi təhlükəli atmosfer hadisələrinin uzunmüddətli proqnozunda mühüm irəliləyişə nail olunmuşdur. Simaların tapılması nəzəriyyəsindən və Furye analizdən istifadə etməklə uzunmüddətli proqnozlaşdırma üsulundan istifadə əsasında L.V.Eppelbaum (2013) geyri-stoxastik uzunmüddətli öncədən xəbərvermə üsulunu işləmişdir. O, il ərzində tornadonun ümumi miqdarı və qabarma effektləri yaradan qravitasiya sisteminin parametrləri əsasında sıx korrelyasiya aşkar etmişdir. Lakin bu əlaqənin fiziki mənası açılmamış qalmışdır. Təqdim olunan işdə biz güclü tornadoların yaranmasını izah edən yeni fiziki-riyazi model təklif edirik. Təqdim olunan model iki başlıca etapdan ibarətdir. Başlanğıcda yuxarı troposferdə qravitasiya qüvvələri və çox güclü küləklər aşağı troposferdə, adətən tufanlı dumanlıq və yağış daşıyan sürətli sinoptik siklonlarla bağlı olan, qeyri-xətti uzun dalğalar əmələ gətirir. Sonra, yuxarı troposferdə fırtına külәkləri yaranır (isti rayonlarda havanın soyuq kütlələri soxulanda). Yaranan qravitasiya qeyri-xətti dalğaları subdumanlığın inversiyası boyunca qabarma dalğalarının sürəti ilə $V=(gH)^{1/2}$ cumur (hücum edir). Bundan sonra qravitasiya dalğaları soyuq atmosfer cəbhəsinin daxilində formalaşan tufanın superözəyi ilə udulur. Meteoroloji sahənin adaptasiyası nəticəsində tufan superözəyinin daxilində təzyiq azalır, küləyin fırlanması şiddətlənir və bu da güclü tornado yaradır. Müxtəlif nümunələr işlənilmiş yanaşmanın tətbiq edilməsini əks etdirir, həm də nəzəri nəticələr praktiki müşahidələrlə yaxşı uzlaşır. Təklif olunan yeni fiziki-riyazi metodologiya Yer atmosferində baş verən digər hadisələrin təhlili üçün konseptual tətbiq oluna bilər.

Açar sözlər*: tornado, uzun qabarma qravitasiya dalğaları, Yer-Ay-Günəş qravitasiya sistemi, soliton, təhlükəli atmosfer fenomenləri*

ANAS Transactions **Earth Sciences** **1 / 2019**

Geology and geophysics

http://www.journalesgia.com

RESULTS OF ARCHAEO-GEOPHYSICAL METHODS ON ALKHANTEPE ARCHEOLOGICAL MONUMENT (AZERBAIJAN TERRITORY)

Safarov R.T.[1], Akhundov T.I.[2], Zamanova A.H.[1], Aliyev Ch.S.[1], Sharifova A.T.[1], Abdullayev A.N.[2], Bagirli R.J.[1]

[1]Geology and Geophysics Institute, Azerbaijan National Academy of Science
119, H. Javid Ave., Baku, Azerbaijan, AZ1143: rafiqsafarov@gmail.com
[2]Institute of Archaeology and Ethnography, Azerbaijan National Academy of Sciences
115, H. Javid Ave., Baku, Azerbaijan, AZ1073: tufan_akhundov@mail.ru

***Keywords**; Archeo-geophysical methods, Alkhantepe, preventive archeology, gamma-ray surveying*

Summary. Studying of archaeological sites in the fields of oil and gas pipeline routes, buildings and oil terminals is very important in Azerbaijan. The application of geophysical methods is based on the preliminary detection and investigation of important archeological objects that can be damaged by oil and gas pipelines, oil and gas fields, and construction sites. The application of these methods in our country can extend search opportunities for archaeologists, on the other hand, it could help to take into account the existing archeological monuments in the area and suggest possible adjustments for the planning stage of the industrial operations (such as oil and gas pipelines, oil and gas terminals, oil wells, etc.) and help to take preventive measures. A series of geophysical investigations have been tested in the Alkhantepe archeological zone of Azerbaijan for the purpose of developing the method and technology for the application of geophysics of small depths in the discovery and initial investigation of archaeological monuments. The sensitivity of the archaeological methods used to detect various types of objects was taken into consideration and the reliability of the results was examined on the Alkhantepe archaeological monument and the three-dimensional space and time models of the archeological object were compiled. To identify the topology of the area high-precision surveying has been applied to the area as well as high-precision gravitational field measurements were performed for determination of possible archaeological sites (cavities, fractures, etc.), natural radio-based background of the area and detection of abnormal zones associated with it were performed with pedestrian gamma-planning method.

© 2019 Earth Science Division, Azerbaijan National Academy of Sciences. All rights reserved.

Introduction

Geophysical investigations allow getting the initial information about archeological monuments, their area of coverage and significance. In archeology geophysical methods primarily can be used for search and discovery of important archeological objects and for preventive measures. Latter have led to a new direction called "Preventive Archeology", which gives very good efficiency in the preparation of preventive measures (Clark, 1990; Мартынов, Шер, 1990).

The application of geophysical methods is based on the preliminary detection and investigation of important archeological objects that can be damaged by oil and gas pipelines, oil and gas fields, and construction sites.

The study of archaeological sites in the fields of oil and gas pipeline routes, buildings and oil terminals is very important in Azerbaijan. The application of these methods in our country can extend search opportunities for archaeologists, on the other hand, it could help to take into account the existing archeological monuments in the area and suggest possible adjustments for the planning stage of the industrial operations (such as oil and gas pipelines, oil and gas terminals, oil wells, etc.) and help to take preventive measures.

Area of investigation

A number of geophysical methods have been tested in Mughan archeological field in Azerbaijan to assess the sensitivity of geophysical methods in the discovery and initial investigation of archaeological monuments. The sensitivity of the archeo-geophysical methods used to detect various types of

objects was taken into consideration and the reliability of the results was verified on the Alkhantepe archaeological monument and their three-dimensional space and time models have been constructed. The research was carried out with the support of the State Oil Foundation of the Azerbaijan Republic (04.01.2018-04.01.2019).

The sensitivity of applied geophysical methods depends on geological and ecological environment, the type and character of the archeological monument. Therefore known Alkhantepe archeological field has been selected as a base in order to perform tests of geophysical methods (Figure 1). The monument is located about 4 km to the north of the village of Uchtepe, Jalilabad region.



Figure 1. The view of the Alkhantepe excavation area

While the research area has a broad coverage with rich cultural history, it is located below the modern level of alluvial plain. Therefore it is covered with alluvial sediments and does not show any signs of existence on the surface. This feature of the archeological field creates ideal conditions to test the geophysical methods in order to develop necessary methodology and techniques to discover and investigate of archaeological monuments.

Archeological view of the research area

South-eastern region of Azerbaijan is divided into mountainous and lowland parts. Lowland part consists of Mughan plain situated in the north of the region and Lankaran lowland which is located between Talysh Mountains and Caspian Sea. The object of our research, the settlement Alkhantepe is on the territory of Mughan plain. The results of archaeological research of the revealed monuments and the analysis showed the following picture of settling in the region.

The traces of early inhabitants in the mountainous part of south-eastern Azerbaijan related to 5th millennium B.C. were revealed on the territory of Lerik district in the Buzeyir cave (Cəfərov, 2012). But we have no certification of settling in this region for the later long period of time.

The next settling in the lowland part of the region began in the 5th mil.B.C. and from time to time continued up to now spreading to all areas. At that period of the time tribes and states with different cultures replaced one another and inhabited the areas in accordance with their economic needs.

In the 5th mil. B.C. the tribes known as "Mughan Neoliths" have settled in Mughan plain and mainly on the territory of modern Jalilabad district. Their traces are kept up to our days in more than 20 monuments. The archaeological research was held only on two of them – Alikomektepe and Polutepe which are situated on the territory of Uchtepe village (Mirzəzadə, 2016).

There are traces of Leylatepe tribes in this region which replaced "Mughan Neoliths" tribes in the second half of the IV mil. B.C. At that time the traces of settling embrace the majority of parts of the region, the lowlands as well as the mountainous ones. One of these parts is our object of research – the settlement Alkhantepe (Ахундов, 2014; Akhundov, 2018).

The next settling in south-eastern Azerbaijan replacing Leylatepe tribes and relating to the III mil.B.C. belongs to the bearers of Kur-Araxes culture. Their traces are observed in different parts of the region. But in the meanwhile the reconnoitering excavation was held only on the settlement Misharchay-I which is situated in the east of Jalilabad city, on the crossway of Misharchay and Baku-Astara road (Махмудов, 2008).

We cannot show any common culture characteristic to this region in the second half of the III mln.B.C. and the first half of the III mln.B.C. At that time, the tribes belonging to different cultures mainly cattle-breaders were living here. They are revealed and observed both in the tumuli and in the remains of settlements, belonging to tribes preceding them. The only known settlement of this period was registered in Jalilabad district on the territory of Jafarkhanly village (Axundov, 2009).

In the second half of the II mln.B.C. – first half of the I mln.B.C. in the south-eastern Azerbaijan there was revealed a number of specific culture traces known as "Talysh-Mughan" culture. They appeared as "stone boxes" in mountainous parts and as tumuli in lowland areas.

Thus as we pointed it out, in the south-eastern Azerbaijan, different tribes and states replaced one another, got mixed, settled on this territory, lived

here and left their traces. The researches and the majority of results gave the certifications which show that the most part of traces for a long time of millenniums are beyond the modern earth surface and are not observed visually. The cause of it are geomorphological processes. Traditional archaeological methods are not enough to efficiently reveal these monuments. It is necessary to use different approaches and apply new techniques and geophysical methods.

Research methods

High-precision leveling and gravity measurements were performed in order to determine possible archaeological sites (cavities, fractures, etc.) of Alkhantepe zone. Natural background radioactivity of the area and associated anomalies were detected by the pedestrian gamma-ray surveying.

High-precision leveling

High-precision leveling was performed in order to study the relief features of Alkhantepe archeological zone. Measurements were performed by the high-precision "AFL-320", produced by Pentax and GPS. Nine profiles were selected to carry out high-precision leveling measurements. Figure 2 illustrates the location of measured points on each profile.



Figure 2. Leveling and gravity measurement points on the profiles in Alkhantepe area

High-precision leveling measurements were carried out on stationary bench marks. Point L1 has been selected as the starting point for measurements. The total length of the profiles is 2.7 km (65 pt). The difference between the starting points is 3.216 m. Discrepancy of measurement was 4 m. Acceptable error A was $\pm 3\sqrt{L}$ mm = 18 mm, where L is the average length of one step.

High-precision gravity measurements

High precision gravity measurements were performed in order to identify possible buried archeological objects, gaps, fractures, etc. The gravity measurements were carried out on 9 parallel profiles striking from south-north and all gravity measurements were tied to the fundamental reference points. The measurements step was 20-25 m. Bouguer anomalies were calculated using the density of intermediate layer (2.67 g/cm^3). Gravity measurements were performed with GNU-K2 gravimeter. Temperature changes, the Earth`s tides and the surrounding relief features, as well as the non-linearity of the gravimeter system were taken into account during gravity data processing. Measurement of gravity difference between two neighbor points A and B is done with a simple loop scheme (A1 → B1 → A2). The gravity difference is calculated by the following formula:

$$\Delta g_{ab} = g_{rb_1} - \left[g_{ra_1} + \frac{g_{ra_2} - g_{ra_1}}{t_{a_2} - t_{a_1}} (t_{b_1} - t_{a_1}) \right]$$

Here, g_{ra_1}, g_{ra_2}, g_{rb_1} are the effective estimates of the gravity acceleration obtained for simple loop between A and B points. Δg_{ab} is the difference of the gravity acceleration between A and B. t_{a_1}, t_{b_1}, t_{a_2} are measured times corresponding to A_1, B_1 and A_2 points. The Bouguer anomaly and the Bouguer anomaly gradient were calculated based on the gravity and geodetic measurements results (Figure 3).

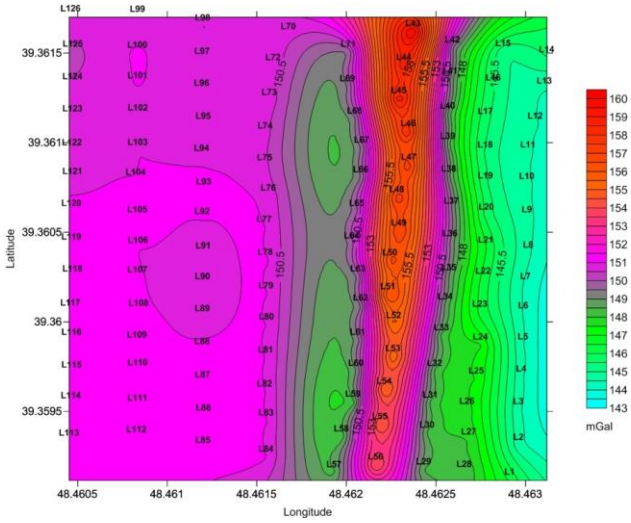


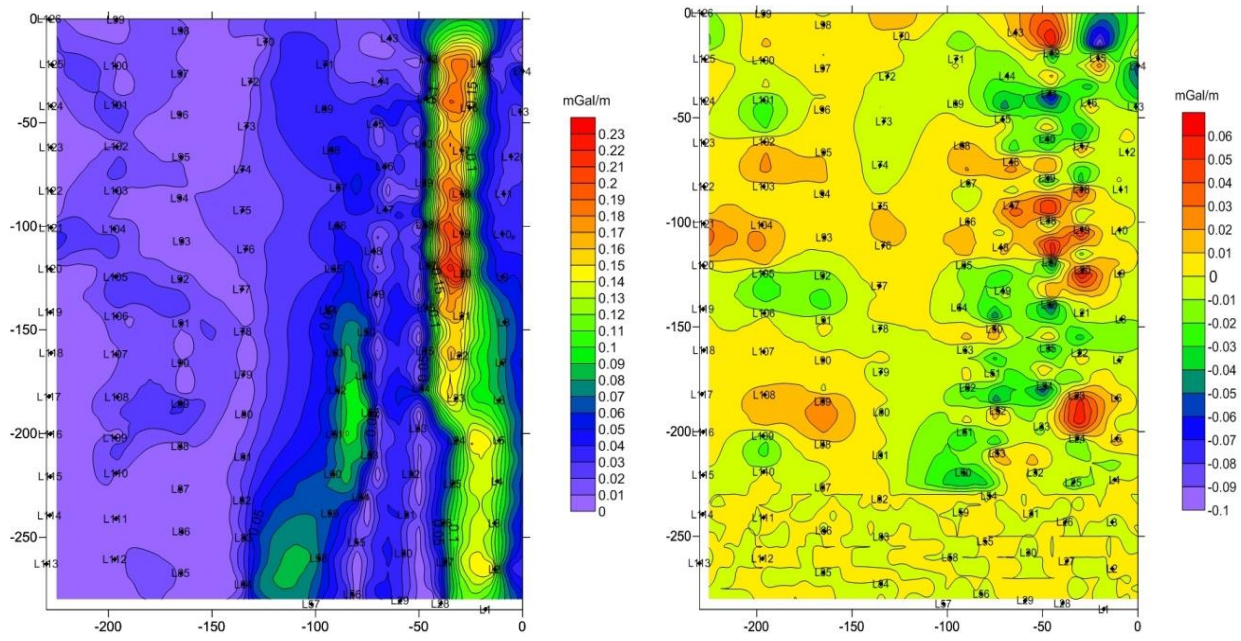
Figure 3. Bouguer anomaly map of Alkhantepe area (calculated using density of 2.67 g/cm^3)

Multiple environments have been detected as a result of the combined analysis of the Bouguer

anomaly and Bouguer anomaly gradient characteristics obtained from high-precision gravity measurements carried out in the study area.

As seen from the Bouguer Anomaly Map (Figure 3) for the Alkhantepe area, the Bouguer anomaly maximums have been observed throughout the L43-L56 measuring points (48.462 to 48.4625 in length) in the eastern part of the study area, where the presence of this maximums stand out by difference from other environmental characteristics in the area.

This is clearly shown in the distribution map of the Bouguer anomaly gradient (Figure 4) calculated for the Alkhantepe area. The boundaries of the anomalous strip found in the distribution map of the Bouguer anomaly gradient are clearly stated. There are two anomalous boundaries in the distribution map of the gradients of the gravitational field. This shows the existence of walls. The results are consistent with the previous archeological researches carried out in Alkhantepe.



(a) backward direction method

(b) central direction method

(c) forward direction method

Figure 4. Bouguer anomaly gradient distribution map of the Alkhantepe area

Radiometric measurements

Radiometric studies in Alkhantepe were performed according to the "Temporary Methodological Guidelines for Pedestrian Gamma-Ray Surveys", "Guides for Radiometric prospecting and analysis" and "RTN 99/2009 Radiation safety norms" (Прудкина, Шашкин, 1984; Нормы радиационной безопасности, 2009; Temporary methodological guidelines…, 1986).

Based on the analysis of radiometric measurements in Alkhantepe archaeological area, maps of gamma-ray and radon gas concentration in underground air has been created (Aliyev Ch.S.). Natural background radiation of the research area and detection of anomalous zones were carried out with pedestrian gamma-ray surveys.

Dose-radiometer MKC-AT1125 is used to conduct the measurements. The background radiation measurements were carried out at 188 points, with a measurement step of about 20 meters by the pedestrian gamma-ray survey. Gamma-ray field of the area was mapped based on the obtained results (Figure 5).

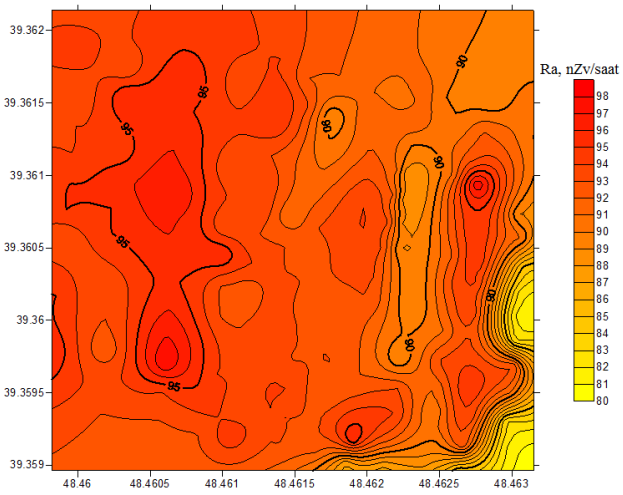


Figure 5. Gamma-ray distribution map of Alkhantepe research area (Aliyev Ch.S.)

The map of the gamma-ray field shows that high values of natural radioactivity (95-98 nZv/h) were observed in the south-western part, whereas north-eastern part of the research area is characterized by relatively low radioactivity (85-90 nZv/h). The background radiation values change between 82-98 nZv/hr.

Also the radon gas concentration of underground air was determined at 9 sites of the study area. Here, the radon gas concentration has been estimated to be about 168-1190 Bk/m^3. Based on these results the map of radon gas content of the underground air has been generated for the research area (Figure 6).

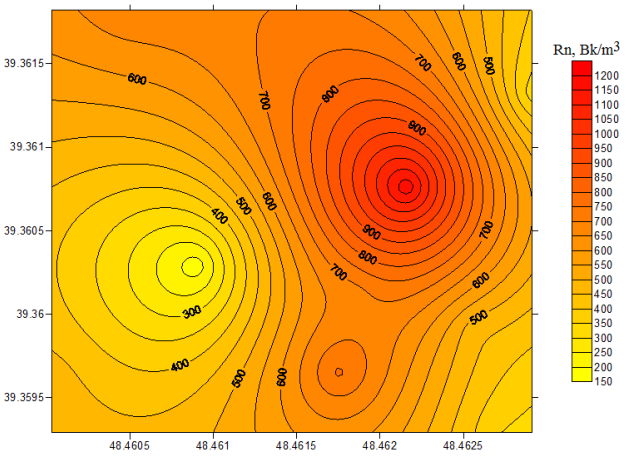


Figure 6. Map of radon gas content in underground air in Alkhantepe research area

According to the map shown in Figure 6 it appears that relatively high values of radon gas in the underground air (900-1200 Bk m^3) are found in the north-eastern part of the area and low concentration (150-400 Bk/m^3) belongs to the south-western part of the area.

Analysis shows that cross-border of the high and low values may be considered as prospective for archaeological investigations. The presence of anomalous boundary in the distribution map of the radon gas content is consistent with previous studies in Alkhantepe.

Conclusions

The first experience of use of near-surface geophysical methods in archeological researches in Azerbaijan (radiometric and gravimetric) can be developed in the future to continue the research in this direction. The following results have been obtained during archeo-geophysical studies:

– the historical archeological scene of the research area is described;

– the possibility of applying of preventive geophysical methods in the complex study of archaeological monuments has been identified and the methodology of modified methods has been developed considering the characteristics of the area;

– the three-dimensional space and time model of the archeological site (Alkhantepe) with different physical parameters has been compiled;

– the sensitivity of the used archeo-geophysical methods to detect different types of objects was assessed and the reliability of the obtained results was tested on Alkhantepe monument.

REFERENCES

Akhundov T.İ. The South Caucasus on the threshold of the metal age. Context and connection: essays on the archaeology of the ancient Near East in honour of Antonio Sagona (Orientalia Lovaniensia Analecta). Peeters Publishers. Hardcover, 2018, pp. 49-77.

Akhundov T.İ. 20 days in Astara. Baku, 2009, 112 p. (in Azerbaijani).

Akhundov T I. Alkhantepe – an early bronze age settlement in Azerbaijan. Transactions of the Institute of the history of material culture, № 10, St.-Petersburg, 2014, pp. 78-92 (in Russian).

Clark A. Seeing beneath the soil. Prospecting methods in archaeology. ISBN 0-415-21440-8. B.T.Batsford Ltd. London, 1990, 196 p.

Jafarov A. Preliminary results of Paleolithic archeological expeditions. Archeological researches in Azerbaijan, 2001. Baku, 2002, pp. 25-28 (in Azerbaijani).

Makhmudov F. Culture of southeastern Azerbaijan in the Bronze Age and early Iron Age. Nafta-Press. Baku, 2008, 216 p. (in Russian).

Martynov A.I., Sher Ya.A. Geophysical methods in architectural-archaeological researches. Research problems of architectural monuments. Moscow, 1990, pp. 102-113 (in Russian).

Mirzazadeh A.A. Mughan material-cultural monuments. Nargiz. Baku, 2016, 160 p. (in Azerbaijani).

Prudkina M.I., Shashkin V.L. Handbook of radiometric survey and radiometric analysis. Energoatomizdat. Moscow, 1984, 168 p. (in Russian).

Radiation safety norms. SanPiN 2.6.1.2523-09. RTN 99/2009 FCH and E. Moscow, 2009, 106 p. (in Russian).

Temporary methodological guidelines for pedestrian gamma-survey in radiation study of urbanized areas. 1986, 17 p. (in Russian).

ЛИТЕРАТУРА

Akhundov T.İ. The South Caucasus on the threshold of the metal age. Context and connection: essays on the archaeology of the ancient Near East in honour of Antonio Sagona (Orientalia Lovaniensia Analecta). Peeters publishers. Hardcover, 2018, pp. 49-77.

Clark A. Seeing beneath the soil. Prospecting methods in archaeology. ISBN 0-415-21440-8. B.T.Batsford Ltd. London, 1990, 196 c.

Ахундов Т.И. Алхантепе – поселение начала эпохи бронзы в Азербайджане. Записки Института истории материальной культуры, № 10, С.-Петербург, 2014, с. 78-92.

Мартынов А.И., Шер Я.А. Геофизические методы в архитектурно-археологических исследованиях. Вопросы исследования памятников архитектуры, Москва, 1990, с. 102-113.

Махмудов Ф. Культура юго-восточного Азербайджана в эпоху бронзы и раннего железа. Nafta-Press. Баку, 2008, 216 с.

Временные методические указания по пешеходной гамма-съемке при изучении радиационной обстановки городских территорий. 1986, 17 с.

Прудкина М.И., Шашкин В.Л. Справочник по радиометрической разведке и радиометрическому анализу. Энергоатомиздат. Москва, 1984, 168 с.

СанПиН 2.6.1.2523-09. Нормы радиационной безопасности (НРБ 99/2009). ФЦГиЭ. Москва, 2009, 106 с.

Axundov T.I. Astarada 20 gün. Elm. Bakı, 2009, 112 s.

Cəfərov Ə. Paleolit arxeoloji ekspedisiyanın apardığı tədqiqatların ilkin nəticələri. Azərbaycanda arxeoloji tədqiqatlar, 2001. Bakı, 2002. s. 25-28.

Mirzəzadə Ə. Muğan, maddi-mədəniyyət abidələri. Nərgiz. Bakı, 2016, 160 s.

РЕЗУЛЬТАТЫ ПРИМЕНЕНИЯ АРХЕОГЕОФИЗИЧЕСКИХ МЕТОДОВ НА ТЕРРИТОРИИ АРХЕОЛОГИЧЕСКОГО ПАМЯТНИКА АЛХАНТЕПЕ (АЗЕРБАЙДЖАН)

Сафаров Р.Т.[1], Ахундов Т.И.[2], Заманова А.Г.[1], Алиев Ч.С.[1], Шарифова А.Т.[1], Абдуллаев А.Н.[2], Багирли Р.Дж.[1]

[1]Институт геологии и геофизики НАНА
AZ1143, г.Баку, просп. Г.Джавида, 119: rafiqsafarov@gmail.com
[2]Институт археологии и этнографии НАНА
AZ1073, г.Баку, просп. Г.Джавида, 115: rafiqsafarov@gmail.com

Резюме. Изучение археологических объектов в районе нахождения нефте- и газопроводов, промышленных зданий и нефтяных терминалов очень актуально для Азербайджана. Применение геофизических методов основано на предварительном выявлении и исследовании археологических объектов, которые могут быть повреждены при возможном строительстве нефте- и газопроводов, разработке нефтегазовых месторождений, а также проведении каких-либо строительных работ. Использование этих методов в нашей стране позволяет археологам расширить возможности поиска археологических памятников, бережно отнестись к таковым существующим и предложить возможные корректировки на стадии планирования работ, а также принять превентивные меры.

Ряд геофизических методов был опробован в археологической зоне Алхантепе в целях разработки методов малоглубинной геофизики для обнаружения и первоначального исследования археологических памятников. Особое внимание было обращено на чувствительность археогеофизических методов, использованных для обнаружения различных типов объектов, а надежность результатов была проверена на археологическом памятнике Алхантепе. Были составлены трехмерные пространственные и временные модели археологических объектов. Для определения рельефа местности применялось высокоточное нивелирование, а для выявления возможных археологических объектов (полостей, трещин и т.д.) – высокоточные измерения гравитационного поля, фон естественной радиоактивности и аномальные зоны были установлены методом пешеходной гамма-съемки.

Ключевые слова*: археогеофизические методы, Алхантепе, профилактическая археология, гамма-съемка*

ARXEOGEOFİZİKİ ÜSULLARIN ALXANTƏPƏ ARXEOLOJİ ABİDƏSİ ƏRAZİSİNDƏ TƏTBİQİNİN NƏTİCƏLƏRİ (AZƏRBAYCAN)

Səfərov R.T.[1], Axundov T.İ.[2], Zamanova A.H.[1], Əliyev Ç.S.[1], Şərifova A.T.[1], Abdullayev A.N.[2], Bağırlı R.C.[1]
[1]AMEA Geologiya və Geofizika İnstitutu
AZ1143, Bakı şəh., H.Cavid prosp., 119A: rafiqsafarov@gmail.com
[2] AMEA Arxeologiya və Etnoqrafiya İnstitutu
AZ1073, Bakı şəh., H.Cavid prosp., 115: tufan_akhundov@mail.ru

Xülasə. Arxeoloji abidələrin aşkarlanması və ilkin tədqiqində kiçik dərinliklər geofizikasının tətbiqi metodunun və texnologiyasının hazırlanması məqsədilə Azərbaycan ərazisinin Alxantəpə arxeoloji zonasında bir sıra geofiziki tədqiqatlar sınaqdan keçirilmişdir. İstifadə edilən arxeogeofiziki üsulların müxtəlif tipli obyektlərin müəyyən edilməsində həssaslığı nəzərə alınmış və nəticələrin etibarlılığı Alxantəpə arxeoloji abidəsi üzərində yoxlanılaraq, obyektin üçölçülü məkan və zaman modelləri tərtib edilmişdir. Tədqiqat ərazisində relyef xüsusiyyətlərinin öyrənilməsi üçün yüksək dəqiqlikli nivelirləmə, ehtimal olunan arxeoloji obyektlərin (boşluqlar, qırılmalar və s.) aşkarlanması məqsədilə yüksək dəqiqlikli qravitasiya sahə ölçmələri, ərazinin təbii radiasiya fonunun təyini və anomal zonaların aşkar edilməsində piyada qammaplanalma işləri həyata keçirilmişdir. Bu üsulların ölkəmizdə tətbiqi arxeoloqların axtarış imkanlarını genişləndirə bilər, digər tərəfdən – sənaye işlərinin planlaşdırılması (neft-qaz kəmərlərinin çəkilisi, neft-qaz terminallarının və neft quyularının yerlərinin seçilməsi və s.) mərhələsində ərazidə mövcud olan arxeoloji abidələri nəzərə almağa, layihələrə lazım olan düzəlişləri verməyə və preventiv tədbirlər görməyə imkan verər.

Açar sözlər: *Arxeogeofiziki üsullar, Alxantəpə, preventiv arxeologiya, qammaplanalma*

ANAS Transactions **Earth Sciences** **1 / 2019**

Geology and geophysics

http://www.journalesgia.com

3D ГЕОФИЗИЧЕСКАЯ МОДЕЛЬ БЛИЗПОВЕРХНОСТНОЙ СТРУКТУРЫ ГРЯЗЕВОГО ВУЛКАНА ДАШГИЛЬ

Саламов А.М., Мухтаров А.Ш., Маммадов В.А.
Институт геологии и геофизики НАНА
AZ1143, г.Баку, просп. Г.Джавида, 119: avazsalamov@mail.ru

3D GEOPHYSICAL MODEL OF NEAR SURFACE STRUCTURE OF THE DASHGIL MUD VOLCANO

Salamov A.M., Mukhtarov A.Sh., Mammadov V.A.
Geology and Geophysics Institute, Azerbaijan National Academy of Sciences
119, H.Cavid ave., Baku, AZ1143: avazsalamov@mail.ru

Keywords: *mud volcano, structure, crater, throat, geophysical investigations, Vertical Electrical Sounding (VES), model, temperature, gradient, heat flow*

Summary. The article discusses the results of geophysical studies (electrical, geothermal and gravimetric) conducted in the crater area of some mud volcanoes. Despite the shallow depth (up to 200 m) of electrical exploration, in combination with other methods, they provide a convincing insight into the structure of the studied area (the crater zone of the Dashgil mud volcano). A joint analysis of these results suggests the existence of subvertical zones in the cross-section with physical properties differing from the ones of the rocks characterizing the environment. Roots (an area where erupting fluids are accumulated) and channels of mud volcanoes are defined as decompressed objects. Fluids that carry heat from the deeper areas to the surface constantly leak through these channels. Therefore, the channels of mud volcanoes relative to the surrounding rocks are distinguished by high temperatures and temperature gradients. On the surface, thermal anomalies are noted only with the activation of volcano or its eruption. The three-dimensional model built based VES (Vertical Electrical Sounding) results allows visually assuming this assumption. According to the VES data, a supposed lithographic-geophysical section was plotted allowing distinguishing the layers of breccia of each eruption case.

© 2019 Earth Science Division, Azerbaijan National Academy of Sciences. All rights reserved.

Введение

Грязевые вулканы относятся к одним из интересных геологических явлений и широко развиты на территории Азербайджана (в Южно-Каспийской мегавпадине).

Некоторые вулканы-гиганты, особенно часто встречающиеся в пределах Азербайджана, имеют высоту 400-450 м, площадь их кратерного поля достигает 900-1000 м^2, а общий объем твердых выбросов в момент извержения иногда превышает 2400 млн.м^3. Особо крупных размеров достигают грязевые вулканы Алятской гряды – Торагай, Беюк Кянизадаг, Дашгиль, Готурдаг, Айрантекен, Кара-кюре, Солахай и др. (Якубов и др., 1971; Холодов 2012).

В районе распространения грязевых вулканов преобладает умеренно-теплый климат полупустынь и сухих степей с сухим летом. Среднегодовая температура составляет +14,6ºС. В летнее время поверхность почвенного покрова нагревается до 46-47ºС.

Тепловой поток в таких областях ниже континентального среднего значения этого параметра. На этом фоне выделяются локальные положительные аномалии температурного поля. К регионам с низкими значениями теплового потока относятся Черноморская и Южно-Каспийская впадины, Таманский полуостров, Западно-Туркменская впадина, Мексиканский залив и др. (Mukhtarov, 2003; Мухтаров и Адыгезалов, 1997; Смирнов, 1980; Hamza et al., 2006; Kopf et al., 2009; Mukhtarov et al., 2003). Это свидетельствует об особой роли грязевых вулканов в формировании теплового поля региона, заключающейся в том, что грязевые вулканы являются проводящими зонами для флюидов из глубинных горизонтов на поверхность и мощными каналами выноса тепла.

Геологический фон

Четвертичные отложения в рассматриваемом регионе распространены довольно широко и покрывают мощным чехлом всю территорию Гобустанской области. Морские четвертичные отложения в осевой полосе прогибов залегают согласно на подстилающих отложениях без существенных следов размыва, почти не затронуты складчатостью и в большинстве случаев залегают на размытых поверхностях отложений абшеронского яруса. Литологически они представлены прибрежно-мелководными грубообломочными, реже песчано-алевритовыми образованиями, глинами, ракушняками, местами дислоцированными под углом 40-50°. В отрицательных формах рельефа выше них лежат галечники, гравелиты, конгломераты, грубозернистые пески и плохо отсортированные породы с прослоями глин и ракушняков.

На юго-востоке их замещают песчано-алевритовые и глинистые отложения с многочисленными прослоями грязевулканической брекчии. Стратиграфически выше них залегают слабо дислоцированные грубообломочные и песчаные, а на востоке – песчано-алевритовые образования с прослоями глин. Еще выше располагаются отложения, представленные песчано-ракушечными и ракушечными фациями, которые на востоке замещаются глинисто-алевролитовыми образованиями и глинами с прослоями песков. Завершают разрез четвертичных отложений суглинки и песчано-ракушечные образования. Мощность четвертичных отложений в пределах Гобустана колеблется в больших пределах и местами достигает первых сотен метров (Ализаде и др., 1978).

По степени дислоцированности и структурному стилю четвертичные отложения существенно отличаются от подстилающих комплексов пород. Они образуют самостоятельный структурный подэтаж и отделены от подстилающих образований региональным перерывом и несогласием. Эти области в четвертичном периоде пережили более интенсивные и мощные тектонические движения.

Иной характер и направленность четвертичные тектонические движения имели в соседней Южно-Каспийской впадине. На преобладающей территории впадины в течение всего четвертичного периода преобладали процессы погружения и накопления осадков.

Площадь исследования

Площадь геофизических исследований расположена на юго-западной окраине Абшеронского полуострова. Здесь в области кратера грязевого вулкана Дашгиль (включая зону распространения грифонов, две грязевые сальзы) несколько раз (в разные годы, начиная с 1990 года) проводились температурные исследования. Измерения температуры производились полутораметровыми зондами в грифонах и на краю сальзы.

В 2018 году на этой площади по десяти профилям впервые проводились полевые электроразведочные работы методом вертикального электрического зондирования (ВЭЗ) (рис.1).

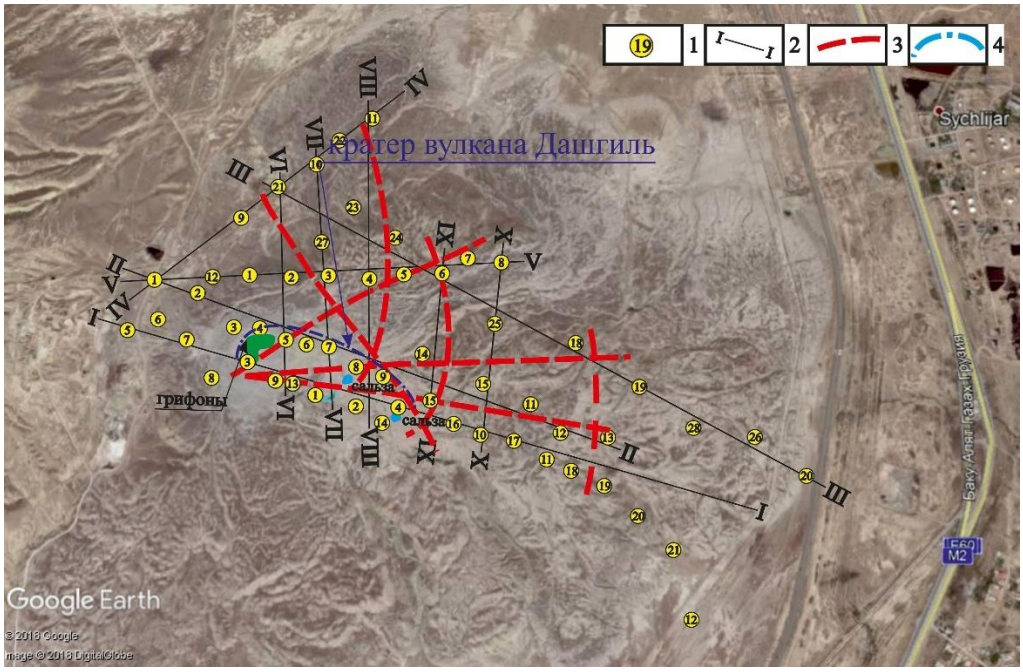


Рис. 1. Площадь исследования. Схема расположения геофизических профилей
1 – точки ВЭЗ и их номера; 2 – линии геофизических профилей; 3 – предполагаемые разрывные нарушения, выявленные по данным ВЭЗ; 4 – предполагаемая зона кратера

Методика исследований и интерпретации

Температурные замеры на грязевых вулканах производились с помощью специальных термозондов длиной 1,5 м. Зонд состоит из металлической трубы диаметром 15 мм. Термочувствительным элементом (датчиком температуры) является терморезистор, который расположен внутри теплопроводящей (медной) головки в конце зонда.

Калибровка терморезисторов производится перед полевыми работами в лабораторных условиях с использованием термостата и ртутного термометра с точностью 0,01°С.

При полевых исследованиях зонд внедряется в рыхлый грунт на определенную глубину. В этом положении выдерживается 30 минут для установления температуры среды, после чего производится измерение температуры.

Полевые электроразведочные работы выполнены по десяти профилям с применением четырехэлектродной симметричной установки AMNB.

Для определения глубины залегания горизонтальных границ раздела и удельных электрических сопротивлений отдельных слоев по совокупности значений $\rho_к$, полученных при измерениях с различными установками, построена новая модель расчета, основанная на введении следующих упрощающих предположений о характере распределения тока в горизонтально-слоистой среде при размещении электродов на дневной поверхности:

– замеряемая величина $\rho_к$ характеризует разрез до некоторой глубины H, целиком определяемой соотношением между размерами приемной (MN) и питающей (AB) линий, причем при MN<<AB величина H составляет AB/2 (практически MN должен быть не более 0,1 AB);

– величина $\rho_к$ определяется только вертикальной составляющей плотности тока, т.е. представляет собой некоторую осредненную электрическую характеристику среды в вертикальном направлении, зависящую от удельных электрических сопротивлений ρ_i каждого слоя, причем "вклад" в величину $\rho_к$ каждого ρ_i зависит от мощности данного слоя h_i (Галин, 1989; Попов и др.,1990).

Принятые допущения позволяют сконструировать следующую простую формулу, устанавливающую соответствие между совокупностью значений ρ_i, h_i многослойного разреза и величиной $\rho_к$:

$$\rho_k = \frac{\rho_1 h_1+\rho_2 h_2+\cdots+\rho_i h_i}{h_1+h_2+\cdots+h_i} = \sum_{i=1}^{n} h_i\rho_i / \sum_{i=1}^{n} h_i, \quad (1)$$

где $\sum_{i=1}^{n} h_{i,m} = H_{i,m}$ – глубина залегания подошвы n-ого слоя.

Поскольку согласно принятому допущению величина H_i полностью определяется соотношением между MN и AB и, следовательно, является известной, формула (1) может быть использована для решения обратной задачи – определения параметров геоэлектрического разреза по совокупности значений $\rho_к$, полученных при различных размерах измерительной установки. Действительно, имея ряд последовательных значений $\rho_{кi}$ и H_i (i=1, 2, ... n), можно последовательно определить h_i и ρ_i, т.е. мощность и удельное сопротивление каждого слоя.

Значит для любого i-го слоя

$$h_i = H_i - H_{i-1} \quad \text{или} \quad h_i = (AB/2)_i - (AB/2)_{i-1} \quad (2)$$

Для вычисления кажущегося электрического сопротивления $\rho_к$ использовалась формула:

$$\rho_k^i = k_{\text{вез.}i}\frac{\Delta U_{i,m}B}{I_{i,m}A}, \quad (3)$$

а удельное электрическое сопротивление отдельных слоев определялось с помощью формулы (4), когда $\rho_i > \rho_{i-1}$ (Галин, 1989; Попов и др., 1990).

$$\rho_i = [\rho_{ki}(AB/2)_i - \rho_{ki-1}(AB/2)_{i-1}]/[(AB/2)_i - (AB/2)_{i-1}] \quad (4)$$

А в случае $\rho_{i-1} > \rho_i$ применяется формула (5) (Попов и др.,1990; Саламов и др., 2015)

$$\sum_k^i \rho i = \frac{\left\{\left[\left(\frac{AB}{2}\right)i - \left(\frac{AB}{2}\right)i-1\right] * \rho\kappa i-1 * \rho\kappa i\right\}}{\left[\rho\kappa i-1 * \left(\frac{AB}{2}\right)i - \rho\kappa i * \left(\frac{AB}{2}\right)i-1\right]}. \quad (5)$$

В отличие от палеточной интерпретации кривых ВЭЗ в данной работе применяется математическая интерпретация формулами (4) и (5). Выражения (2), (3) и (4) являются основными расчетными формулами в предлагаемом способе определения параметров геоэлектрического разреза по данным ВЭЗ для установок с MN<<AB.

Как следует из формул (2), (4) и (5), использование предложенной модели обеспечивает возможность определения мощности и удельного электрического сопротивления любого слоя независимо от параметров вышележащей толщи.

Принимая во внимание вышеизложенное, с целью детального расчленения разреза и более точного определения глубины залегания отдельных литологических разновидностей количество измерений в одной точке наблюдения увеличено в четыре раза. В результате проведенных опытных измерений методом ВЭЗ были приняты следующие размеры питающей AB/2 и приемной MN/2 линий соответственно (в метрах) AB/2 =1; 2; 3; 4; 5; 6; 7; 8; 9; 10,10; 12,12; 14; 16; 18; 20; 22; 24,24; 26,26; 28; 30; 32; 34; 36,36; 38,38; 40,40; 42; 44; 46; 48; 50,50; 52; 54; 56; 58; 60; 63; 66; 69; 72,72; 75,75; 78; 81; 84; 87; 90,90; 93,93; 96; 99;

102; 105; 108; 111; 114; 117; 120; 125,125; 130,130; 135, 140; 145; 150; 155; 160; 165; 170; 175; 180; 185; 190; 195; 200, 200 и MN/2=0,3; 0,3; 0,3; 0,3; 0,3; 0,3; 0,3; 0,3; 0,3; 0,3; 0,3; 0,3; 0,3; 0,3, 1; 0,3, 1; 1; 1; 1; 1; 1; 1,2; 1,2; 2, 2, 2, 2; 2,3; 2,3; 2,3; 3; 3; 3; 3; 3,5; 3,5; 5; 5; 5; 5; 5; 5; 5; 5; 5,7; 5,7; 7; 7; 7; 7; 7,9; 7,9; 9; 9; 9; 9; 9; 9; 9; 9; 9; 9,12; 9,12; 12; 12; 12; 12; 12; 12; 12; 12; 12; 12; 12; 12; 12; 12; 12; 12,15.

Увеличение количества измерений на одной точке наблюдения позволило выявлять маломощные слои в геологическом разрезе (Галин, 1989; Попов и др., 1990; Саламов и др., 2015; Электроразведка…, 2005).

Для полевых измерений использовалась аппаратура АМС-1 с рабочей частотой 4,88 Гц. Измерительная установка ориентирована по направлению северо-запад – юго-восток.

Обсуждение результатов исследования

Измерение температуры производилось в зоне кратера, где главным образом происходят процессы тепломассопереноса при постоянной грифонно-сальзовой деятельности грязевого вулкана. Результаты показали, что температура приповерхностной части грунта обычно близка к температуре приповерхностного воздуха. Тем не менее, удалось обнаружить, что тепловое поле в кратерной части грязевых вулканов преимущественно контролируется тепломассопотоком по выводящим каналам грифонов и сальз.

Обычно измерения температуры производились на двух и более уровнях в интервале глубин 0,5-1,5 м, а при измерении внутри грифона иногда глубина достигала 16 метров и более. Это давало возможность определить температурные градиенты в области кратера грязевого вулкана.

Изучение распределения температурных градиентов по глубине и по площади, а также на отдельных грязевых вулканах позволяет судить об их термальной активности. В табл. 1 приведены некоторые результаты определения температурного градиента в приповерхностных слоях области кратера некоторых грязевых вулканов, произведенного во второй половине октября 1992 года. Интересно, что, за исключением грязевого вулкана Хамамдаг, получены положительные градиенты температур, свидетельствующие о поступлении тепла из глубины на поверхность.

При замерах, сделанных 29 июня 2006 года на грязевом вулкане Дашгиль, получены совсем другие результаты. На этот раз градиенты температуры в большинстве случаев оказались отрицательными, что указывает на перенос тепла с поверхности на глубину. Это нормальное явление в летнее время, когда температура на поверхности достигает 30°C, а температура «нейтрального слоя» составляет около 15°C. Зимой температура поверхности оказывается ниже 10°C и температурный градиент меняет знак. Кратерная зона грязевого вулкана характеризуется множеством активных грифонов и сальз. Поэтому приповерхностный градиент температуры в этой зоне контролируется флюидопотоком по жерлу вулкана. В активные периоды грифонно-сальзовой деятельности увеличивается поток флюидов (тем самым и поток тепла) из глубины, и приповерхностный градиент температуры может менять знак под влиянием этого потока тепла.

Таблица 1

Грязевой вулкан	Градиент температуры				Плотность ТП (среднее), мВт/м^2
	Значения, К/м (°C/м)		n	Интервал глубины, м	
	min/max	Средний			
Бахар*	16,66/19,94	17,25(в области кратера) 9,85(вне кратера)	3 1	0,5 - 1,0 0,5 - 0,7	$23{,}29\cdot10^3$ $13{,}3\cdot10^3$
Дашгиль	1,58/3,58	2,55	3	0,5 - 1,0	$34{,}42\cdot10^2$
Айрантекен	1,82/5,84	3,31	6	0,5 - 1,0	$44{,}68\cdot10^2$
Чеильдаг	0,18/2,12	1,24	5	0,5 - 1,0	$16{,}74\cdot10^2$
Агзыбир	0,08/1,04	0,58	10	0,5-1,5	$78{,}3\cdot10^1$
о. Зенбил*	10,5/21,25	15,62	4	0,5-1,5	$21{,}09\cdot10^3$
о. Харе-Зиря	0,07/2,42	0,87	7	0,5-15,0	$11{,}75\cdot10^2$
Хамамдаг	-2,76/0,09	–	14	0,5-12,0	–
Отманбоздаг	2,35/6,67	3,51	6	0,6-1,5	$47{,}38\cdot10^2$

*) Примечание: замеры температуры на грязевом вулкане Бахар производились через 13 суток, а на грязевом вулкане о. Зенбил – через два месяца после извержения

Результаты температурной съемки в кратерной области грязевых вулканов показали, что поверхностное распределение температуры для некоторых из них описываются концентрическими изотермами с одним центром, а для других характерны максимумы температуры в области кратера. По этим данным можно судить о том, что форма выводного канала у различных грязевых вулканов различная. Выводной канал некоторых грязевых вулканов (например, Отман-Боздага, Кейреки и др.) не разветвляется у поверхности. У других (например, Локбатана, Бахара, Дашгиля и т.п.) канал разветвляется, образуя множество грифонов, сальз и т.п. Поэтому распределение температуры в кратере различных грязевых вулканов отличается друг от друга (Мухтаров и Адыгезалов, 1997; Kadirov, Mukhtarov, 2004; Mukhtarov, 2003; Mukhtarov et al., 2003).

Результаты электроразведочных работ также подтвердили это предположение. Интерпретация данных ВЭЗ показала, что кажущееся сопротивление горных пород, слагающих геологический разрез площади исследования, меняется в интервале 1-14 Ом·м, а удельное электрическое сопротивление – 0,1-35 Ом·м. По этим данным можно обнаружить близвертикальные зоны с низким электрическим сопротивлением, которые предположительно соответствуют жерлу и выводящим каналам и иногда разветвляются вблизи поверхности (рис. 2a).

В результате проведенных исследований методом ВЭЗ по профилями I-I…X-X (рис. 1) были построены разрезы кажущегося электрического сопротивления ($\rho_{к.э.с}$) и геоэлектрические разрезы по значениям удельного электрического сопротивлений ($\rho_{у.э.с}$), которые затем были преобразованы в предполагаемый литолого-геофизический разрез (рис. 2a).

Как было отмечено, площадь исследования покрыта грязевулканическими отложениями. В литолого-геофизических разрезах прослеживаются три слоя, мощность которых меняется примерно от 3,0 до 130 м. По данным геофизических исследований мощность этих отложений по площади составляет в среднем 50-60 м, у.э.с. – 2-8 Ом·м на ЮВ, а на СЗ – 10-15 Ом·м. В составе этих отложений имеются обломки разных литологических разновидностей, таких как песчаники, гравий, глины и др. (рис.2b).

Предполагаемые физические, физико-химические и физико-механические параметры грязевулканической брекчии на площади исследования меняются в среднем в следующих пределах: у.э.с – ρ=2,1-8,7 Ом·м, плотность – $\gamma_т$= 1,62-1,89 т/м^3, плотность под водой – $\gamma_{тw}$= 0,52-1,01 т/м^3, плотность скелета – γ =1,13-1,57т/м^3, естественная влажность –$W_т$=29,5-39,8%, полная влагоемкость – $W_о$=29,1-53,4%, поры, заполненные водой – $W_п$ = 40,2-45,3%, коэффициент водонасыщения – K_w = 0,6894-0,8240, пористость – n=40,9-69,5%, глинистость – G=38,1-54,1 %, пластичность – t=15,4-20,3% (Оленченко и др., 2015).

В подошве вулканической брекчии прослеживается пласт, составленный из глин мощностью примерно 40-130 м, которые являются коренными отложениями с у.э.с. 3-10 Ом·м и выходят в юго-восточной части площади на дневную поверхность (ВЭЗ № 21-12). В северо-западной части профиля кровля этого пласта залегает на уровне минус 16 м по абсолютным отметкам, в районе жерла вулкана – минус 20 м, а на юго-восточном окончании профиля – минус 3 м. Снизу первый пласт мощностью 35-80 м с у.э.с. 10-25 Ом·м прослеживается по всему разрезу профиля, в литологическом отношении предположительно составленный из глин с прослойками песков.

В интервале исследованных глубин обнаруживается субвертикальная зона с низким у.э.с. 0,2-1,3 Ом·м (что соответствует легко проницаемым породам), которую можно считать выводящим каналом грязевого вулкана Дашгиль (рис. 2a, 3). Помимо этого, при интерпретации профилей ВЭЗ выделяется ряд разрывных нарушений, отраженных на рис. 1 и 2a.

Результаты проведенных геофизических исследований позволяют предполагать, что после завершения осадконакопления в морских условиях произошло семь извержений грязевого вулкана Дашгиль (по «Каталогу …» – шесть (Алиев и др., 2009)). Предполагается, что в периоды извержений после каждого излияния брекчии ее поверхность высыхает и отвердевает быстрее, чем подошва, и в подошве каждого слоя брекчии остается неотвердевший легко проницаемый слой с у.э.с. 0,2-1,3 Ом·м. В дальнейшем при каждом новом извержении происходит проникновение жидкой фазы продуктов извержения в эти легко проницаемые зоны (рис. 2c). Предполагаемые физические, физико-химические и физико-механические параметры слоев, составленных из сопочной брекчии, отличаются друг от друга. Это дает основание предполагать, что каждое очередное извержение грязевого вулкана происходит из разных пластов, расположенных на разных глубинах и характеризующихся различным литологическим составом (рис. 2c).

На основе данных малоглубинной электроразведки составлена 3D модель кратерной области грязевого вулкана Дашгиль (рис. 3). На ри-

сунке выделяется субвертикальная низкоомная область – предполагаемый канал грязевого вулкана, который расщепляется с приближением к поверхности. Одному из них на поверхности соответствует поле грифонов, а другому – сальза. У.э.с. этой субвертикальной зоны составляет 0,2-1,3 Ом·м. Возможность существования подобной легко проницаемой субвертикальной зоны под кратером грязевого вулкана отмечалась еще и в более ранних геотермических и гравиметрических работах (Mukhtarov et al., 2003; Kadirov and Mukhtarov, 2004).

Результаты настоящих исследований позволили показать, что кратер и выводящие каналы грязевого вулкана Дашгиль расположены на участке пересечения разнонаправленных разрывных нарушений, что отражено на вышеприведенных рисунках (рис. 1, 3).

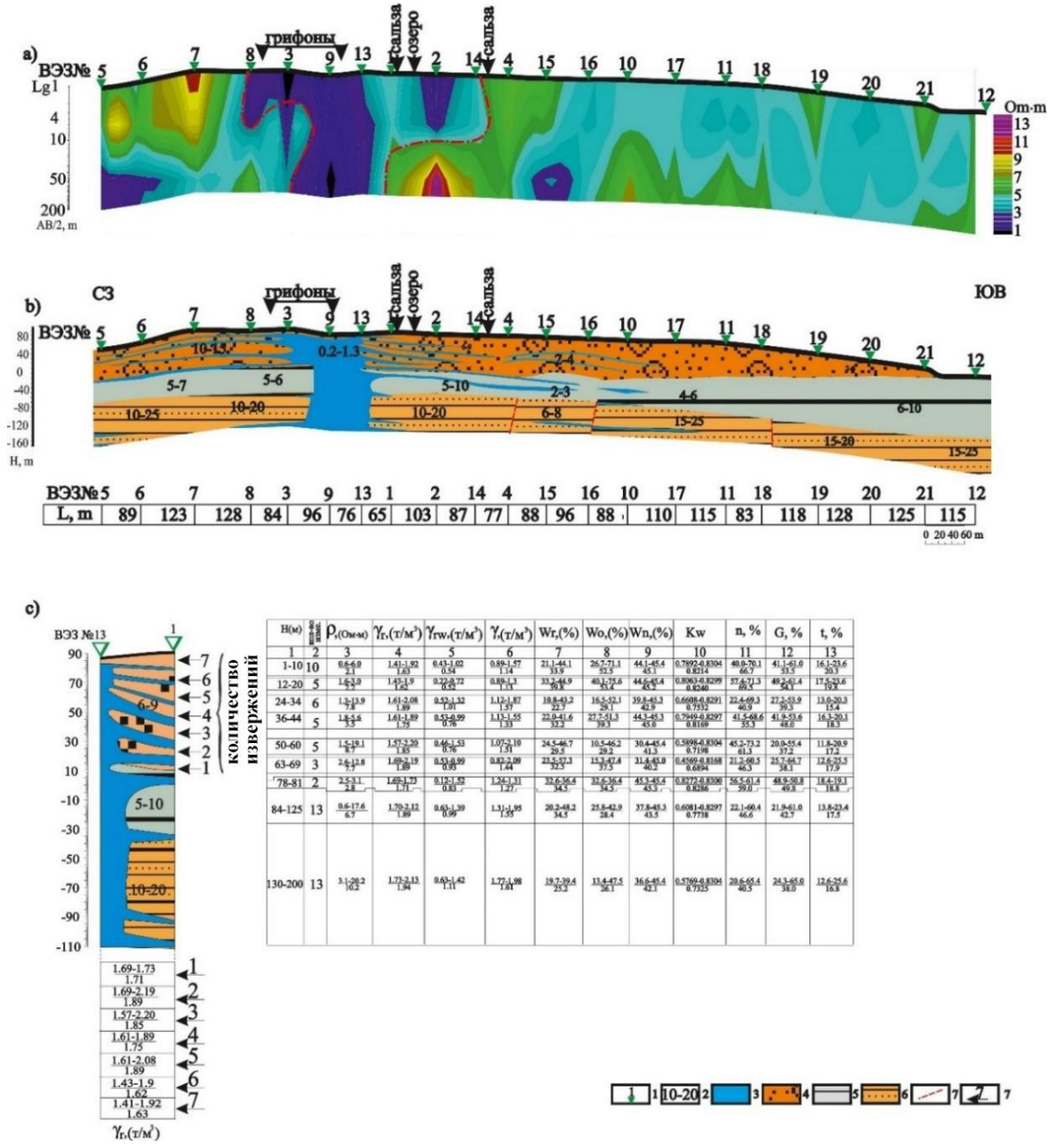


Рис. 2. Разрезы кажущегося электрического сопротивления (а) и предполагаемый литолого-геофизический (б), составленный по данным ВЭЗ по профилю I-I.
1 – номера точек ВЭЗ; 2 – удельное электрическое сопротивление пород, слагающих геологический разрез; 3 – грязевулканические флюиды, проникающие через жерло грязевого вулкана; 4 – грязевулканическая брекчия; 5 – глины; 6 – глины, чередующиеся с мелкозернистыми слабоцементированными песками; 7 – предполагаемые разрывные нарушения, выявленные по данным ВЭЗ

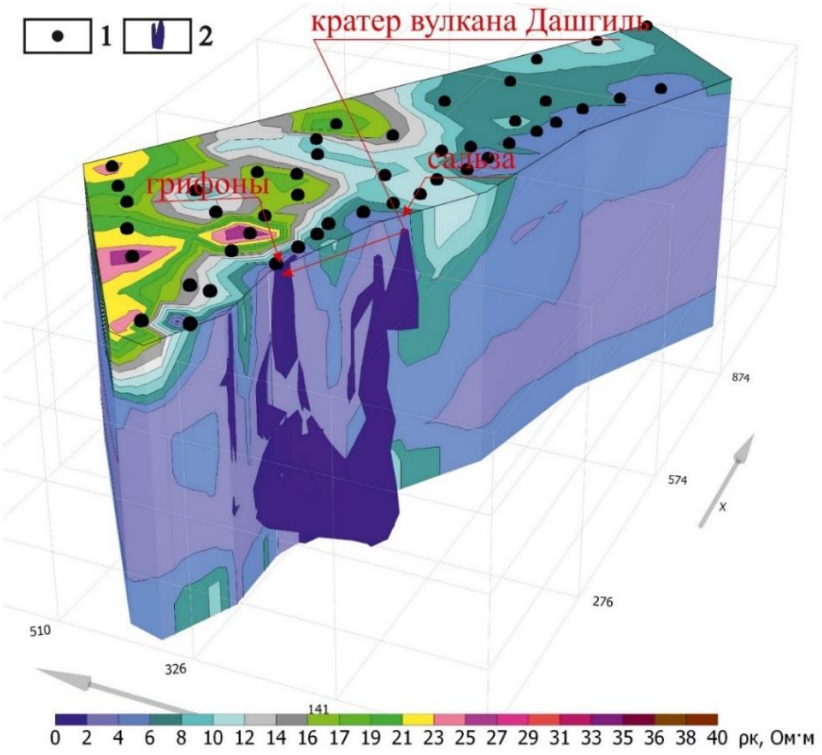


Рис. 3. 3D модель грязевого вулкана Дашгиль.
1 – точки ВЭЗ; 2 – предполагаемые выводящие каналы вулкана

Заключение

В заключении можно отметить, что грязевые вулканы – это геологические объекты, которые выделяются на поверхности Земли не только своими внешними, морфологическими признаками, но и геофизическими полями. На гравитационном поле они выявляются гравитационными минимумами. Корни (область, где накапливаются извергаемые флюиды) и каналы грязевых вулканов определяются как разуплотненные объекты (Kadirov and Mukhtarov, 2004). По этим каналам постоянно просачиваются флюиды, которые переносят тепло из глубинных участков на поверхность. Поэтому каналы грязевых вулканов характеризуются высокими относительно окружающих пород температурами и температурными градиентами. На поверхности тепловые аномалии отмечаются только при активизации деятельности вулкана или при его извержении. Эти данные подтверждаются результатами электроразведочных исследований. На 3D модели выделяется расположенная под грифонами и сальзами субвертикальная зона с физическими свойствами (низкоомные, с низкой плотностью и высокой проницаемостью), отличными от окружающих пород. Таким образом, грязевой вулкан состоит из основного глубинного теплового очага (5-10 км), насыщенного флюидами очага извержения (3-6 км), а также некоторых промежуточных очагов, соединенных между собой выходящим на поверхность субвертикальным выводящим каналом с высокой флюидопроницаемостью (Мухтаров и Адыгезалов, 1997). Верхний двухсотметровый участок этого канала выявлен в результате исследований авторов методом ВЭЗ и показан на трехмерной модели (рис. 3).

Благодарности

Данная работа была выполнена при финансовой поддержке Фонда Развития Науки при Президенте Азербайджанской Республики – **Грант № EİF KEPTL-2-2015-1(25)-56/31/2.**

ЛИТЕРАТУРА

Али-заде С.А., Байрамов А.А., Мамедов А.В., Ширинов Н.Ш. Геология четвертичных отложений Азербайджана. Элм. Баку, 1978, 159 с.

Алиев Ад.А., Гулиев И.С., Рахманов Р.Р. Каталог извержений грязевых вулканов Азербайджана (1810-2007 гг.). Nafta-Press. Баку, 2009, 110 с.

Галин Д.Л. Интерпретация данных инженерной геофизики.

REFERENCES

Aliyev Ad.A., Guliyev I.S., Rakhmanov R.R. Catalog of eruptions of mud volcanoes of Azerbaijan (1810-2007). Nafta-Press. Baku, 2009, 110 p. (in Russian).

Alizadeh S.A., Bayramov A.A., Mammadov A.V., Shirinov N.Sh. Geology of Quaternary sediments of Azerbaijan. Elm. Baku, 1978, 159 p. (in Russian).

Electrical survey. Textbook on electrical exploration practice for

Недра, 1989, 114 с.

Мухтаров А.Ш., Адыгезалов Н.З. Термальный режим грязевых вулканов Восточного Азербайджана. Труды Института геологии АН Азербайджана, № 26, Баку, 1997, с. 221-228.

Оленченко В.В., Шнюков Е.Ф., Гаськова О.Л., Кох С.Н., Сокол Э.В., Бортникова С.Б., Ельцов И.Н. Динамика извержения грязевого вулкана на примере сопки Андрусова (Булганакский грязевулканический очаг, Керченский полуостров). ДАН, Т. 464, № 2, 2015, с. 214-219.

Попов Е.А., Тен К.М., Фунтиков Г.Н., Селяков В.И., Глушко С.П. Методические рекомендации по использованию ВЭЗ для детального расчленения разреза при решении геологических и инженерно-геологических задач. Ротапринт. Москва, 1990, 52 с.

Саламов А.М., Кадыров А.Г., Саламов Ф.А., Пашаев Т.Р. Исследование оползня в Хызынском районе Азербайджана методом вертикального электрического зондирования. Инженерные изыскания, № 5-6, 2015, с. 50-56.

Смирнов Я.Б. Тепловое поле территории СССР (пояснительная записка к картам теплового потока и глубинных температур в масштабе 1:10000000). ГУГК. Москва, 1980, 150 с.

Холодов В.Н. Грязевые вулканы: распространение и генезис. Геология и полезные ископаемые Мирового океана, № 4, Москва, 2012, 5-27 с.

Электроразведка: пособие по электроразведочной практике для студентов геофизических специальностей. В.К.Хмелевский, И.Н.Модин, А.Г.Яковлев (под ред.). Научный мир. Москва, 2005, 311 с.

Якубов А.А., Ализаде А.А., Зейналов М.М. Атлас грязевых вулканов Азербайджанской ССР. Элм. Баку, 1971, 258 с.

Hamza V.M., Cardoso R.R., Ponte Neto C.F. Global heat flow: fantasy and facts. Sixth Intern. Meeting “Heat flow and the structure of the lithosphere”, Bykov near Pilsen, Czech Republic, 2006, 24 p.

Kadirov F.A., Mukhtarov A.Sh. Geophysical fields, deep structure, and dynamics of the Lokbatan mud volcano. Izvestiya, Physics of the Solid Earth, V. 40, № 4, 2004, pp. 327-333.

Kopf A., Stegmann S., Delisle G. et al. In situ cone penetration tests at the active Dashgil mud volcano, Azerbaijan: Evidence for excess fluid pressure, updoming, and possible future violent eruption. Marine and Petroleum Geology, V. 26, 2009, pp. 1716-1723.

Mukhtarov A. Heat transfer by fluids of mud volcanoes and hydrothermal processes. Proceedings of the 38th Conference of Sosiete Internationale des Techniques Hydrothermales and the 56th Annual Meeting of the Balneological Society of Japan. Beppu, Japan, 2003, pp. 295-300.

Mukhtarov A., Kadirov F., Guliyev I., Lerche I. Temperature evolution in the Lokbatan mud volcano crater (Azerbaijan) after the eruption of 25 October 2001. Energy Exploration & Exploitation, V. 23, № 3, 2003, pp. 187-207.

students of geophysical specialities. Khmelevsky V.K., Modin I.H. and Yakovlev A.G. (ed.). Nauchny mir. Moscow, 2005, 311 c. (in Russian).

Galin D.L. Interpretation of engineering geophysics data. Nedra. Moscow, 1989, 114 p. (in Russian).

Hamza V.M., Cardoso R.R., Ponte Neto C.F. Global heat flow: fantasy and facts. Sixth Intern. Meeting “Heat flow and the structure of the lithosphere”, Bykov near Pilsen, Czech Republic, 2006, 24 p.

Kadirov F.A., Mukhtarov A.Sh. Geophysical fields, deep structure, and dynamics of the Lokbatan mud volcano. Izvestiya, Physics of the Solid Earth, V. 40, № 4, 2004, pp. 327-333.

Kholodov V.N. Mud volcanoes: distribution and genesis. Geology and mineral resources of the World Ocean, № 4, Moscow, 2012, pp. 5-27 (in Russian).

Kopf A., Stegmann S., Delisle G. et al. In situ cone penetration tests at the active Dashgil mud volcano, Azerbaijan: Evidence for excess fluid pressure, updoming, and possible future violent eruption. Marine and Petroleum Geology, V. 26, 2009, pp. 1716-1723.

Mukhtarov A.S., Adigozelov N.Z. Thermal regime of East Azerbaijan mud volcanoes. Proceedings of Geology Institute of AS Azerbaijan, № 26, 1997, pp. 221-228 (in Russian).

Mukhtarov A. Heat transfer by fluids of mud volcanoes and hydrothermal processes. Proceedings of the 38th Conference of Sosiete Internationale des Techniques Hydrothermales and the 56th Annual Meeting of the Balneological Society of Japan. Beppu, Japan, 2003, pp. 295-300.

Mukhtarov A., Kadirov F., Guliyev I., Lerche I. Temperature evolution in the Lokbatan mud volcano crater (Azerbaijan) after the eruption of 25 October 2001. Energy Exploration & Exploitation, V. 23, № 3, 2003, pp.187-207.

Olenchenko V.V., Shnyukov E.F., Gaskova O.L., Kokh S.N., Sokol E.V., Bortnikova S.B., Eltsov I.N. Dinamics of eruption of mud volcano sopka Andrusova (Bulganak mud volcanic focus, Kerch peninsula). Doklady AS, V. 464, № 2, 2015, pp. 214-219 (in Russian).

Popov E.A., Ten K.M., Funtikov G.N., Selyakov V.I., Glushko S.P. Guidelines for the use of VES for the detailed dissection of the section in solving geological and engineering-geological problems. Rotaprint. Moscow, 1990, 52 p. (in Russian).

Salamov A.M., Kadirov A.G., Salamov F.A., Pashayev T.R. Investigation of the landslide in the Khizi region of Azerbaijan by the method of Vertical Electrical Sounding. Inzhenerniye izyskaniya (engineering survey), № 5-6, 2015, pp. 50-56 (in Russian).

Smirnov Ya.B. Thermal field of the USSR territory (explanatory note to the maps of heat flow and deep temperatures on a scale of 1: 10,000,000). GUGK. Moscow, 1980, 150 p. (in Russian).

Yakubov A.A., Alizadeh A.A., Zeynalov M.M. Atlas of mud volcanoes of the Azerbaijan SSR. Elm. Baku, 1971, 258 p. (in Russian).

3D ГЕОФИЗИЧЕСКАЯ МОДЕЛЬ БЛИЗПОВЕРХНОСТНОЙ СТРУКТУРЫ ГРЯЗЕВОГО ВУЛКАНА ДАШГИЛЬ

Саламов А.М., Мухтаров А.Ш., Маммадов В.А.
Институт геологии и геофизики НАН Азербайджана,
AZ1143, г.Баку, просп. Г.Джавида, 119: avazsalamov@mail.ru

Резюме. В статье рассматриваются результаты (электроразведочных, геотермических и гравиметрических) геофизических исследований, проведенных в кратерной области некоторых грязевых вулканов. Несмотря на малую глубину (до 200 м) электроразведочных работ, в комплексе с другими методами они дают убедительное представление о строении рассматриваемого участка земной коры (зоне кратера грязевого вулкана Дашгиль). Совместный анализ этих результатов позволяет

предполагать существование в разрезе субвертикальных зон, физические свойства которых отличаются от свойств пород, характеризующих окружающую среду. Корни (область, где накапливаются извергаемые флюиды) и каналы грязевых вулканов выделяются как разуплотненные объекты. По этим каналам постоянно просачиваются флюиды, которые переносят тепло из глубинных участков на поверхность. Поэтому каналы грязевых вулканов относительно окружающих пород выявляются высокими температурами и температурными градиентами. На поверхности тепловые аномалии отмечаются только при активизации деятельности вулкана или при его извержении. Эти данные подтверждаются результатами электроразведочных исследований. Трехмерная модель, построенная по результатам ВЭЗ (вертикального электрического зондирования), позволяет визуально отобразить это предположение. По данным ВЭЗ также составлен предполагаемый литолого-геофизический разрез, позволяющий выделять слои сопочной брекчии каждого извержения.

***Ключевые слова**: грязевой вулкан, структура, кратер, жерло, геофизические исследования, вертикальное электрическое зондирование (ВЭЗ), модель, температура, градиент, тепловой поток*

DAŞGİL PALÇIQ VULKANI SƏTHƏ YAXIN STRUKTURUNUN 3D GEOFİZİKİ MODELİ

Salamov A.M., Muxtarov A.Ş., Məmmədov V.A.
AMEA Geologiya və Geofizika İnstitutu
AZ1143, Bakı, H.Cavid prosp., 119: avazsalamov@mail.ru

Xülasə. Məqalədə bəzi palçıq vulkanlarının krater sahəsində aparılan geofiziki (elektrik kəşfiyyatı, geotermik və qravimetrik) tədqiqatların nəticələrinə baxılır. Elektrik kəşfiyyat işlərinin kiçik dərinlikdə (200 m-ə qədər) aparılmasına baxmayaraq, onlar başqa üsullarla birlikdə yer qabığının baxılan sahəsinin (Daşgil palçıq vulkanının krater zonasının) quruluşu haqda əsaslı təsəvvür verir. Palçıq vulkanlarının kökləri və kanalları (püskürmə materiallarının toplandığı əsas həcm-məkan) sıxlığı az olan parçalanmış məsaməli obyekt kimi seçilir. Flüidlər daima bu kanallar boyunca süzülərək səthə çıxır və dərin layların istiliyini səthə daşıyır. Buna görə də palçıq vulkanlarının kanalları ətraf süxurlara nisbətən yüksək temperatur və temperatur qradiyenti ilə seçilirlər. Alınan nəticələrin birgə təhlili kəsilişdə xassələri vulkanın çıxış kanallarının fiziki xassələrinə uygun olan, lakin ətraf süxurların fiziki xassələrindən fərqlənən subşaquli zonaların mövcud olmasını fərz etməyə imkan verir. Şaquli Elektrik Zondlamanın (ŞEZ) nəticələri əsasında qurulmuş üçölçülü model bu fərziyyəni vizual əks etdirməyə imkan verir. Həmçinin ŞEZ-ın məlumatları əsasında hər püskürmənin brekçiya layını ayırmağa imkan verən fərz edilən litoloji-geofiziki kəsiliş qurulmuşdur.

***Açar sözlər**: palçıq vulkanı, struktur, krater, vulkan boğazı, geofiziki tədqiqatlar, Şaquli Elektrik Zondlaması (ŞEZ), model, temperatur, qradient, istilik seli*

ANAS Transactions Earth Sciences 1 / 2019

Geography

http://www.journalesgia.com

FEATURES OF SEASONAL CHANGES OF THE CASPIAN SEA LEVEL

Safarov E.S.[1], Cretaux J.-F.[2], Mammadov R.M.[1], Arsen A.[3], Safarov S.H.[1]

[1]*Institute of Geography of ANAS*

115, H.Cavid av., Baku, Azerbaijan, AZ1143: elnur.safarov@geo.az

[2]*CNES/Legos*

14, avenue Edouard Belin, Toulouse, France, 31400

[3]*Freelancer, Warsaw, Poland*

Keywords: *The Caspian Sea, Volga River, satellite altimetry, track, Jason 1-2, ENVISAT, amplitude, phase, sea level*

Summary. The Caspian Sea is the largest closed reservoir in the world. In the absence of a direct connection with the world ocean, the closed Caspian Sea is characterized by significant secular changes, inter-annual and seasonal variability in the level. In the work, according to observations of radar altimetry of ENVISAT, Jason 1 and Jason 2 satellites, seasonal variations in the level of the Caspian Sea, as well as features of their amplitude distribution, also the phases of their appearance over the entire sea area, are investigated. According to a special method, the average annual values of the amplitude and the occurrence phase of seasonal fluctuations of water level for various areas of the sea area were calculated using pre-determined satellite tracks. The influence of the Volga River flow on the amplitude and phase of seasonal variations in the various areas of the Caspian Sea level has been studied. Studies have shown that the amplitude of seasonal fluctuations in sea level of the North Caspian Sea is greater than in the Middle and South Caspian. They also differ in direction from east to west. The earliest phases of the sea level amplitudes were recorded in the Northern Caspian, below the Volga delta (in May), and in the rest of the sea – much later (June-July). It has been established that the influence of the Volga River flow is most sensitive in the northern part of the sea, and towards the south its influence gradually decreases, and other factors start to prevail (evaporation, precipitation). The paper discusses the reasons for this difference.

© 2018 Earth Science Division, Azerbaijan National Academy of Sciences. All rights reserved.

Introduction

One of the main factors affecting to seasonal fluctuations of the Caspian Sea level is river water input (Volga, Ural, Kura, Terek, etc.). The Volga provides 78-82% of the total river input to the Caspian Sea (Гидрометеорология и гидрохимия морей, 1990). Even though other rivers have some slightly different physical-geographical conditions, the intra-annual variations of the surface waters flowing to the sea, in general correspond to intra-annual river inflow of the Volga River. High water period with maximal discharge of the Volga River is observed in May and June (Fig. 1).

In order to analyze the spatial and temporal distribution of seasonal sea water level fluctuations and the influence of the river flow of the Volga River on this distribution, it is necessary to create spatial and temporal distribution maps of the sea level amplitude and phases of its occurrence for the whole surface of the Caspian Sea. However, it is impossible to solve this problem according to the in-situ observations, because they cover only coastal regions. Thus, for this purpose it is more expedient to use remote sensing data, which are much attractive in case when contact measurements cannot be conducted because of geographic, political or economic reasons (Troitskaya et al., 2011).

Since the launch of Topex/Poseidon in 1992 many studies have shown the high potential of radar altimetry for the monitoring of lake height variations (Birkett, 1995; Coe and Birkett, 2004; Aladin et al., 2005; Crétaux et al., 2005; Hwang et al., 2005; Crétaux and Birkett, 2006; Crétaux et al., 2009; Crétaux et al., 2011b; Hwang et al., 2011; Lee et al., 2011; Gao et al., 2012; Zheng and Bastiaanssen, 2013; Arsen et al., 2015; Chen et al., 2017). The main advantages of this remote sensing method is global coverage and high penetrating ability of radio waves through the atmosphere and clouds. This

allows to perform investigation practically in all weather conditions, as well as in condition of the presence of sufficiently high aerosol concentrations in the air (Troitskaya et al., 2011). For the Caspian Sea satellite radar altimetry data were successfully used since Topex/Poseidon launch in 1993 (Kouraev et al., 2011). However, taking into account the temporal variability of the water regime of the Caspian Sea, it is of great interest to study sea level amplitude and phase distribution using recent data of Jason 2. It should be taken into consideration that the satellites of the Jason series have an advantage in the frequency of data repetition, and the ENVISAT satellite is preferable regarding the density of track distribution over the sea's water area. The accuracy of measuring by Jason satellites over the oceans is 2 cm (Fu et al., 2001), but the error in calculating the altitude of the sea surface in relation to the reference ellipsoid reaches 4.2 cm (Chelton et al., 2001). The accuracy of measurements by ENVISAT vary depending on target size (Arsen et al., 2015) and is generally 4-5 cm for big open water bodies (Crétaux et al., 2011a; Lebedev et al., 2005).

Used material and research methodology

The satellite altimetry observation data of ENVISAT (2002-2009) GDR v2, Jason 1 (2002-2009) GDR-C and Jason 2 (2008-2013) GDR-D data used in this work were obtained from Centre of Topography of the Oceans and the Hydrosphere (ctoh.legos.obs-mip.fr) and processed in collaboration with LEGOS/ECHOS research group (www.legos.obs-mip.fr).

The Caspian Sea surface intersects with 8 Jason 1-2-3 tracks (016, 031, 057, 092, 107, 133, 168, 209 and 244). Four of them are ascending, and 4 descending (Fig. 2). The revisit time for each of these tracks is about 10 (9.9156) days. The longest track (092) is about 1000 km long and crosses the sea from Iranian coast in the South to the southern boundary of the Volga Delta (territory of the Russian Federation) in the North. The Caspian Sea intersects with 25 tracks of the ENVISAT satellite as well. Of these, 14 are ascending, and 11 are descending. The revisit time for each of these tracks was about 35 days. The gaps between ENVISAT tracks are smaller then that of Jason 1, Jason 2 which allow us to retrieve more information about the distribution of seasonal sea-level amplitudes and their phases of occurrence throughout the water area.

In order to identify the annual maximum amplitudes and their phases of occurrence in the entire water area of the Caspian Sea, an integrated research along the corresponding tracks, consisting of three stages was carried out.

In the first stage, satellite data for the Jason 1, Jason 2 and ENVISAT were geographically delimited. For each track for each satellite the sea level was calculated using LEGOS processing chain which was described by Cretaux et al., 2011a. The sea level is calculated as follows:

$$SSH = \text{altitude} - \text{corrected range},$$

where SSH is the sea surface height, altitude is the satellite orbit, and corrected range is the measured range with atmospheric path delay and geophysical corrections. The expression for the sea level anomaly is as follows:

$$SLA = SSH - MSS,$$

where SLA is the sea level anomaly, and MSS is the mean sea surface.

In an open sea and in the ocean, estimation of sea level is usually done with averaged 1 Hz data. For the Caspian Sea the averaging of the sea level was carried out over 10 km strips. Outliners inside each patch were filtered using a 3-sigma test.

At the second stage of the study the spatial and temporal distribution of sea level is analyzed. For each satellite for each track, the 10 km averaged sea level time series are used to determine annual mean, annual maximum and minimum values of the sea level anomalies and phase (the day of the year of their occurrence). Here, the definition of the amplitude is considered as half of the difference between the maximum and minimum level anomalies, observed in one year. For each 10 km patch the average multi-annual amplitudes and the phases were also calculated.

Finally, after the completion of the first and second stages of the studies, based on satellite altimetry observations data maps of the distribution of the mean annual maximum amplitudes and the phases of their occurrence throughout the all water area were created using ArcGIS 10.3 (Fig. 2 and 3).

Results and discussions

Fig. 1 reflects monthly distribution of the Volga River water discharge based on in-situ observation data, conducted from measurement point Verkhnee Lebyazhye during 2002-2013. As seen, the value of the river flow begins to grow in March and reaches the maximum in May. Despite the fact that the maximum water discharge in Volga is observed in May, the spatial variability of the amplitude and phases of sea level observations indicate the complexity of these changes (Fig. 2 and 3).

According to the data taken from Jason 1 and Jason 2 satellites for the 2002-2013 period of observations, the largest amplitudes (43-48 cm) of seasonal sea level changes (Fig. 2a) were observed in the eastern part of the North Caspian (track 133) from June 25 to July 5 (Fig. 2b). In the Northern Caspian, south to the Volga Delta (tracks 57 and 168), relatively high values (33-38 cm) of amplitude in the sea level were also observed (Fig. 2a) from mid-May to early June (Fig. 2b). The relatively bigger values of the seasonal sea level fluctuations amplitude, can be explained by the enormous influence of the flow from the Volga and Ural rivers, as well as such factors as the shallow waters, the nature of surface currents and, partially, the effect of relatively light fresh water that enters the sea with rivers discharge.

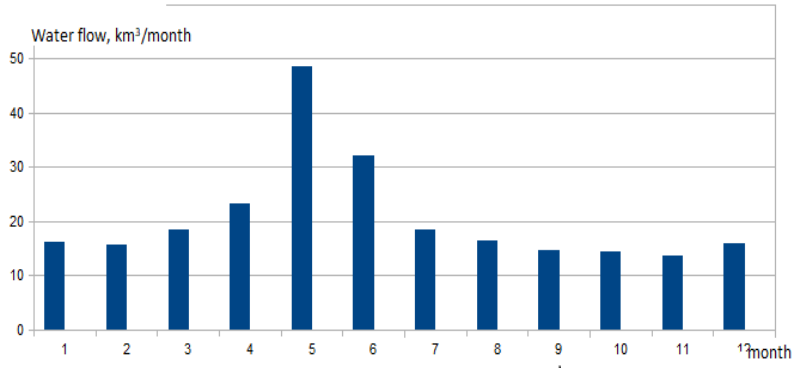


Figure 1. The histogram of intra-annual average water flow discharge of the Volga River based on the observation data for 2002-2013

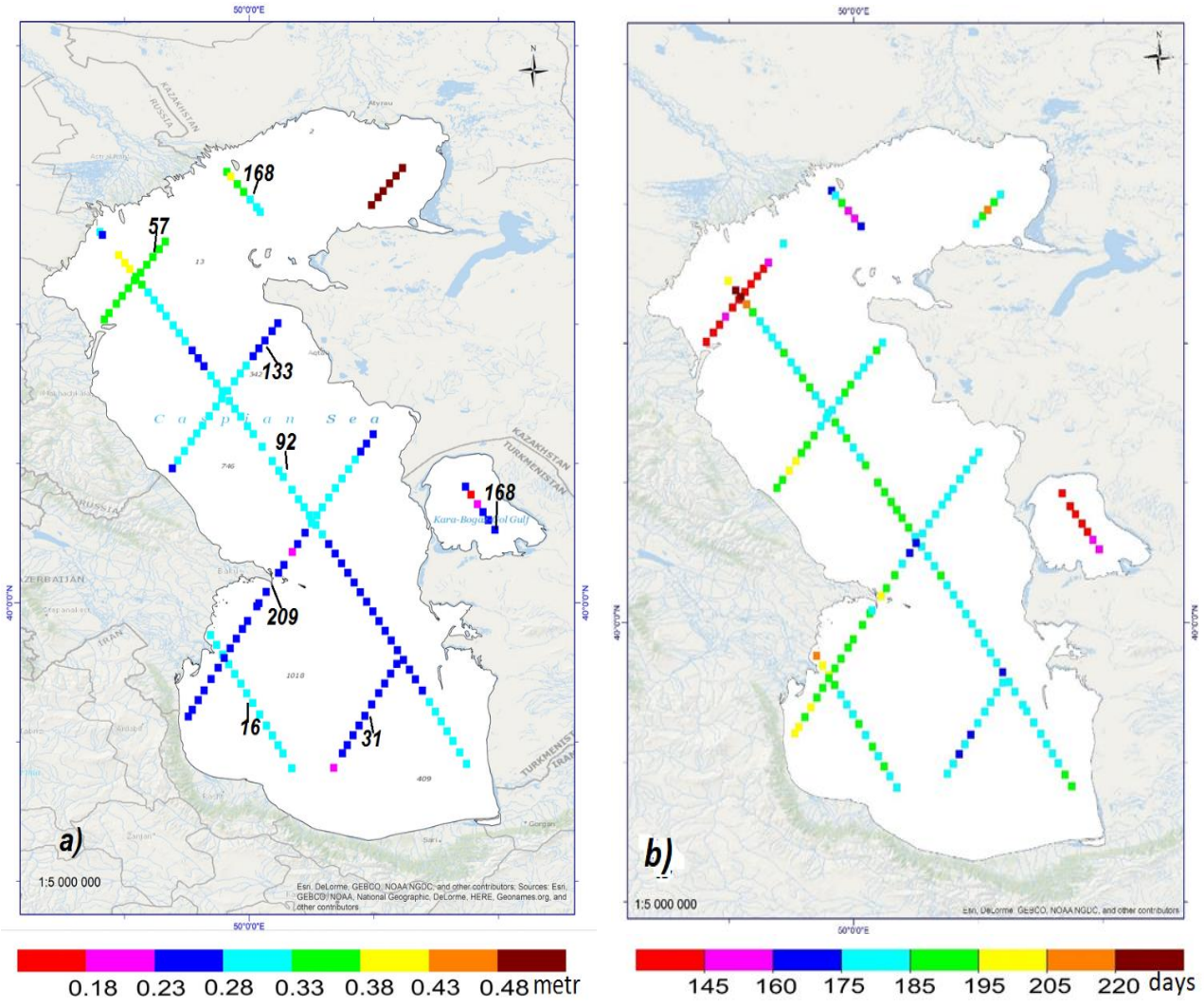


Figure 2. Distribution maps for tracks of annual level amplitudes in the Caspian Sea (a) and the phases of their occurrence (b) based on the data of the altimetry observations of the Jason 1, Jason 2 satellites for 2002-2013

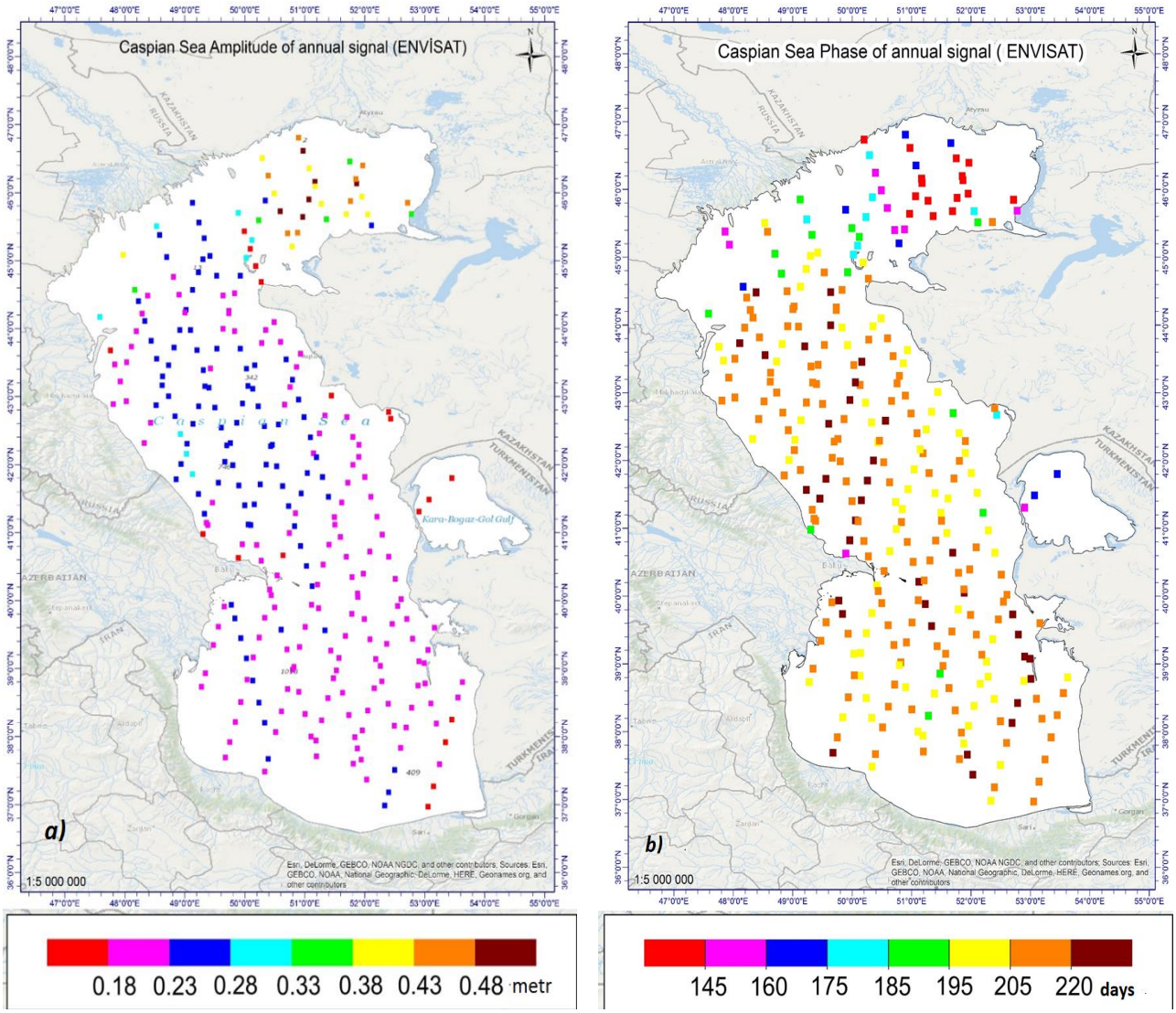


Figure 3. Maps of distribution for tracks of annual level amplitudes (a) in the Caspian Sea and the phases of their occurrence (b) based on the data of the altimetry observations of the ENVISAT satellite for 2002-2013

It should be noted that the results obtained here are slightly different from those obtained with the help of Topex/Poseidon data (Kouraev et al., 2011), where the available seasonal amplitude values are smaller, and observation phases of them are bigger. However, the comparison with the data of ground in-situ stations (Abuzyarov, 2011) shows that the values of amplitudes and phases of observation, obtained in this study are much closer to the real values. This, incidentally, is also noticeable from the graphs of sea level evolution basing on data of ground and satellite observations.

In the Middle Caspian, the sea level amplitude is relatively lower than in the Northern Caspian. Along the track 092 in the deep-water areas, it varies around 28-33 cm (Fig. 2a). This result has a good agreement with the observation data from the coastal region stations (Abuzyarov, 2011). In the relatively northern part of the deep-water area, the phases of occurrence of the sea level amplitudes are observed from June 25 to July 5, and in the southern part – in July 5-15 (Fig. 2b). The amplitude phases to the east of track number 92 are related to an earlier period, whereas to the west – on the opposite (tracks 133 and 209). If we compare with the bottom topography map, it can be concluded that in the shallow water areas of the Middle Caspian, seasonal amplitudes of the level are observed at an earlier time than in the deep waters. The reason is apparently because of warming of the sea water which causes the evaporation to increase, which prevents a further rise in sea level due to the flows of the Volga and other rivers.

In the Southern Caspian (tracks 31, 92, 209), the values of the sea level amplitude are generally getting lower values (23-28 cm) than in Northern and Middle Caspian regions, and only in the western part, where the Kura River flows into the sea (track 16), as well as surrounding areas it reaches the value of 28-31 cm. In the western part of the Southern Caspian, the water level and the

amplitude of its fluctuation is slightly bigger compared to the eastern part (Fig. 2a). This can be explained by relatively huge river flow and huge amount of atmospheric precipitation in the western part. The phases of the occurrence of sea level amplitudes in the eastern territories are observed earlier than in the western areas (Fig. 2b). The reason for that probably lies in the fact that in Southern Caspian region the impact of the Volga River decreases and unlike western territories the amount of precipitation here is low, whereas evaporation is high. In other words, rapid evaporation in the eastern part of the sea leads to an earlier formation of the amplitude.

Maps of distributions of seasonal amplitudes and phases of their occurrence, obtained with the help of the altimetry observation data from the ENVISAT satellite, are shown in Fig. 3, where it can be seen that the nature of these distributions is generally similar to those obtained from the Jason 1, Jason 2 satellites (Fig. 2). However, the difference lies in the fact that the amplitudes obtained from ENVISAT data turned out to be relatively smaller, and the phases, on the contrary, are bigger than for the Jason 1, Jason 2 satellites. This can be explained by a much longer period of track repetition of the ENVISAT satellite (35 days) compared to Jason 1, Jason 2 (10 days). Longer track repetition period leads to a bigger error in establishing correct values of the amplitude of the level and the phase of its occurrence, and therefore the measured values of the amplitude turn out to be understated, and its phases are overvalued.

Conclusion

Summarizing the results obtained from the satellite altimetry of Jason 1, Jason 2 and ENVISAT, it can be concluded that, in general, the biggest seasonal sea level amplitudes are observed in the Northern Caspian, and the smallest – in the Southern Caspian. The earliest phases of the sea level amplitudes are fixed in the Northern Caspian, below the Volga Delta (in May), and in the remaining parts of the sea – much later (in June-July). In the Middle and Southern parts of the Caspian Sea, to the east of track 92, the phases of amplitudes are observed earlier than in the western part. All this shows that in different parts of the sea, besides the impact of flow of the Volga River, the formation and distribution of phases of amplitudes are influenced also by evaporation, precipitation and short-period phenolmena (wind and related movement of water).

A comparison of the results obtained in this work with the results concluded by other authors shows that depending on the combination of various factors (river flow, evaporation, precipitation, etc.), the nature of the spatial distribution and phases of seasonal sea level amplitudes may be slightly different.

REFERENCES

Abuzyarov Z.K. Some features of the spatio-temporal variability of the level of the Caspian Sea. Proceedings of the SHC of RF, V. 345, 2011, pp. 5-23.

Aladin N., Crétaux J.-F., Plotnikov I.S., Kouraev A.V., Smurov A.O., Cazenave A., Egorov A.N., Papa F. Modern hydrobiological state of the Small Aral Sea. Environmetrics, V. 16, Iss. 4, 2005, pp. 375-392. DOI: 10.1002/env.709.

Arsen A., Crétaux J.-F., Abarca Del Rio R. Use of SARAL/ AltiKa over Mountainous Lakes, intercomparison with Envisat mission. Marine Geodesy, V. 38, 2015, pp. 534-548. DOI: 10.1080/01490419.2014.1002590.

Birkett C.M. The contribution of TOPEX/POSEIDON to the global monitoring of climatically sensitive lakes. J. Geophys. Res., V. 100, Iss. C12, 1995, pp. 25179-25204. DOI: 10.1029/95JC02125.

Chelton D.B., Ries J.C., Haines B.J. et al. Satellite altimetry. In: Satellite altimetry and earth sciences. A handbook of techniques and applications. L.-L.Fu and A.Cazenave (eds.), Academic Press. San Diego, USA, 2001, pp. 1-131.

Chen J.L., Pekker T., Wilson C.R., Tapley B.D., Kostianoy A.G., Cretaux J.-F., Safarov E.S. Long-term Caspian Sea level change. Geophys. Res. Lett., V. 44, Iss. 13, 2017, pp. 6993-7001. DOI.org/10.1002/2017GL073958.

Coe M.T., Birkett C.M. Calculation of river discharge and prediction of lake height from satellite radar altimetry: Example for the Lake Chad basin. Water Resour. Res., V. 40, Iss. 10, 2004, W10205. DOI: 10.1029/2003WR002543.

ЛИТЕРАТУРА

Abuzyarov Z.K. Some features of the spatio-temporal variability of the level of the Caspian Sea. Proceedings of the SHC of RF, V. 345, 2011, pp. 5-23.

Aladin N., Crétaux J.-F., Plotnikov I.S., Kouraev A.V., Smurov A.O., Cazenave A., Egorov A.N., Papa F. Modern hydrobiological state of the Small Aral Sea. Environmetrics, V. 16, Iss. 4, 2005, pp. 375-392. DOI: 10.1002/env.709.

Arsen A., Crétaux J.-F., Abarca Del Rio R. Use of SARAL/ AltiKa over Mountainous Lakes, intercomparison with Envisat mission. Marine Geodesy, V. 38, 2015, pp. 534-548. DOI: 10.1080/01490419.2014.1002590.

Birkett C.M. The contribution of TOPEX/POSEIDON to the global monitoring of climatically sensitive lakes. J. Geophys. Res., V. 100, Iss. C12, 1995, pp. 25179-25204. DOI: 10.1029/95JC02125.

Chelton D.B., Ries J.C., Haines B.J. et al. Satellite altimetry. In: Satellite altimetry and earth sciences. A handbook of techniques and applications. L.-L.Fu and A.Cazenave (eds.), Academic Press. San Diego, USA, 2001, pp. 1-131.

Chen J.L., Pekker T., Wilson C.R., Tapley B.D., Kostianoy A.G., Cretaux J.-F., Safarov E.S. Long-term Caspian Sea level change. Geophys. Res. Lett., V. 44, Iss. 13, 2017, pp. 6993-7001. DOI.org/10.1002/2017GL073958.

Coe M.T., Birkett C.M. Calculation of river discharge and prediction of lake height from satellite radar altimetry: Example for the Lake Chad basin. Water Resour. Res., V. 40, Iss. 10, 2004, W10205. DOI: 10.1029/2003WR002543.

Crétaux J.-F., Calmant S., Abarca Del Rio R. et al. Lakes studies from satellite altimetry. In: Handbook on Coastal altimetry. Springer. Ch. 19, 2011a, pp. 509-513.

Crétaux J.-F., Jelinski W., Calmant S., Kouraev A., Vuglinski V., Bergé-Nguen M., Gennero M.C. et al. SOLS: A lake database to monitor in the Near Real Time water level and storage variations from remote sensing data. Advances in Space Research, Elsevier. V. 47, Iss. 9, 2011b, pp. 1497-1507. DOI:10.1016/j.asr.2011.01.004.

Crétaux J.-F., Kouraev A.V., Papa F., Bergé M.N., Cazenave A., Aladin N., Plotnikov I.S. Evolution of sea level of the Big Aral Sea from satellite altimetry and its implications for water balance. Journal of Great Lakes Research, V. 31, Iss. 4, 2005, pp. 520-534. DOI: 10.1016/S0380-1330(05)70281-1.

Crétaux J.-F., Birkett C. Lake studies from satellite radar altimetry. Comptes Rendus Geoscience, V. 338, Iss.14-15, 2006, pp. 1098-1112. DOI: 10.1016/j.crte.2006.08.002.

Crétaux J.-F., Calmant S., Romanovski V., Shabunin A., Lyard F., Bergé M., Cazenave A., Hernandez F., Perosanz F. An absolute calibration site for radar altimeters in the continental domain: Lake Issykkul in Central Asia. J. Geod., V. 83, Iss. 8, 2009, pp. 723-735. DOI: 10.1007/s 00190-008-0289-7.

Fu L.-L., Cazenave A. Satellite altimetry and Earth science. A handbook of techniques and applications. International Geophysics Series, Academic press. V. 69, 2001, 463 p.

Gao H., Birkett C., Lettenmaier D.P. Global monitoring of large reservoir storage room satellite remote sensing. Water Resour. Res., V. 48, Iss. 9, 2012, W09504. DOI: 10.1029/2012WR012063.

Hydrometeorology and hydrochemistry of the seas. Project "The Seas". V. 6 – Caspian Sea. Issue 1 – Hydrometeorological conditions. F.S. Terzieva, A.N. Kosareva and A.A. Kerimov (eds.). Gidrometeoizdat. St.-Petersburg, 1990, 359 p. (in Russian).

Hwang C., Kao Y., Natthachet T. A preliminary analysis of lake level and water storage changes over lakes Baikal and Balkhash from satellite altimetry and gravimetry. Terrestrial, Atmospheric and Oceanic Sciences, V. 22, № 2, 2011, pp. 97-108. DOI: 10.3319/TAO.2010.05.19.01(TibXS).

Hwang C., Peng M., Ning J., Luo J., Sui C. Lake level variations in China from TOPEX/Poseidon altimetry: data quality assessment and links to precipitation and ENSO. Geophysical Journal International, V. 161, Iss. 1, 2005, pp. 1-11. DOI: 10.1111/j.1365- 246X.2005.02518.x.

Kouraev A.V., Crétaux J.-F., Lebedev S.A. et al. Satellite altimetry applications in the Caspian Sea. In: Handbook on Coastal altimetry. S.Vignudelli, A.G.Kostianoy, P.Cipollini, J.Benveniste (eds.). Springer Berlin Heiderberg. ch. 13, 2011, pp. 331-366.

Lebedev S.A., Kostianoy A.G. Satellite altimetry of the Caspian Sea. Publisher "More". Intern. Institute of the Ocean. Moscow, 2005, 366 p. (in Russian).

Lee H., Shum C.K., Tseng K-H., J. Guo, C.-Y. Kuo. Present-day lake level variation from Envisat altimetry over the Northeastern Qinghai-Tibetan Plateau: links with precipitation and temperature. Terrestrial, Atmospheric and Oceanic Sciences, V. 22, Iss. 2, 2011, pp. 169-175. DOI: 10.3319/TAO.2010.08.09.01(TibXS).

Troitskaya Yu.I., Balandina G.N., Rybushkina G.V., Soustova I.A., Kostyanoy A.G., Lebedev S.A., Panyutin A.A., Filina L.V. Investigations of the water level variability in the Gorky reservoir on the basis of satellite altimetry data. Research of the Earth from Space, № 1, 2011, pp. 48-56.

Zheng Duan, Bastiaanssen W.G.M. Estimating water volume variations in lakes and reservoirs from four operational satellite altimetry databases and satellite imagery data. Remote Sensing of Environment, V. 134, 2013, pp. 403-416. DOI: 10.1016/j.rse.2013.03.010.

Crétaux J.-F., Calmant S., Abarca Del Rio R. et al. Lakes studies from satellite altimetry. In: Handbook on Coastal altimetry. Springer. Ch. 19, 2011a, pp. 509-513.

Crétaux J.-F., Jelinski W., Calmant S., Kouraev A., Vuglinski V., Bergé-Nguen M., Gennero M.C. et al. SOLS: A lake database to monitor in the Near Real Time water level and storage variations from remote sensing data. Advances in Space Research, Elsevier. V. 47, Iss. 9, 2011b, pp. 1497-1507. DOI:10.1016/j.asr.2011.01.004.

Crétaux J.-F., Kouraev A.V., Papa F., Bergé M.N., Cazenave A., Aladin N., Plotnikov I.S. Evolution of sea level of the Big Aral Sea from satellite altimetry and its implications for water balance. Journal of Great Lakes Research, V. 31, Iss. 4, 2005, pp. 520-534. DOI: 10.1016/S0380-1330(05)70281-1.

Crétaux J.-F., Birkett C. Lake studies from satellite radar altimetry. Comptes Rendus Geoscience, V. 338, Iss.14-15, 2006, pp. 1098-1112. DOI: 10.1016/j.crte.2006.08.002.

Crétaux J.-F., Calmant S., Romanovski V., Shabunin A., Lyard F., Bergé M., Cazenave A., Hernandez F., Perosanz F. An absolute calibration site for radar altimeters in the continental domain: Lake Issykkul in Central Asia. J. Geod., V. 83, Iss. 8, 2009, pp. 723-735. DOI: 10.1007/s 00190-008-0289-7.

Fu L.-L., Cazenave A. Satellite altimetry and Earth science. A handbook of techniques and applications. International Geophysics Series. Academic press. V. 69, 2001, 463 p.

Gao H., Birkett C., Lettenmaier D.P. Global monitoring of large reservoir storage room satellite remote sensing. Water Resour. Res., V. 48, Iss. 9, 2012, W09504. DOI: 10.1029/2012WR012063.

Hwang C., Kao Y., Natthachet T. A preliminary analysis of lake level and water storage changes over lakes Baikal and Balkhash from satellite altimetry and gravimetry. Terrestrial, Atmospheric and Oceanic Sciences, V. 22, № 2, 2011, pp. 97-108. DOI: 10.3319/TAO.2010.05.19.01(TibXS).

Hwang C., Peng M., Ning J., Luo J., Sui C. Lake level variations in China from TOPEX/Poseidon altimetry: data quality assessment and links to precipitation and ENSO. Geophysical Journal International, V. 161, Iss. 1, 2005, pp. 1-11. DOI: 10.1111/j.1365- 246X.2005.02518.x.

Kouraev A.V., Crétaux J.-F., Lebedev S.A. et al. Satellite altimetry applications in the Caspian Sea. In: Handbook on Coastal altimetry. S.Vignudelli, A.G.Kostianoy, P.Cipollini, J.Benveniste (eds.). Springer Berlin Heiderberg. ch. 13, 2011, pp. 331-366.

Lee H., Shum C.K., Tseng K-H., J. Guo, C.-Y. Kuo. Present-day lake level variation from Envisat altimetry over the Northeastern Qinghai-Tibetan Plateau: links with precipitation and temperature. Terrestrial, Atmospheric and Oceanic Sciences, V. 22, Iss. 2, 2011, pp. 169-175. DOI: 10.3319/TAO.2010.08.09.01(TibXS).

Troitskaya Yu.I., Balandina G.N., Rybushkina G.V., Soustova I.A., Kostianoy A.G., Lebedev S.A., Panyutin A.A., Filina L.V. Investigations of the water level variability in the Gorky reservoir on the basis of satellite altimetry data. Research of the Earth from Space, № 1, 2011, pp. 48-56.

Zheng Duan, Bastiaanssen W.G.M. Estimating water volume variations in lakes and reservoirs from four operational satellite altimetry databases and satellite imagery data. Remote Sensing of Environment, V. 134, 2013, pp. 403-416. DOI: 10.1016/j.rse.2013.03.010.

Гидрометеорология и гидрохимия морей (под ред. Ф.С. Терзиевой, А.Н. Косаревой, А.А. Керимова). Том 6 – Каспийское море. Вып. 1 – Гидрометеорологические условия. Гидрометеоиздат. Санкт-Петербург, 1990, 359 с.

Лебедев С.А., Костяной А.Г. Спутниковая альтиметрия Каспийского моря. Издательский центр «МОРЕ» Международного института океана. Москва, 2005, 366 с.

ОСОБЕННОСТИ СЕЗОННЫХ ИЗМЕНЕНИЙ УРОВНЯ КАСПИЙСКОГО МОРЯ

Сафаров Э.С.[1], Крето Ж.-Ф.[2], Мамедов Р.М.[1], Арсен А.[3], Сафаров С.Г.[1]
[1]Институт Географии НАНА
AZ1143, г.Баку, просп. Г.Джавида, 115: elnur.safarov@geo.ab.az
[2]CNES/Legos
31400, Франция, Тулуза, просп.Эдуарда Белин,14
[3]Freelancer
Варшава, Польша

Резюме. Каспийское море является самым большим закрытым водоемом во всем мире. В отсутствии непосредственной связи с мировым океаном замкнутому Каспийскому морю свойственны значительные вековые, межгодовые и сезонные изменения уровня. В работе по данным наблюдений радиолокационной альтиметрии спутников ENVISAT, Jason 1 и Jason 2 рассматриваются сезонные колебания уровня Каспийского моря, особенности распределения их амплитуды, а также фазы появления по всей акватории моря. По специальной методике рассчитаны среднегодовые значения амплитуды и фазы появления сезонных колебаний уровня воды для различных районов акватории моря по заранее установленным спутниковым трекам. Изучено влияние стока реки Волга на амплитуду и фазу сезонных колебаний уровня различных районов Каспийского моря. Исследования показали, что в Северном Каспии значение амплитуды сезонных колебаний уровня моря больше, чем в Среднем и Южном Каспии. Они также отличаются в направлении с востока на запад. Самые ранние фазы амплитуд уровня моря зафиксированы в Северном Каспии, ниже дельты Волги (в мае), а в остальных частях моря – значительно позже (июнь-июль). Установлено, что влияние стока реки Волга наиболее чувствительно в северной части моря, а в направлении к югу оно постепенно уменьшается, и начинает преобладать воздействие других факторов (испарение, атмосферные осадки). В работе обсуждаются причины такого различия.

Ключевые слова: *Каспийское море, Волга река, спутниковая альтиметрия, трек, Jason 1-2, ENVISAT, амплитуда, фаза, уровень моря*

XƏZƏR DƏNİZİNİN MÖVSÜMİ SƏVİYYƏ DƏYİŞİLMƏLƏRİNİN XÜSUSİYYƏTLƏRİ

Səfərov E.S. [1], Kreto J.-F.[2], Məmmədov R.M.[1], Arsen A.[3], Səfərov S.H.[1]
[1]AMEA Coğrafiya İnstitutu,
AZ1143, Bakı şəh., H.Cavid prosp., 115: elnur.safarov@geo.ab.az
[2]CNES/Legos
31400, Fransa, Tuluza, av. Edouard Belin, 14
[3]Freelancer
Varşava, Polşa

Xülasə. Məlum olduğu kimi, Xəzər dənizi dünyanın ən böyük qapalı su hövzəsidir. Dünya okeanı ilə birbaşa əlaqəsi olmayan qapalı Xəzər dənizi əhəmiyyətli səviyyə dəyişilmələri (əsrlik, illərarası və mövsümi) ilə xarakterizə olunur. Məqalə Xəzər dənizi səviyyəsinin mövsümi səviyyə tərəddüdlərinə, həmçinin onların amplituda və başvermə fazalarının fəza-zaman paylanmasının tədqiqinə həsr olunmuşdur. Tədqiqatda Envisat, Jason 1 и Jason 2 peyklərinin radar altimetriya məlumtlarından istifadə olunub. Müvafiq peyk trekləri üzrə Xəzər dənizi akvatoriyasının müxtəlif ərazilərində mövsümi səviyyə tərəddüdlərinin orta çoxillik amplitudaları və onların fazaları müəyyənləşdirilmiş, həmçinin Volqa çayı axımının onlara mümkün təsiri araşdırılmışdır. Tədqiqatın nəticələrinə əsasən müəyyənləşdirilmişdir ki, Şimali Xəzərdə dəniz səviyyəsinin mövsümi dəyişmələrinin amplitudaları Cənubi Xəzərə nisbətən daha böyükdür. Belə bir fərq dənizin şərq və qərb əraziləri üçün də mövcuddur. Dənizin səviyyə dəyişilmə amplitudalarının ən erkən fazaları may ayında Şimali Xəzərdə, Volqa çayının deltasından aşağıda, dənizin qalan hissələrində isə - nəzərəçarpacaq dərəcədə sonra - iyun-iyul aylarında qeydə alınır. Beləliklə, göstərilmişdir ki, dənizin şimal əraziləri Volqa çayı axımına daha həssasdır və cənuba doğru bu təsir tədricən azalır və digər amillər üstünlük təşkil etməyə başlayır (buxarlanma, atmosfer yağıntıları). Tədqiqatda alınan nəticələrin səbəbləri məqalədə müzakirə olunur.

Açar sözlər: *Xəzər dənizi, Volqa çayı, peyk altimetriyası, trek, Jason 1-2, ENVISAT, amplitude, faza, dəniz səviyyəsi*

ANAS Transactions **Earth Sciences** **1 / 2019**

Geography

http://www.journalesgia.com

THE INFLUENCE OF TRANSCONTINENTAL RAILROADS ON THE GEOPOLITICAL AND ECONOMIC SITUATION OF AZERBAIJAN

Orujov P.Sh.
Baku State University
Baku, Azerbaijan, Z.Khalilov str., 23, AZ114: porucov@bsu.edu.az

Keywords: *railway, international transport corridors, economic development, Baki-Tbilisi-Kars and North-South Railways, TRACECA*

Summary. The article examines economic-geographical study of the railway infrastructure of Azerbaijan Republic and the efficiency of transit potential of the country in the Europe-Asia region. Also, the paper discusses the importance of transport and international transportation in the context of the globalization of the world economy and their impact on Azerbaijan's international economic relations. Transcontinental railroads play significant role in the growth of both the country and its regions, in the international economic and political integration of countries. In the process of integration in world economy, Azerbaijan sets tasks for expanding their transport complex, also, for joining to global transport corridors. The target is to estimate the potential of the international railroad corridors, to substantiate its socio-economic benefits for our country. Azerbaijan plans to improve transport and railway infrastructure along the Great Silk Road and to expand trade links with Europe and Asia. We researched transcontinental railroad corridors demonstrating economic, political and cultural significance to ensure sustainable socio-economic development of Azerbaijan during the integration into the world economy. The role of the large transport corridors in Eurasia like Baku-Tbilisi-Kars, TRACECA, North-South and their impact for the economic integration of Europe and Asia was investigated. Additionally, the influence of the Baku-Tbilisi-Kars railway and the North-South international transport corridor on integration of Azerbaijan to global economy was studied.

© 2018 Earth Science Division, Azerbaijan National Academy of Sciences. All rights reserved.

The relevance of research. The main economic priorities of Azerbaijan after gaining independence are the development of the non-oil sector, spreading of industry sectors, growing of agricultural production, increasing of investment, strengthening of infrastructure, expanding non-oil exports, and making stronger family business. For promoting these priorities our government implemented different state programs, incentive mechanisms and awareness-raising activities. Of course, the main goal is to achieve the growth of domestic production, increase the employment level and improve the living conditions of the population. In the implementation of the above, the transport factor has a crucial importance. In the twentieth century, the transport sector has been shaped as an important infrastructure in the dynamic development of the world economy and has turned into the most actual area of the economy as a whole. Transcontinental transport corridors play an important role in the economic development of the modern world, as well as Azerbaijan. It is only through these transport routes that large-scale loads can be transmitted directly and shortly between long distances. Thus, with the development and diversification of this field, foreign investment is focused not only on the oil sector, but on other sectors of the economy – mechanical engineering, microelectronics, agriculture, light industry, food, textile and so on. Also through these corridors the economic security of our country will be strengthened and geopolitical situation in the region will be even better.

Purpose of the study. Assess the potential of international railways that passes through Azerbaijan's territory and substantiate the socio-economic benefits of improving transport infrastructure along the Baku-Tbilisi-Kars and North-South routes and expanding trade links with European and Asian railway complexes.

Theoretical bases. One of the fundamental conditions for the overall economic development and overall security of any country in the world is the availability of transport corridors and developing some of the major types of transport in key global routes. At present, Azerbaijan has the potential to develop trans-

portation of goods and passengers to different directions of the world using of main transport modes – land, air and water. This creates a continuing opportunity for establishing international economic relations with various means of transport, as well as the implementation of import-export operations.

The historical outcomes of the strategy implemented by national leader Heydar Aliyev were the launch of the Baku-Tbilisi-Ceyhan Main Export Pipeline and the initiation of the Baku-Tbilisi-Erzurum South Caucasus Pipeline. These projects provided an access of Azerbaijan to the world market. Successful implementation of these global projects from a historic point of view has led to the fact that our country has gained leadership positions in the region and has increased its weight in political and economic processes in the world (Alekperova, Seidova, 2009).

At the same time, with its geopolitical position and placing in the crossroads of trade routes that connect different parts of Eurasia Azerbaijan has become one of the key participants of the TRACECA program, which was aimed at creating natural transport corridor Europe-Caucasus-Asia. This project has been carried out within the framework of the rehabilitation of the Historic Silk Road. As a result of all these, the beneficial economic relations established with the near and far abroad have been expanded, the trade turnover has increased rapidly, and as a result, Azerbaijan has become an important country in terms of transit cargo transportation (Mamedov, 2002).

Also, the completion of the Baku-Tbilisi-Kars railway, Astara-Astara (Iran) railway bridge, reconstruction of Baku-Boyuk Kasik, Baku-Astara, Baku-Yalama railways and Baku-Ganja speed railway enhance the role of Azerbaijan in global economic integration.

Baku-Tbilisi-Kars railway project. Transport being an integral part of the geographical division of labor, also considered a factor of globalization, is an important tool for promoting regionalization and enhancing the reputation of the leading transnational corporations. In this context, the restoration of the Great Silk Road will help eliminate employment problems, accelerate the flow of investment and reduce political and economic pressure on our country, isolate hidden blockades and embargoes.

Owing to efforts of Heydar Aliyev in Azerbaijan there was held international forum for restoring and developing of Great Silk route, in which representatives of 42 countries of the world took participation, among whom 8 were represented by presidents. As H.Aliyev noticed at this forum on September, 1998: "Baku summit will play its historical role in decision of co-operation, provision with peace, prosperity in every country and all Eurasian space". The main purposes of developing of Great Silk Route are expressed in the following:

– developing of trade-economic relations of the regional countries;

– developing of transport connections of international transportation of trucks and passengers;

– creation of propitious conditions for transit transportation;

– acceleration of delivery terms and saving of transported truck;

– harmonization of transport policy;

– privileges on tariffs on transportation and collection of taxes;

– coordination of relationships between different fields of transport;

– tariff policy on international and internal tariffs on truck and passenger transportation;

– development of the programs of coordinated actions for organization of multi-modal (combined) transportation.

It must be noticed that geographic situation of Azerbaijan and its role in Great Silk route are one of the main (central), if take into consideration the fact that there are well developed all kinds of transports and main roads (air, sea and automobile) in the republic.

The Intergovernmental Commission (IGC) TRACECA is open for all the initiatives promoting the development of regional transport dialogue and ensuring the efficient and reliable Euro-Asian transport links, promoting the regional economy on the whole.

TRACECA corridor is involved in gradually developing trends of trade and economic development. Major traffic flows passing through a corridor formed on the one hand, in Western and Central Europe, and on the other – in Central and South-East Asia.

Baku-Tbilisi-Kars railway is a regional rail link project to directly connect Azerbaijan, Georgia and Turkey through the South Caucasus which becomes an integral part for the international transport corridor TRACECA and through Turkey offers a unique opportunity for uninterrupted and reliable rail communication with the European continent.

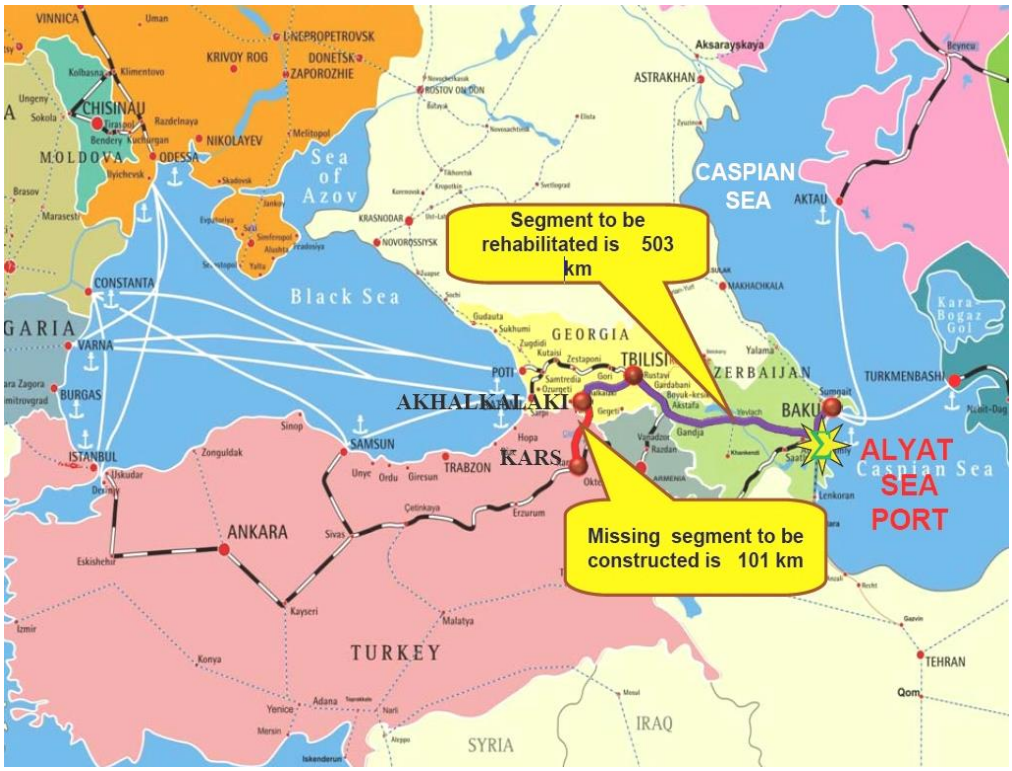
Being the most advantageous transit option and the short haul between the Caspian Sea and the Black Sea, the railway line Baku-Tbilisi-Kars is creating an alternative at the intersection of both between West and East and between a number of northern and southern countries. This rail line is designed to become a key part of the southern route of the emerging new Silk Road network of trade and transport corridors that are coming together between China and Europe.

The Baku-Tbilisi-Kars railway is the final destination for transportation between Europe and Asia.

The creation of this project on the Great Silk Road increases its attractiveness for the countries of the region. China, the country which is the main source of cargo in Asia, is also interested in this project. And also, the possibilities of Afghanistan in this region should not be forgotten. In the near future, NATO plans to withdraw its martial contingent from Afghanistan, this is approximately 130,000 TEU containers and 60,000 vehicles, and there are no alternatives to the Baku-Tbilisi-Kars transport corridor. The project envisages the construction of numerous stations, bridges, a 4350-meter tunnel on the Turkish-Georgian border. It should be noted that the construction of a new railway line on the Kars-Akhalkalaki section as well as the rehabilitation and reconstruction of the Akhalkalaki-Marabda section will be carried out in accordance with the standards of the International Railway Union (UIC) (The official web site of International Union of Railways, 2018).

The total length of the Baku-Tbilisi-Kars railway line is 825.0 km; 503 km in Azerbaijan, 244.5 km in Georgia and 77.5 km in Turkey. It is expected that the maximum speed will be 120 km/h after commissioning of the entire line. It will be possible to get from Baku to Kars in just one day and two days to Istanbul. After commissioning of the Baku-Tbilisi-Kars railway, this line is supposed to carry 1 million passengers and 6.5 million tons of cargo per year, as well as 3 million passengers and 17 million tons of cargo in 2034. The minimum annual income of Azerbaijan from transit in the first years will be $ 50 million. In the future, attracting European and Asian rail freight to this railway will increase the volume of container and intermodal transportation (carriage of goods by several modes of transport) in both directions. Thus, the Baku-Tbilisi-Kars railway will serve to increase the transit potential of the countries of the region, speed up the integration process in Europe, further develop cooperation within the European Neighborhood Policy and expand our country's foreign economic relation (The official web site of TRACECA, 2018) (map 1).

The Baku-Tbilisi-Kars railway project is considered a very important project not only for the countries of the region, but also for other countries that will join this line. The railway will lead to an increase in cargo and passenger traffic between Asia and Europe, will contribute to the development of its tourism potential and link the Caspian Sea and the Black Sea. With the launch of the BTK railway, ferry and container traffic will continue to grow. In the future, the Marmaray railway tunnel, which will pass through the Bosphorus Strait, will add the significance of this project. The Baku-Tbilisi-Kars railway will transport bridge continents and is projected to begin operating in 2018. Passengers will be able to travel from Beijing to London in just 12 days (Hajizadeh, 2014). As we approach the implementation of this gigantic project, potential carriers are increasingly showing interest in it.



Source: "Azerbaijan in figures". Publications of the State Statistical Committee of the Republic of Azerbaijan, 2018.
Map 1. Baku-Tbilisi-Kars railway corridor

In global terms, the BTK route is designed to connect China and Central Asia with Europe. Regionally, it aims to strengthen trade between the three countries involved – Azerbaijan, Turkey and Georgia – while isolating Armenia to help bring an end to its occupation of Nagorny Karabakh.

Countries of Central Asia, including Kazakhstan, are showing great interest in this railway project. This is clearly illustrated by the participation of delegations and high-ranking officials from these countries at this ceremony. We are sure that there will be additional opportunities in cargo transportation, and our traditional friendship with countries of Central Asia will strengthen further thanks to this railway. This railway is of great importance for Europe. Azerbaijan has already held talks with several European countries. European states are also very interested in this railway.

North-South transport corridor. The transport sector of Azerbaijan has produced many large-scale projects in last 20 years. Highway construction and railway modernisation, the new Baku International Sea Port complex, modern international airports and global transport corridors all aim to make Azerbaijan a regional transport hub and expand the country's global reach. Azerbaijan's significance as a transit country between Europe and Asia will increase further after the completion of the Baku-Tbilisi-Kars railway line in this year. Another key project nearing completion is the International North-South Transport Corridor.

One of the key characteristics of globalization and the integration process is the renewal, restoration and reuse of historical transit routes. In this regard, the North-South transport corridor, one of the international transport corridors connecting the countries of Eurasia, has a great importance. The use of the North-South transport corridor, which is largely considered an alternative to the TRACECA program, allows transit cargo to be 3 times faster than the sea route through the Suez Canal, but also stimulates the creation of conditions for further expansion of economic relations between the South Caucasus and Central Asia and Iran (The official web site of Azerbaijan Railway, 2018).

The creation of the North-South Transport Corridor was laid on the basis of the intergovernmental agreement signed between Russia, Iran and India on September 12, 2000. Azerbaijan joined to this agreement in 2005. Totally, 13 countries have ratified the agreement (the Republic of Azerbaijan, the Republic of Belarus, the Republic of Bulgaria, the Republic of Armenia, India, Islamic Republic of Iran, the Republic of Kazakhstan, the Kyrgyz Republic, Oman Sultanate, the Russian Federation, the Republic of Tajikistan, the Republic of Turkey, Ukraine) (Dergachev, 2015).

Azerbaijan is geographically located in close proximity to two huge transport corridors. Full-scale operation of these transport lines will be of great importance for enhancing the economic power of Azerbaijan. Also passing through different natural zones and countries with different culture, the transport corridors of the West-East and North-South, which intersect in the territory of Azerbaijan, will create favorable conditions not only for the transportation of goods, but also for the organization of tourist routes. Countries and regions will benefit from such conditions.

This corridor will be of great importance for travel to Islam's pilgrimage sites, especially to the cities of Mecca and Medina, providing a transport alternative between Arab countries and Europe.

Russia shows a greater interest in the implementation of the North-South transport corridor and places it on the list of key priorities of its transport strategy. To this end, Russia intends to create a consortium for the construction of a 300-kilometer railway line connecting Astara and the Iranian city of Anzali and Rasht. Initially, this project is estimated at about $ 600 million. Russia hopes that along with the socio-economic significance of this line, it will also bring favorable political dividends to strengthen mutual trust between the countries of the region (Azerbaijan in figures, 2018).

In this regard, the full participation of Azerbaijan as a key figure in the project and support for its implementation will be political, social and economically beneficial. It is also important to emphasize that such rapidly developing countries as China and India are interested in the North-South and West-East transport corridors. It is already known that the new route for transportation of various goods from India will be delivered to the Astrakhan port of Russia or to Baku via the Persian port of Bandar Abbas, which will start from the Indian city of Mumbai (formerly Bombay). This is an important factor for the economic progress of Azerbaijan as a transit country.

This corridor will have three routes: the Caucasus – the Persian Gulf – India; Central Asia – Persian Gulf – India; Caspian Sea – Islamic Republic of Iran – Persian Gulf – India (map 2) (The official web site of North-South Transport Corridor, 2018).

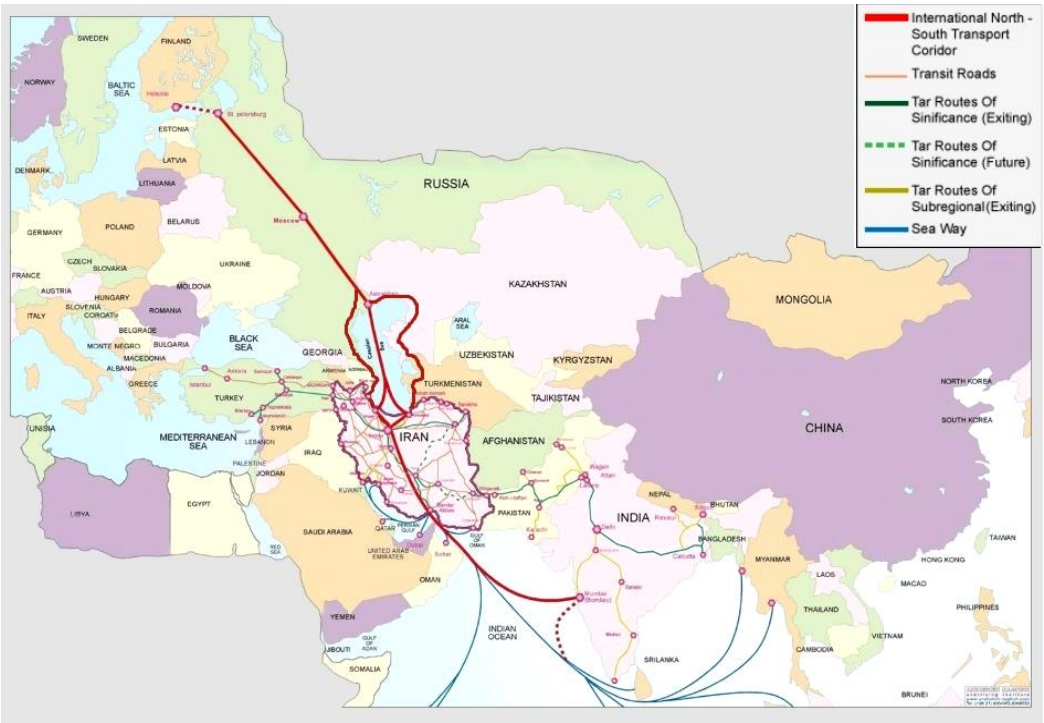
The expected volume of cargo that will be transported over the territory of Azerbaijan through the Corridor: at the first stage – 3 million tons; at the second stage – 5-8 million ton; at the third stage – 15 million ton. The following measures are being taken on the part of the North-South International Transport Corridor passing through the territory of the Republic of Azerbaijan:

– The construction of 8.3 km of new road of Astara (Azerbaijan) – Astara (Iran) railway line up to the Astarachay bridge and the bridge over the Astarachay and 1.4 km of road on the territory of Iran has been completed;

– Negotiations are underway with Iranian side on the construction of Gezvin-Resht (175 km) section of this corridor;

– Construction of Samur (Azerbaijan) – Yaraq Qazmalar (Russia) highway bridge over the Samur River (Azerbaijan in figures, 2018).

Thus, the North-South Corridor will offer a direct transport route between St Petersburg and Mumbai. This means Azerbaijan together with Iran bridging two continents, Europe and Asia. In other words, the Astara-Astara section (a rail link between Astara in Iran and Astara in Azerbaijan) will play a vital role in linking North and South by land and developing relations between individual countries and continents. It will strengthen trade, transport and economic relations between the countries of the Middle East, Southeast Asia, Northern Europe and Russia. In this way the Astara-Astara transit corridor is very important for Azerbaijan and Baku is naturally extremely interested in implementing this project. The North-South Corridor will be a key to realising the country's transit potential, generating additional income and jobs, and strengthening the Azerbaijani economy in the region.



Source: http://instcorridor.com/ - Official web site of North-South transport corridor

Map 2. North-South transport corridor

REFERENCES

Alekperova F.F., Seidova R.T. Transport geography and transport systems of the world. Mulki Aviasiya. Baku, 2009, 174 p. (in Russian).

Azerbaijan in figures. Publications of the State Statistical Committee of the Republic of Azerbaijan. 2018, 264 p. (in Azerbaijani).

Dergachev V. European transport corridors (Electronic resource). 2015 http://dergachev.ru/geop_events/260909.html (in Russian).

Hajizadeh E.M. The role of the Baku-Tbilisi-Kars railway project in improving the regional transport infrastructure. Azerbaijan Tax Journal, № 3 (117), Baku, 2014, pp. 123-160 (in Azerbaijani).

Mamedov Z.S. The transport factor of the economic development of the XXI century. Azerneshr. Baku, 2002, 386 p. (in Azerbaijani).

ЛИТЕРАТУРА

Алекперова Ф.Ф. Сеидова Р.Т. Транспортная география и транспортные системы мира. Mülki Aviasiya. Баку. 2009, 174 с.

Дергачев В. Европейские транспортные коридоры (Электронный ресурс). Аналитический и образовательный портал: 2015. http://dergachev.ru/geop_events/260909.html

Azərbaycan rəqəmlərdə. Azərbaycan Respublikası Dövlət Statistika Komitəsinin nəşrləri. 2018, 264 s.

Hacızadə E.M. Regional nəqliyyat infrastrukturunun təkmilləşdirilməsində Bakı-Tbilisi-Qars dəmir yolu xətti layihəsinin rolu. Azərbaycanın Vergi Jurnalı, № 3(117), Bakı, 2014, s.123-160.

Məmmədov Z.S. XXI əsr iqtisadi inkişafın nəqliyyat faktoru. Azərnəşr. Bakı, 2002, 386 s.

Azərbaycan Dəmir Yolları rəsmi internet saytı. 2018. https://view.officeapps.live.com/op/view.aspx?src=https://ady.az/uploads/ada03-kpi-az.docx/ 2018.

The official web site of Azerbaijan Railway. 2018. https:// view.officeapps.live.com/op/view.aspx?src=https://ady.az/uploads/ada03-kpi-az.docx/ 2018
The official web site of International Union of Railways. 2018. https://uic.org/corridors#Transcontinental-corridors/2018.
The official web site of North-South Transport Corridor. 2018. http://instcorridor.com/wp-content/uploads/2018/01/ Azerbaijan.pdf /2018.
The official web site of TRACECA. 2018. http://www.traceca. org.org/en/countries/azerbaijan/azerbaijan -in-traceca/2018.
The official web site of International Union of Railways. 2018. https://uic.org/corridors#Transcontinental-corridors/2018.
The official website of North-South Transport Corridor. 2018. http://instcorridor.com/wp-content/uploads/2018/01/ Azerbaijan.pdf /2018.
The official web site of TRACECA. 2018. http://www.traceca. org.org/en/countries/azerbaijan/azerbaijan-in-traceca/2018

ВЛИЯНИЕ ТРАНСКОНТИНЕНТАЛЬНЫХ ЖЕЛЕЗНОДОРОЖНЫХ КОРИДОРОВ НА ГЕОПОЛИТИЧЕСКОЕ И ЭКОНОМИЧЕСКОЕ СОСТОЯНИЕ АЗЕРБАЙДЖАНА

Оруджев П.Ш.
Бакинский Государственный Университет
AZ1148, г.Баку, ул. З.Халилова, 23: porucov@bsu.edu.az

Резюме. В статье даются результаты экономико-географического исследования железнодорожной инфраструктуры Азербайджанской Республики и показана эффективность транзитного потенциала страны в регионе Европа-Азия. Также обсуждается важность транспорта и международных перевозок в контексте глобализации мировой экономики и их влияние на международные экономические отношения Азербайджана. Трансконтинентальные железные дороги играют большую роль в росте экономики как страны, так и ее регионов, международной экономической и политической интеграции стран. В процессе интеграции в мировую экономику Азербайджан ставит задачи по расширению своего транспортного комплекса, а также по присоединению к глобальным транспортным коридорам. Цель – оценить потенциал международных железнодорожных коридоров, обосновать его социально-экономическую выгоду для нашей страны. Азербайджан планирует улучшить транспортную, а также железнодорожную инфраструктуру вдоль трассы Великого шелкового пути и расширить торговые связи с Европой и Азией. Изучены трансконтинентальные железнодорожные коридоры, имеющие важное экономическое, политическое и культурное значение для обеспечения устойчивого социально-экономического развития Азербайджана в процессе интеграции в мировую экономику. Исследована роль крупных транспортных коридоров в Евразии, таких как Баку-Тбилиси-Карс, TPACEKA, Север-Юг и их влияние на экономическую интеграцию Европы и Азии. Кроме того, изучается влияние железной дороги Баку-Тбилиси-Карс и международного транспортного коридора Север-Юг на интеграцию Азербайджана в мировую экономику.

Ключевые слова: *железная дорога, международные транспортные коридоры, экономическое развитие, железные дороги Баки-Тбилиси-Карс и Север-Юг, TPACEKA*

TRANSKONTİNENTAL DƏMİRYOLU DƏHLİZLƏRİNİN AZƏRBAYCANIN GEOSİYASİ VƏ İQTİSADİ ŞƏRAİTİNƏ TƏSİRİ

Orucov P.Ş.
Bakı Dövlət Universiteti
AZ1148, Bakı şəh., Z. Xəlilov küç., 23: porucov@bsu.edu.az

Xülasə. Məqalədə Azərbaycan Respublikasının dəmir yolu infrastrukturunun iqtisadi-coğrafi təhlili və Avropa-Asiya regionunda ölkənin tranzit potensialının səmərəliliyi araşdırılır.Habelə, dünya iqtisadiyyatının qloballaşması şəraitində nəqliyyatın və beynəlxalq yük daşımalarının əhəmiyyəti və onların Azərbaycanın beynəlxalq iqtisadi əlaqələrinə təsirləri müzakirə olunur. Transkontinental dəmir yolları ölkənin və onun bölgələrinin inkişafında, həmçinin ölkələrin beynəlxalq iqtisadi və siyasi inteqrasiyasında mühüm rol oynayır. Dünya iqtisadiyyatına inteqrasiya prosesində Azərbaycan öz qarşısına nəqliyyat kompleksinin genişləndirilməsi, həmçinin qlobal nəqliyyat dəhlizlərinə qoşulması məsələlərini qoyub. Məqsəd beynəlxalq dəmir yolu dəhlizlərinin potensialını qiymətləndirmək və onların ölkəmiz üçün sosial və iqtisadi faydalarını əsaslandırmaqdır. Azərbaycan Böyük İpək Yolu boyunca nəqliyyat və dəmir yolu infrastrukturunun təkmilləşdirilməsini və Avropanın və Asiyanın ticarət əlaqələrinin genişləndirilməsini planlaşdırır. Məqalədə dünya iqtisadiyyatına inteqrasiya prosesində Azərbaycanın davamlı sosial-iqtisadi inkişafının təmin edilməsi üçün böyük iqtisadi, siyasi və mədəni əhəmiyyətə malik transkontinental dəmir yolu dəhlizləri araşdırılıb. Avrasiyada Bakı-Tbilisi-Qars, TRASEKA, Şimal-Cənub kimi böyük nəqliyyat dəhlizlərinin rolu və onların Avropanın və Asiyanın iqtisadi inteqrasiyasına təsiri araşdırılmışdır. Bundan əlavə, Bakı-Tbilisi-Qars dəmir yolunun və Şimal-Cənub beynəlxalq nəqliyyat dəhlizinin Azərbaycanın beynəlxalq arenaya inteqrasiyasına təsiri öyrənilir. Həmçinin, Avropanı Asiya ilə birləşdirən təbii tranzit körpülərindən biri kimi aparıcı beynəlxalq təşkilatlar tərəfindən rəsmən tanınmış TRASEKA beynəlxalq nəqliyyat dəhlizi araşdırılır.

Açar sözlər: *dəmir yolu, beynəlxalq nəqliyyat dəhlizləri, iqtisadi inkişaf, Baki-Tbilisi-Qars və Şimal-Cənub dəmir yolları, TRASEKA*